Molecular mechanisms of severe congenital neutropenia (SCN) associated with deficiencies in vacuolar protein sorting homolog 45 (VPS45)

Dissertation an der Fakultät für Biologie

der Ludwig-Maximilians-Universität München

Laura Frey

München, den 26.05.2021

Diese Dissertation wurde unter Leitung von Prof. Dr. Christoph Klein am Dr. von Haunerschen Kinderspital der Ludwig-Maximilians-Universität München angefertigt und von Prof. Dr. Wolfgang Enard vertreten.

Erstgutachter: Prof. Dr. Wolfgang Enard

Zweitgutachter: Prof. Dr. Christoph Klein

Tag der Abgabe: 26.05.2021

Tag der mündlichen Prüfung: 12.01.2022

Eidesstattliche Erklärung

Ich versichere hiermit an Eides statt, dass die vorgelegte Dissertation selbstständig und ohne unerlaubte Hilfsmittel angefertigt worden ist. Die vorliegende Dissertation wurde weder ganz noch teilweise bei einer anderen Prüfungskommission vorgelegt. Ich habe noch zu keinem früheren Zeitpunkt versucht, eine Dissertation einzureichen oder an einer Doktorprüfung teilzunehmen.

München, den 14.01.2022 Laura Frey

Acknowledgements

I would like to express my sincere gratitude to all people who have made a great contribution to this work:

First and foremost, I would like to thank my supervisor Prof. Christoph Klein for giving me the opportunity to conduct this research and providing me with all the expertise and resources. I am particularly grateful for the critical discussions and the support throughout these years.

I owe special thanks to Prof. Wolfgang Enard for his willingness to represent this thesis at the Faculty of Biology at the Ludwig-Maximilins-Universität München. Along with him I would like to thank all members of my PhD examination board—Prof. Christoph Klein, Prof. Wolfgang Frank, Prof. Bettina Kempkes, Prof. Heinrich Leonhardt and Prof. Kirsten Jung—for reviewing my thesis and participating in my defense.

A big thanks goes to my former colleagues and friends at the Klein lab for your companionship. I could always rely on you: no matter whether it was about solving the mysteries of the wet lab, administrative issues or where to get lunch. In particular, I would like to thank Dr. Natalia Zietara and Dr. Marcin Lyszkiewicz for their endless support and daily guidance. Without you, my research would not have come this far.

Furthermore, I would like to thank the international doctorate training program “i-Target: Immunotargeting of Cancer” of the Elite Network of Bavaria for not only providing funding, but also the opportunity to participate in international conferences and workshops.

My deepest gratitude goes to my family for their unconditional support and encouragement. Tobi, I am beyond grateful to have you in my life. I dedicate this thesis to you.

Abstract

Vacuolar protein sorting 45 homolog (VPS45) is a member of the Sec1/Munc18 (SM) family and controls vesicle trafficking through the endosomal system. VPS45-deficient patients suffer from severe congenital neutropenia (SCN) and clinically manifest with bone marrow fibrosis as well as aberrant hematopoiesis. Furthermore, patients are refractory to the mainstay of treatment with granulocyte colony-stimulating factor (G-CSF). The molecular mechanisms underlying these diseases and the regulation of vesicular trafficking by VPS45 remain elusive. Thus, the overall goal of this thesis was to investigate the molecular mechanisms underlying VPS45 deficiencies.

The data presented here reveal an essential role of VPS45 in maintaining the morphology and distribution of endosomal and lysosomal vesicles in human cells. Moreover, it was shown that VPS45 is crucial for the efficient recycling of cargo proteins. Besides, the depletion of VPS45 results in disrupted endosome maturation. Consequently, cargos are trapped in early endosomes and prevented from efficient processing in the lysosomal compartment in the absence of VPS45. In this context, aberrant trafficking of the G-CSF receptor (G-CSFR) was demonstrated in VPS45-deficient cells. Furthermore, a complete lack of VPS45 leads to embryonic death at an early stage in mice.

Thus, this thesis identifies mammalian VPS45 as a crucial regulator of endosomal cargo transport and an essential protein during early embryogenesis of mice. It further deepens the understanding of VPS45-driven cellular processes in health and disease.

Table of contents

List of abbreviations

Abbreviation	Meaning
APC	Antigen-presenting cell
BSA	Bovine serum albumin
CATCHR	Complex associated with tethering containing helical rods
CAV1-3	Caveolin 1-3
CCP	Clathrin-coated pit
CCR7	C-C chemokine receptor type 7
CCV	Clathrin-coated vesicle
CHS	Chediak-Higashi syndrome
CME	Clathrin-mediated endocytosis
COG	Conserved oligomeric Golgi
CP	Complement receptor
COPI	Coat protein complex I
COPII	Coat protein complex II
CQ	Chloroquine
CORVET	Class C core vacuole/endosome tethering
DC	Dendritic cell
DQ BSA	DQ bovine serum albumin
DQ OVA	DQ ovalbumin
EARP	Endosome-associated recycling protein
EEA1	Early endosome antigen 1
EGF	Epidermal growth factor
EGFR	Epidermal growth factor receptor
EHD	EPS15 homology domain
EPS15	Epidermal growth factor receptor substrate 15
ER	Endoplasmic reticulum
ESCRT	Endosomal sorting complex required for transport
FRT	Flippase recognition target
FYCO1	FYVE and coiled-coil domain-containing protein 1

FYVE	Fab1-YotB-Vac1p-EEA1
G6PC3	Glucose-6-phosphatase 3
GARP	Golgi-associated retrograde protein
G-CSF	Granulocyte colony-stimulating factor
G-CSFR	Granulocyte colony-stimulating factor receptor
GDP	Guanosine diphosphate
GEF	Guanine exchange factor
GFP	Green fluorescent protein
GS2	Griscelli syndrome type 2
GTP	Guanine triphosphate
HOPS	Homotypic fusion and protein sorting
HPS2	Hermansky-Pudlak syndrome type 2
IFN	Interferon
ILV	Intraluminal vesicle
KO	Knockout
LC3	Microtubule-associated protein light chain 3
LAMP1	Lysosome-associated membrane protein 1
LAMP2	Lysosome-associated membrane protein 2
LAMTOR2	Late endosomal/lysosomal adaptor and MAPK and mTOR activator 2
LSK	Lineage-negative (Lin^-), Sca-1-positive ($Sca\text{-}1^+$), c-Kit-positive ($c\text{-}Kit^+$)
LYST	Lysosomal trafficking regulator
M6P	Mannose 6-phosphate
M6PR	Mannose 6-phosphate receptor
M6PRBP1	Mannose-6-phosphate receptor binding protein 1
Mac-1	Macrophage-1 antigen
MAPK	Mitogen-activated protein kinase
MHC	Major histocompatibility complex
MTC	Multisubunit tethering complex
mTOR	Mechanistic target of rapamycin
MVB	Multivesicular body
ORP1L	Oxysterol-binding protein-related protein 1L

OVA	Ovalbumin
PBS	Phosphate-buffered saline
PCR	Polymerase chain reaction
PEI	Polyethylenimine
PI3K	Phosphoinositide 3-kinase
PIC	Protease inhibitor cocktail
PI(3)P	Phosphatidylinositol 3-phosphate
$PI(3,5)P_2$	Phosphatidylinositol 3,5-bisphosphate
PLEKHM1	Pleckstrin homology domain-containing family M member 1
PM	Plasma membrane
PMSF	Phenylmethanesulfonylfluoride
$PtdIns(4,5)P_2$	Phosphatidylinositol 4,5-bisphosphate
PVDF	Polyvinylidene difluoride
Rab	Ras-related in brain
RFP	Red fluorescent protein
rhG-CSF	Recombinant human G-CSF
RILP	Rab-interacting lysosomal protein
RTK	Receptor tyrosine kinase
Rubicon	RUN domain protein as Beclin1 interacting and cysteine-rich containing
RUN	RPIP8-UNC-14-NESCA
SDS	Sodium dodecylsulfate
SCN	Severe congenital neutropenia
SM	Sec1/Munc18
SNARE	Soluble N-ethylmaleimide-sensitive factor attachment protein receptor
SNX9	Sorting nexin 9
SNX4	Sorting nexin 4
SRP	Signal recognition particle
STAT	Signal transducers and activators of transcription
t-SNARE	Target-SNARE
TCR	T cell receptor
Tf	Transferrin

TfR	Transferrin receptor
TGN	Trans-Golgi network
TLR	Toll-like receptor
TNF	Tumor necrosis factor
TRAPP	Transport protein particle
VPS	Vacuolar protein sorting
VPS45	Vacuolar protein sorting 45 homolog
v-SNARE	Vesicle-SNARE
WDR91	WD repeat-containing protein 91
WT	Wild type

1 Introduction

1.1 The endomembrane system

The endomembrane system constitutes a network of membrane-enclosed compartments, which are functionally interrelated. The compartmentalization allows the organelles to specialize in their function by maintaining distinct compositions, resulting in an increased efficiency of cellular processes (Rothman and Wieland, 1996; Chen and Silver, 2012). The main components of the cellular membrane system comprise the nuclear envelope, the endoplasmic reticulum (ER), the Golgi apparatus, endolysosomal vesicles, and the plasma membrane (PM). The highly dynamic exchange of proteins and lipids between these compartments is facilitated by vesicle budding, fission, and fusion with the membrane of the acceptor organelle (Misteli, 2001). The simultaneous movement of hundreds of cargo carriers accounts for the complexity of the intracellular trafficking network. In order to cope with the huge amount of traffic, the cell requires tight regulation and coordination of these processes. Proper membrane trafficking is essential for maintaining homeostasis and multiple fundamental cellular functions, such as the uptake of nutrients, signaling, secretion, removal of dysfunctional organelles and proteins, motility, and immunity. Intact trafficking not only ensures communication between the organelles in the cell interior but also enables communication with the extracellular environment (Amara et al., 1992; Cobbold, 2003; Gissen and Maher, 2007). The importance of functional membrane trafficking and cargo transport is further highlighted by the occurrence of multiple human diseases, in which genes encoding members of the vesicular trafficking machinery are mutated (described later in chapter 1.5).

The intracellular vesicle trafficking system consists of two main pathways: the endocytic pathway, which directs vesicle trafficking from the plasma membrane to the cell interior and the biosynthetic or secretory pathway, which involves cargo transport from the cell interior to the exterior (Figure 1-1).

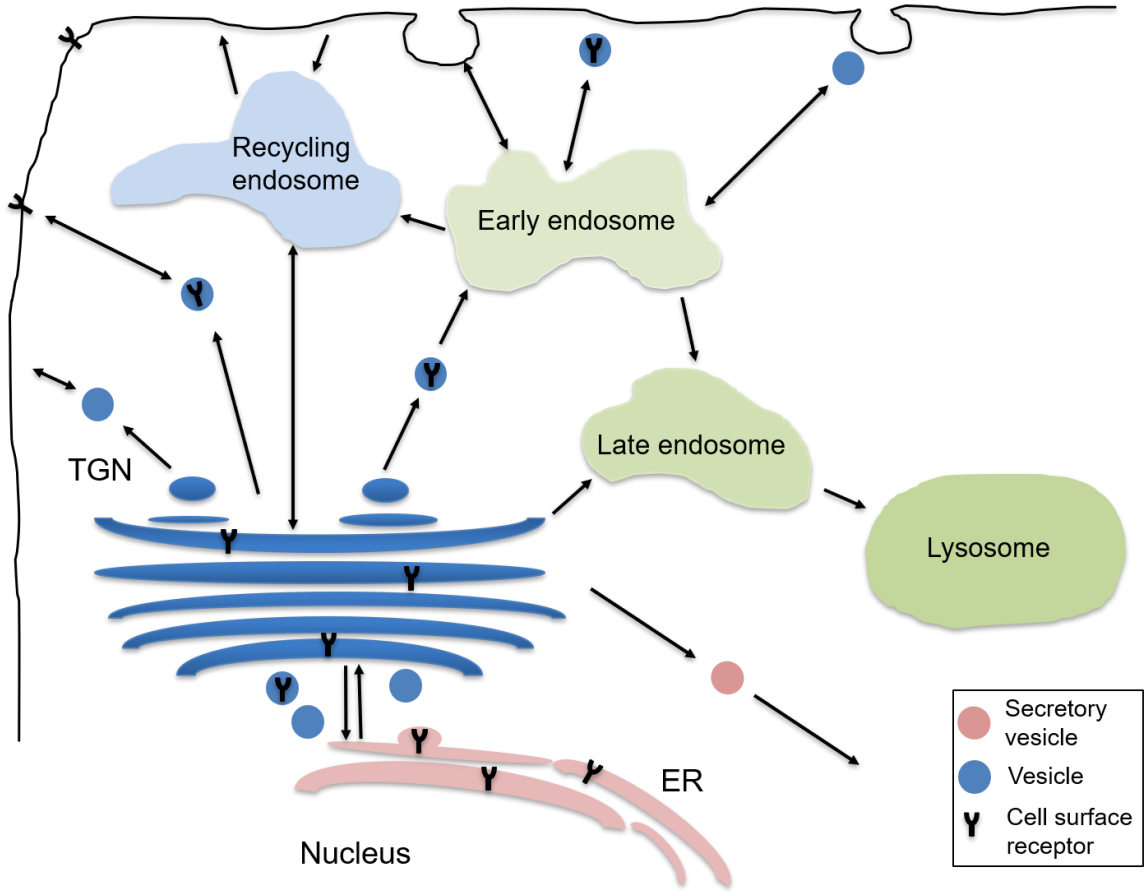

Figure 1-1 Vesicular trafficking pathways.

Newly synthesized proteins are transported from the ER to the trans-Golgi network (TGN), where protein sorting occurs. Internalized cargos are sorted at the early endosomes to be either recycled to the cell surface or degraded in lysosomes.

1.2 The biosynthetic pathway

The secretory or biosynthetic pathway mediates the transport of newly synthesized proteins from the ER to either intracellular compartments, including the Golgi apparatus, endosomes, and lysosomes or the plasma membrane and the extracellular space. The ER constitutes the first stage of the secretory pathway. The signal sequence of the secretory protein is recognized by the signal recognition particle (SRP) complex, which initiates its targeting to the Sec61 pore complex (Benham, 2012; Akopian et al., 2013). Upon translocation across the ER membrane, the SRP complex is disassembled and the signal peptide is removed from the secretory protein. Proteins destined for secretion are post-translationally modified and folded by chaperones in the ER lumen (Benham, 2012; Ellgaard et al., 2016). Aberrantly modified and misfolded proteins are either retained in the ER for refolding or degraded by the proteasome in the ER-associated degradation (ERAD) pathway (Ruggiano et al., 2014; Needham et al., 2019). ER-resident proteins are marked by sorting motifs, such as the

KDEL sequence, and kept in the ER (Munro and Pelham, 1987). Other proteins, which exhibit correct folding and post-translational modifications, are packed into coat protein complex II (COPII)-coated vesicles and delivered to the cis-Golgi network. On the anterograde transport route, the cargo is further transported to the trans-Golgi network (TGN) through the cis-cisterna, the medial-cisterna, and the trans-cisterna (Federica Brandizzi and Charles Barlowe; Jackson, 2009). During the passage through the distinct cisternae of the Golgi apparatus, proteins undergo further post-translational modifications (Stanley, 2011; Zhang and Wang, 2016). In the TGN, secretory proteins are sorted into distinct vesicle types, which do not belong to the COPI/COPII system (Robinson, 2004). Based on their sorting motifs or post-translational modifications, secretory proteins are subsequently targeted to their specialized compartments, such as endosomes, lysosomes, and the plasma membrane (Bonifacino and Traub, 2003; Matteis and Luini, 2008). One of the best-characterized sorting mechanisms is the lysosomal targeting of proteases, such as the aspartic protease cathepsin D. It involves the addition of mannose-6-phosphate (M6P) residues to the N-linked oligosaccharides of the proteins. These proteins are recognized by M6P receptors in the TGN and sorted into clathrin-coated vesicles, which are transported to endolysosomal vesicles. There, the receptor releases the hydrolases due to a drop in pH and is targeted back to the TGN for another round of transport. Recycling of the M6P receptor to the TGN is assisted by a specific signal sequence in its cytoplasmic domain and carrier proteins, such as the M6P receptor-binding protein 1 (M6PRBP1) (Kurt von Figura and Andrej Hasilik; Díaz and Pfeffer, 1998; Hirst et al., 1998).

In parallel to anterograde trafficking, retrieval mechanisms ensure that ER-resident proteins and components of the anterograde transport machinery are returned to the ER (Cosson and Letourneur, 1994). The transport of cargo material from the Golgi apparatus on the retrograde route is facilitated by COPI-coated vesicles. This mechanism constitutes an important balance between the secretory and the endocytic trafficking pathway (Federica Brandizzi and Charles Barlowe; Johannes and Popoff, 2008; Progida and Bakke, 2016).

1.3 The endocytic pathway

The endocytic transport route plays a pivotal role in many cellular processes including the activation and regulation of signal transduction, nutrient uptake, cell development, cargo entry, as well as lysosomal digestion. The first step of the endocytic pathway is the internalization of cargo material, such as receptor-ligand complexes, fluids, lipids, proteins, plasma membrane components, or pathogens. The distinct uptake mechanisms are described in 1.3.1. Following internalization, membrane-enclosed cargos are

delivered to pre-existing early endosomes in the periphery of the cell. Early endosomes function as major sorting stations, where further transport to various destinations is coordinated. Vesicles and their cargos are either recycled to the PM (1.3.2) or targeted to lysosomes via the degradation pathway (1.3.3) (Mayor and Pagano, 2007; Kumari et al., 2010; Cossart and Helenius, 2014). Alternatively, they can be sent to the TGN via the retrograde transport route, where additional cargo sorting occurs (Mallard et al., 1998). Differential sorting of receptor-ligand complexes in early endosomes is partly facilitated by the intraluminal pH of endosomal vesicles. Receptors destined to return to the PM, such as the transferrin receptor (TfR), dissociate from their ligands already in a mildly acidic pH, thus enabling recycling at an early step of the endocytic pathway. In contrast, receptors following the retrograde pathway, such as the M6PR, or the lysosomal degradation route, such as the epidermal growth factor receptor (EGFR), remain associated with their respective ligands and dissociate in the low pH environments of late endosomes or lysosomes (Elkin et al., 2016). Organelles involved in the endocytic route mainly comprise early endosomes, recycling endosomes, late endosomes, and lysosomes. Each specialized compartment has its unique set of proteins by which it can be identified. However, the endosomal network relies on dynamic exchanges between compartments, thus the properties and characteristics of organelles can change and merge during endocytic flux.

1.3.1 Internalization

Cargo internalization to pre-existing early endosomes in the cell periphery comprises four main uptake mechanisms: clathrin-mediated endocytosis, caveolar endocytosis, pinocytosis, and phagocytosis.

Clathrin-mediated endocytosis (CME)

CME is mainly used by receptor-ligand complexes, including the EGFR, TfR, and antibody complexes (Mellman, 1996). In addition, this uptake mechanism is employed by various bacteria and viruses to enter the cells (Cossart and Helenius, 2014).

The first step in CME is the generation of clathrin-coated pits (CCPs), which are small membrane invaginations. The formation of CCPs is initiated by the recruitment of a complex consisting of FCH domain only 1 and 2 (FCHo1 and FCHo2) proteins, epidermal growth factor receptor substrate 15 (EPS15), and intersectins to phosphatidylinositol 4,5-bisphosphate (PtdIns(4,5)P_2)-enriched regions at the PM (McMahon and Boucrot, 2011; Kirchhausen et al., 2014). The subsequent recruitment and enrichment of adaptor proteins, such as the adaptor protein 2 (AP2) complex, enables cargo selection and recruitment of clathrin triskelia, which are polymers of the clathrin heavy chain (Mellman, 1996; McMahon and Boucrot, 2011). Upon the formation of a clathrin coat,

membrane constriction and fission are initiated by binding of BAR domain-containing proteins, such as amphiphysin, endophilin, and sorting nexin 9 (SNX9) (Shin et al., 2008; McMahon and Boucrot, 2011). These proteins recruit the GTPase dynamin to the neck of the vesicle, where it facilitates membrane fission and the formation of a clathrin-coated vesicle (CCV). The subsequent removal of the clathrin coat is triggered by auxilin-mediated targeting of the chaperone heat shock cognate 70 (HSC70) to the coats. The disassembly of the clathrin coat results in the formation of an endocytic vesicle, which fuses with early endosomes (McMahon and Boucrot, 2011; Yu et al., 2014). Components of the complex are then released and reused in another cycle of CME (McMahon and Boucrot, 2011; Mettlen et al., 2018).

Caveolar endocytosis

Caveloar endocytosis is a clathrin-independent and dynamin-dependent process, which mediates the uptake of extracellular ligands, bacterial toxins, different types of viruses, as well as membrane proteins and lipids. Caveolae are small membrane invaginations of roughly 50-100 nm, which are enriched in caveolin proteins, sphingolipids, and cholesterol (Yamada, 1955; Harder and Simons, 1997; Parton, 2018). Essential proteins involved in the formation and stabilization of caveolae are caveolin proteins, cavin proteins, pacsin proteins, and EPS15 homology domain (EHD) proteins (Parton, 2018). Humans possess three caveolin genes, caveolin-1 (CAV1), caveolin-2 (CAV2), and caveolin-3 (CAV3), which have cholesterol-binding properties. CAV1 is mainly expressed in non-muscle tissues, whereas CAV3 is expressed in muscle cells. CAV2 is usually coexpressed with CAV1. The expression of CAV1 and CAV3 is essential for the formation of caveolae in their respective tissues. In contrast, CAV2 expression is not fundamental for this process (Almeida, 2017; Parton, 2018). Cavin1 is another lipid-binding protein essential for the induction of membrane invagination and stabilization of the caveolae by binding to PtdIns(4,5)P_2 and phosphatidylserine at the PM. Moreover, pacsins play an important role in shaping and stabilizing the caveolae (Hansen et al., 2011; Parton, 2018). The neck of the caveolae is further stabilized by the recruitment of EHD proteins (Yeow et al., 2017; Parton, 2018). Similar to CME, the scission of endocytic vesicles is dependent on the GTPase dynamin, in particular dynamin 2 (Henley et al., 1998; Shajahan et al., 2004).

Internalized caveolar vesicles can either fuse with early endosomes or with an organelle termed caveosome. Like early endosomes, caveosomes act as sorting stations but differ in their composition and properties: the pH of caveosomes is neutral and the early endosome antigen (EEA1) protein is absent on these structures (Parton and Simons, 2007; Parton and Howes, 2010). Upon sorting at the caveosomes, caveolar vesicles fuse with early endosomes, the Golgi apparatus, and the ER or recycle to the

PM. To date, the exact mechanism of the disassembly and recycling of the caveolar machinery is not fully understood (Parton and Simons, 2007; Parton, 2018).

Phagocytosis

Phagocytosis is typically employed by professional phagocytic cells, including neutrophil granulocytes, monocytes, macrophages, and dendritic cells (DCs), during the internalization and elimination of pathogenic microorganisms, large solid particles or debris and dead cells. Recognition of material destined for phagocytosis is facilitated by non-opsonic and opsonic receptors. Non-opsonic receptors comprise lectin-like recognition molecules, such as CD169 (Sialoadhesin) or CD33 (Siglec-3), related C-type lectins, such as Dectin-2 or Mincle, scavenger receptors, and Dectin-1. Receptors belonging to the group of opsonic receptors comprise Fc receptors and the complement receptors. Examples for opsonins targeting material for digestion are antibodies (IgG), fibronectin, the mannose-binding lectin, and the milk fat globulin (Mellman, 1996; Gordon, 2016; Rosales and Uribe-Querol, 2017). Fc receptors bind to the Fc portion of antibodies and are crucial for the host's innate and adaptive immunity. These receptors are expressed by multiple cells of the immune system, comprising macrophages and monocytes, granulocytes, DCs, as well as natural killer (NK) cells and B cells. The best-characterized Fc receptors are the Fcγ receptors, which recognize the Fc fragment of IgGs. The family of Fcγ receptors has several members, including FcγRI (CD64), FcγRIIA (CD32a), FcγRIIB (CD32b), FcγRIIIA (CD16a), and FcγRIIIB (CD16b). These receptors have different affinities to bind IgG subclasses. Whereas FcγRI shows a high affinity, the other receptors reveal low to medium affinities. The FcγRIIB is the only inhibitory receptor containing an immunoreceptor tyrosine-based inhibitory motif (ITIM) in the cytoplasmic domain, while all other receptors have activating properties (Nimmerjahn and Ravetch, 2008; Koenderman, 2019). Complement receptors (CRs) are essential for the efficient destruction of invading pathogens, recruitment of immune cells to sites of inflammation, and cell adhesion. These receptors are expressed on both myelocytes and lymphocytes and bind to the portions of the complement components 3 and 4. The members comprise CR1 (CD35), CR2 (CD21), CR3 (CD11b/CD18 or Macrophage-1 antigen (Mac-1)), and CR4 (CD11c/CD18). CR3 and CR4 belong to the family of β2 integrins of adhesion molecules and are heterodimers consisting of a common β2 chain (CD18) and different α subunits comprising integrin αM (CD11b) and integrin αX (CD11c), respectively (Holers, 2014; Vorup-Jensen and Jensen, 2018). Once the phagocytic material is recognized by receptors, a signaling cascade is triggered and pseudopod extensions are formed. The pseudopods eventually engulf the phagocytic material in a vesicle and form a non-coated phagosome. The phagosomal vesicle is transported to the endosomal compartment, where phagosome maturation occurs by the switch of Rab5 to Rab7. This results in the delivery of the cargo to lysosomes, where it is degraded (Mellman, 1996; Gordon, 2016; Rosales and

Uribe-Querol, 2017). The process of phagocytosis, comprising membrane invagination and pseudopod formation, is highly dependent on actin remodeling and polymerization (Freeman and Grinstein, 2014).

Macropinocytosis

Macropinocytosis constitutes a fluid-phase and less specific form of endocytosis, as it is not initiated by ligand binding to specific receptors. In some cells macropinocytosis is triggered by extracellular stimuli, including the epidermal growth factor (EGF) and the macrophage colony-stimulating factor (MCSF) (Racoosin and Swanson, 1992; Araki et al., 2007). In DCs, the main professional antigen-presenting cells (APCs), micropinocytosis is one of the key mechanisms of antigen uptake (Sallusto et al., 1995). The uptake process resembles phagocytosis, except that internalized matter is soluble. Engulfment of soluble cargo requires membrane ruffling and the formation of protrusions surrounding the cargo, which subsequently fold back with the plasma membrane. Like phagocytosis, actin rearrangement and polymerization play a crucial role in this process. Moreover, Ras, class-1 phosphoinositide 3-kinase (PI3K), and phosphatidylinositol (3,4,5)-triphosphate (PIP3) phosphoinositides are important regulators of these steps (Bar-Sagi and Feramisco, 1986; Araki et al., 2007; Swanson, 2014). Membrane-enclosed non-coated vesicles are termed macropinosomes and are heterogeneous in size, ranging from 0.2 to 5 µm (Swanson, 1989). Macropinosomes eventually bud off the plasma membrane and fuse with Rab5-positive early endosomes (Feliciano et al., 2011; Egami et al., 2014). Subsequent maturation of macropinosomes is characterized by an exchange of Rab5 to Rab7 and mediates the delivery of cellular cargo to the degradative compartment (Feliciano et al., 2011).

1.3.2 The recycling pathway

Upon internalization into early endosomes, cargo is either sorted to late endosomes and lysosomes for degradation or to recycling endosomes for the delivery to the PM. The recycling process balances the endocytic pathway by regulating levels of plasma membrane components, thus ensuring membrane homeostasis. Moreover, the recycling pathway is crucial for various cellular functions, including nutrient uptake, adhesion, and signal transduction (Grant and Donaldson, 2009; Goldenring, 2015). Additionally, the recycling of adhesion molecules, such as integrins, affects cell migration (Caswell et al., 2009). Return of cellular cargo to the PM occurs via either the fast or the slow recycling pathway and is regulated by GTPases, their respective effectors, and EHD proteins.

The fast route has been characterized by the direct recycling of cargo through the formation and budding of CCVs from early endosomes. Important components of the fast

recycling machinery include the GTPases Rab4 and Rab35 (van der Sluijs et al., 1992; Kouranti et al., 2006). The role of Rab4 in recycling is controversial since the siRNA-mediated knockdown of Rab4 has revealed an increased rapid recycling rate of transferrin (Tf), whereas the expression of a dominant-negative form delayed the recycling of Tf (McCaffrey et al., 2001; Deneka et al., 2003).

The slow route involves the sorting of cellular cargo into tubular structures, which dissociate from early endosomes and mature to form recycling endosomes (Hopkins, 1983). Recycling endosomes are typically identified by the presence of the GTPase Rab11 (van der Sluijs et al., 1992; Sönnichsen et al., 2000). The transfer of cargo from early endosomes to recycling endosomes is mediated by various proteins, including sorting nexin 4 (SNX4), EHD3, the Rab11 effector FIP5, as well as the GTPases Rab22 and Rab10 (Weigert et al., 2004; Chen et al., 2006; Traer et al., 2007; Schonteich et al., 2008; Bahl et al., 2016).

Independent of the distinct recycling routes, newly vacated receptors and components of the PM are eventually returned and incorporated in the PM to ensure its homeostasis (Maxfield and McGraw, 2004; Goldenring, 2015).

Recycling of the transferrin receptor (TfR)

Tf and the TfR are critical regulators of iron homeostasis and are widely used to study the recycling pathway (Hopkins, 1983; Grant and Donaldson, 2009; Goldenring, 2015). The serum glycoprotein Tf possesses two Fe^{3+}-binding sites and acts as an iron carrier. After the iron is bound to Tf, it binds to its receptor with a markedly increased affinity as compared to unbound Tf (Dautry-Varsat et al., 1983; Yersin et al., 2007). The complex is internalized via CME and subsequently translocated to early endosomes (Maxfield and McGraw, 2004). The mildly acidic pH in these organelles facilitates iron dissociation from the complex (Dautry-Varsat et al., 1983; Eckenroth et al., 2011). In contrast, iron-free Tf remains bound to its receptor and is sorted into vesicles trafficking along either the fast or the slow recycling route (Sönnichsen et al., 2000). Upon delivery to the PM, iron-free Tf is released from the receptor at neutral pH and is ready for another round of iron loading and delivery (Dautry-Varsat et al., 1983; Maxfield and McGraw, 2004).

1.3.3 Endosome maturation and lysosomal degradation

Early endosomal cargos, which are not recycled to the plasma membrane or follow the retrograde route to the TGN, are typically destined for degradation in lysosomes. Proteolytic processing of cargo is crucial for a multitude of cellular processes, such as the regulation and termination of signaling cascades, membrane turnover, or destruction

of pathogens. It is facilitated by the conversion of early endosomes to late endosomes, a process termed endosome maturation, as well as the subsequent fusion of late endosomes with lysosomes (Sorkin and Zastrow, 2009; Di Fiore and Zastrow, 2014).

During the process of endosomes maturation, the composition of membrane proteins and lipids is continuously remodeled. Early endosomes are enriched in the lipid phosphatidylinositol 3-phosphate (PI(3)P), which is phosphorylated by the kinase PIKFYVE to generate phosphatidylinositol 3,5-bisphosphate ($PI(3,5)P_2$) on late endosomal membranes (Marat and Haucke, 2016). Moreover, the identity and functional property of each endosomal compartment are defined by a specific subset of proteins. Proteins that carry out crucial functions at early endosomes include EEA1 and Rab5. In contrast, late endosomes require the presence of the lysosomal-associated membrane protein 2 (LAMP2) and Rab7 proteins, whereas lysosomal membranes typically contain the lysosome-associated membrane protein 1 (LAMP1) (Duclos et al., 2003). A relevant step in endosome maturation is the gradual loss of early endosomal Rab5 and continuous acquisition of late endosomal Rab7 (Rink et al., 2005). The Mon1-Ccz1 complex is one of the crucial complexes controlling the exchange of Rab5 by Rab7 (Kinchen and Ravichandran, 2010). The recruitment of the Mon1-Ccz1 complex displaces the Rab5 guanine exchange factor Rabex-5 and results in the inactivation of Rab5. In turn, Rab7 gets activated through the release of bound GDI by the Mon1-Ccz1 complex (Huotari and Helenius, 2011). Other complexes involved in endosome maturation are the CORVET (class C core vacuole/endosome tethering) and HOPS (homotypic fusion and protein sorting) hexameric tethering complexes, which interact with Rab5 on early endosomes and Rab7 on late endosomes, respectively. Together with the switch of Rab5 to Rab7, the CORVET complex is converted into the HOPS complex during endosome maturation (Cabrera and Ungermann, 2010; Balderhaar and Ungermann, 2013). Endosome maturation is further accompanied by a change in the intracellular localization of endolysosomal vesicles. Whereas early endosomes are mainly located in the cell periphery, late endosomes and lysosomes are primarily concentrated in the perinuclear region (Huotari and Helenius, 2011). The movement of endolysosomal vesicles along microtubules and actin filaments is facilitated through the interaction with family members of the motor proteins dynein and kinesin. The transition of early endosomes to late endosomes further involves the enhanced inward budding of endosomal membranes, leading to the formation of intraluminal vesicles (ILVs) and multivesicular bodies (MVBs). Sorting of ubiquitinated cargo proteins and lipids into these ILVs is coordinated by the endosomal sorting complexes required for transport (ESCRT) machinery (ESCRT complexes 0-III) (Frankel and Audhya, 2017). Upon fusion of late endosomes and MVBs with lysosomes, cargos and ILVs are degraded in the lysosomal compartment. The efficient processing of cargos is facilitated by the enhanced acquisition of acidic hydrolases and increased acidification of vesicles

during endosome maturation (Hu et al., 2015). Typically, early endosomes exhibit a mildly acidic pH of about 6.2, whereas the pH decreases in the lumen of late endosomes to roughly 5.5, and to 4.5 in the highly acidic lumen of lysosomes (Casey et al., 2010). The increased acidification is mainly mediated by the multi-subunit protein pump V-ATPase and is a prerequisite for the activation of hydrolases, such as the aspartic protease cathepsin D.

Endosomal sorting of the epidermal growth factor receptor (EGFR)

The EGFR belongs to the ErbB family of receptor tyrosine kinases (RTKs), which besides EGFR/ErbB1/HER1 comprises ErbB2/HER2, ErbB3/HER3, and ErbB4/HER4. The transmembrane receptors transduce signals via the phosphorylation of tyrosine residues in their intracellular domain, resulting in the activation of AKT and MAPK pathways. These are essential for many cellular functions, such as the survival, growth, proliferation, and migration (Scartozzi et al., 2007; Wieduwilt and Moasser, 2008; Lemmon et al., 2014). Notably, dysregulated expression and signaling of members of the ErbB family of RTKs are implicated in multiple human diseases, including cancer, diabetes, and autoimmune disorders (Lemmon et al., 2014; Roskoski, 2014).

The EGFR is widely used to study trafficking along the degradation pathway. CME is the main route of EGF-mediated EGFR internalization. It remains controversial, whether clathrin-independent endocytosis occurs under certain conditions, such as the low availability of EGF ligands (Sigismund et al., 2005; Madshus and Stang, 2009; Hurley and Stenmark, 2011; Bakker et al., 2017). Ligand binding induces dimerization of the receptor and activation of the EGFR kinase. The kinase activation results in the autophosphorylation of tyrosine residues, of which pTyr1045, pTyr1068, and pTyr1086 have been shown to be crucial for binding of the ubiquitin ligase Casitas B-lineage lymphoma (CBL) and the adaptor protein growth factor receptor-bound protein 2 (GRB2) (Madshus and Stang, 2009; Hurley and Stenmark, 2011; Bakker et al., 2017). Subsequent ubiquitylation and recruitment of further ubiquitin-binding adaptor proteins, such as EPS15 and epsin-1, facilitate the translocation of EGFR to CCPs (Torrisi et al., 1999; Kazazic et al., 2009; Hurley and Stenmark, 2011). Following CME, the receptor-ligand complex is transported to early endosomes, which possess a mildly acidic pH of 5.5-6.0. EGF stably binds to EGFR in this environment, ensuring a sustained kinase activity and ubiquitylation of the residues. Thus, the dissociation and potential recycling of the complex is prevented (Longva et al., 2002). Further sorting of the complex for lysosomal degradation and signal termination is mediated by four ESCRT complexes, comprising ESCRT-0, ESCRT-I, ESCRT-II, and ESCRT-III (Tanaka et al., 2008; Hurley and Stenmark, 2011). Endosome maturation facilitates

the translocation of the complex to late endosomes. Eventually, the complex is delivered to the lysosomal compartment, where it is degraded (Madshus and Stang, 2009; Hurley and Stenmark, 2011; Bakker et al., 2017).

Endocytosis and lysosomal processing of various cargo proteins

Cargo proteins, which are widely used to study the endocytic pathway, include ovalbumin (OVA), bovine serum albumin (BSA), and dextran. These compounds differ in their route of entry into the endolysosomal system of the cell. Ovalbumin and its conjugates are mainly internalized via the mannose receptor-mediated CME pathway (Burgdorf et al., 2006; Autenrieth and Autenrieth, 2009). The endocytic route of uptake of BSA and BSA conjugates is not completely understood, however, they are likely endocytosed via macropinocytosis (Tejeda-Muñoz et al., 2019). Depending on the cell type, alternative routes of BSA uptake might be involved, including caveolar endocytosis and clathrin-dependent endocytosis (Francis, 2010; Li et al., 2013). Similarly, macropinocytosis is suggested to be the main route of uptake of dextran, though CME has been observed as well (Li et al., 2015; Tejeda-Muñoz et al., 2019). This is probably due to the large size of dextran. Whereas CME was described for the uptake of 10 kD dextran, macropinocytosis was ascribed to the internalization of 70 kD dextran (Li et al., 2015). Upon uptake into the cells, the distinct cargo proteins follow the same trafficking pathway: they are transported to early endosomes, where they are sorted for degradation in lysosomes. Thus, these compounds are useful to study the delivery of cargo to the degradative compartment.

Endocytic trafficking of the granulocyte colony-stimulating factor (G-CSFR)

The G-CSFR is a member of the cytokine receptor class I superfamily. Upon ligand binding, the G-CSFR forms homodimers and transduces signals, which are critical for neutrophil proliferation and differentiation. The G-CSFR is internalized via CME and transported to early endosomes, where further sorting occurs: the receptor is preferentially directed to lysosomes for degradation, though recycling of the receptor to the PM occurs as well. In general, the intracellular routes of the G-CSFR-GCSF complex are not well studied. It has been shown, however, that intact internalization and lysosomal routing of the receptor depend on a dileucine-based internalization motif and the ubiquitination of the specific lysine residue K632 by the suppressor of cytokine signaling 2 (SOCS2) protein, respectively (Irandoust et al., 2007; Palande et al., 2013).

1.4 The molecular machinery of endomembrane fusion

Vesicle trafficking involves a cascade of events, such as vesicle budding from the donor membrane, transport of cargo vesicles, and fusion with the acceptor membrane.

The efficiency and specificity of these processes are tightly regulated by a complex molecular machinery, which includes Rab GTPases, soluble N-ethylmaleimide-sensitive factor (NSF) attachment protein receptors (SNAREs), members of the Sec1/Munc18 (SM) protein family, and multisubunit tethering complexes (MTCs) (Gonzalez and Scheller, 1999; Cai et al., 2007).

1.4.1 Rab GTPases

Rab GTPases are small monomeric G proteins and members of the Ras superfamily. To date, more than 60 Rab proteins are known in humans. Each endocytic compartment is defined by the presence of specific Rab GTPases and their effector proteins on membranes. Through their interaction with effector proteins, Rab GTPases coordinate docking and tethering of vesicles (Chavrier et al., 1990; Zerial and McBride, 2001; Pfeffer, 2013).

Rab proteins cycle between the GDP-bound inactive form in the cytoplasm and the GTP-bound active form on membranes. Rab proteins are activated through the exchange of GDP by GTP, which is induced by guanine nucleotide exchange factors (GEFs). In contrast, Rab GTPases are inactivated by GTPase-activating proteins (GAPs), which facilitate the hydrolysis of GTP to GDP. While switching between the active and inactive states, Rab proteins undergo conformational changes, which enable them to execute specific functions, such as membrane budding or vesicle docking (McLauchlan et al., 1998; Wandinger-Ness and Zerial, 2014). Rab effectors are proteins, which primarily interact with the active GTP-bound form of Rab proteins and comprise phosphatases, sorting adaptors, tethering factors, kinases, and motor proteins (Eathiraj et al., 2005).

Early endosomes

Rab 5 is one of the most extensively studied Rab protein in the endocytic system. It is localized at early endosomes, where it regulates the fusion of plasma membrane-derived vesicles, the generation of PI(3)P, the homotypic fusion of endosomes, and the recycling of cargos to the plasma membrane. Rab5 is activated by Rabex-5, which functions as a GEF and subsequently recruits its effector Rabaptin-5, which in turn increases the GEF activity of Rabex-5 (Stenmark et al., 1995; Lippe et al., 2001). The complex consisting of Rab5, Rabex-5, and Rabaptin-5 recruits the PI-3-OH kinase hVPS34/p150, which generates PI3P on the early endosomal membrane (Christoforidis et al., 1999). The concomitant presence of Rab5 and enrichment of PI(3)P result in the recruitment of additional effectors containing the conserved Fab1-YotB-Vac1p-

EEA1 (FYVE) domain. These effectors include EEA1 and Rabenosyn-5, which are required for the homotypic fusion of early endosomal vesicles and the maturation of the early endocytic compartment (Nielsen et al., 2000; Jovic et al., 2010).

Late endosomes

The GTPase Rab7 is present at late endosomes and is a critical component of the degradation pathway. Through the interaction with various effectors, Rab7 plays a role in multiple processes, such as the fusion and motility of late endosomal vesicles. Effectors of Rab7 comprise the Rab-interacting lysosomal protein (RILP), the Rabring7, the oxysterol-binding protein-related protein 1L (ORP1L), the FYVE protein, the coiled-coil domain-containing protein 1 (FYCO1), the Pleckstrin homology domain-containing family M member 1 (PLEKHM1), the WD repeat-containing protein 91 (WDR91), and the RPIP8-UNC-14-NESCA (RUN) domain protein as Beclin 1 interacting and cysteine-rich containing (Rubicon). The complex consisting of Rab7, RILP, and ORP1L binds to dynein and dynactin motor proteins to direct positioning of late endosomal vesicles along microtubules towards the perinuclear region (Harrison et al., 2003; Johansson et al., 2007; Hyttinen et al., 2013). In contrast, the Rab7 effector FYCO1 interacts with kinesin and promotes vesicle transport towards the cell periphery. WDR91 is a Rab7 effector, which inhibits the PI3K complex activity on endosomes, thus facilitating the conversion of early endosomal PI(3)P to late endosomal PI(3,5)P_2 and promoting endolysosomal trafficking (Casanova and Winckler, 2017; Liu et al., 2017). The effectors PLEKHM1 and Rabring7 support the fusion of late endosomes with lysosomes and the biogenesis of lysosomes (Mizuno et al., 2003). Rubicon, in contrast, negatively regulates endosome maturation and fusion with lysosomal vesicles by antagonizing the function of the ultraviolet radiation resistance-associated gene (UVRAG).

Rab9 is another Rab GTPase localizing at late endosomes, where it associates with its effector tail-interacting protein of 47 kD (TIP47) to regulate the sorting of lysosomal hydrolases to late endosomes and retrograde trafficking of M6PRs from late endosomes to the TGN (Aivazian et al., 2006). Moreover, it controls lysosome biogenesis as well as the size and intracellular organization of late endosomal vesicles (Ganley et al., 2004).

Recycling endosomes

Rab4 and Rab11 are involved in the fast and slow endocytic recycling of cellular cargo, respectively.

Rab4 is recruited to early endosomes and supports the shuffling of cargo from early endosomes to recycling vesicles. It exerts its functions by interacting with distinct effectors. These effectors comprise KIF3B, Rabip4, its variant Rabip4`, Rabaptin-4, Rabaptin-5, and Rabenosyn-5. The binding of active GTP-bound Rab4 with KIF3B, a member of the kinesin-2 family, induces the directed transport of cargo vesicles to the plasma membrane, thus regulating the mobility and positioning of recycling endosomes (Nag et al., 2018). The other effectors comprising Rabip4`, Rabapting-4, Rabaptin-5, and Rabenosyn-5 simultaneously interact with active Rab4 and Rab5, hence linking and coordinating the recycling and degradation pathways via Rab4 and Rab5, respectively (Renzis et al., 2002; Grant and Donaldson, 2009).

Endosomes implicated in the slow recycling of cellular cargos are defined by the presence of Rab11. Effectors of Rab11 include the Rab11 binding protein (Rab11BP), the motor protein Myosin Vb, members of the Rab11-family interacting proteins (Rab11-FIPs), such as Rab11-FIP1, Rab11-FIP2, and Rab11-FIP3, as well as the Rab11-interacting protein (Rip11) (Junutula et al., 2004). The interaction of Rab11 and Rab11-FIPs facilitates the association of recycling endosomes with motor proteins and microtubules, thus regulating the trafficking of recycling endosomes to the cell surface (Grant and Donaldson, 2009). Similarly, Rip11 binds to kinesin-II to direct cellular cargo to the slow recycling route (Schonteich et al., 2008).

1.4.2 SNARE proteins

SNAREs are membrane-associated proteins, which are crucial for the final membrane fusion step. They further assist Rab GTPases to ensure the specificity of fusion events. SNARE proteins share a common heptad repeat sequence of about 60 to 70 amino acid residues and the SNARE motif, which forms coiled-coil complexes containing four helices (Fasshauer, 2003; Lou and Shin, 2016). One way to classify SNAREs depends on the type of amino acid present at the central or zero layer. The layer consists of three glutamine residues (Q) termed Qa, Qb, and Qc and one arginine residue (R), which are provided by four SNARE proteins, respectively, and determine their categorization in Qa-, Qb-, Qc-, and R-SNAREs. The second possibility to distinguish SNARE proteins depends on their presence on either the vesicle and donor membrane (v-SNARE) or the target and acceptor membrane (t-SNARE) (Hong, 2005; Kloepper et al., 2007). V-SNAREs usually correspond to R-SNAREs and include mostly VAMP proteins. In contrast, t-SNAREs often correspond to Q-SNAREs. Most of the Syntaxins belong to the Qa-SNAREs, whereas Qb- and Qc-SNAREs include only some Syntaxins, such as Syntaxin6, Syntaxin8, or members of the synaptosome-associated protein (SNAP) subfamily (Hong, 2005). Distinct SNARE complexes control different fusion events and the complex components may vary to some extent, as some components can functionally substitute for others. For instance, the SNARE complex involved in the

fusion of early endosomes with late endosomes comprises Syntaxin7, Syntaxin8, Vti1b, and VAMP8, whereas the SNARE complex mediating fusion of late endosomes with lysosomes consists of Syntaxin7, Syntaxin8, Vti1b, and VAMP7 (Antonin et al., 2000; Pryor et al., 2004). Cargo trafficking from the TGN to late endosomes is mediated by Syntaxin6, Syntaxin16, Vti1a, and VAMP4/7 (Laufman et al., 2011).

Pairing of v- and t-SNAREs brings the two opposing membranes into proximity. Moreover, the formation of the four-helix bundle in a *trans*-SNARE complex provides enough energy to facilitate zippering from the N-terminal region towards the membrane-proximal C-terminal domain and fusion of the lipid bilayers. Subsequently, the *trans*-SNARE complex is converted into a *cis*-SNARE complex on the target membrane. The disassembly of the SNARE complex is facilitated by the soluble NS attachment protein (α-SNAP) and the NSF protein, which uses its ATPase activity to unfold the proteins. The v-SNAREs are recycled to the donor vesicle for another round of membrane fusion (Zorman et al., 2014; Lou and Shin, 2016; Wang et al., 2017).

1.4.3 The Sec1/Munc18 (SM) protein family

The SM protein family comprises only four members: Sec1/Munc18, VPS45, SLY1, and VPS33, which assist with the SNARE complex assembly and stabilize SNARE proteins to enable vesicle fusion (Baker et al., 2013; Munson, 2014). Despite the small number of family members and the conservation of SM proteins throughout eukaryotic evolution, the exact function of SM proteins is not completely understood. Besides, SM proteins neither share a common binding mode nor a universal mechanism of action and they play a role in different stages of vesicular trafficking. Sec1 or Munc18 proteins are involved in exocytosis and interact with secretory Syntaxins, whereas VPS45 controls early endosomal traffic and binds to the Qa-SNARE Syntaxin16. Sly1 regulates the transport from the ER to the Golgi apparatus by interacting with the Qa-SNAREs Syntaxin5 or Synatxin18 and VPS33 is a member of the MTC HOPS, which plays a role in targeting cargos to the lysosomal compartment (Jahn and Südhof, 1999; Dulubova et al., 2002; Lobingier and Merz, 2012; Demircioglu et al., 2014; Nogueira et al., 2014)

1.4.4 Tethers and multisubunit tethering complexes along the endosome/lysosome pathway

Tethering factors are involved in almost all vesicle fusion events and mediate tethering of two opposing membranes prior to SNARE pairing. Together with Rab GTPases, they control the formation of SNARE complexes, thus guaranteeing specificity of the fusion process and preventing the assembly of a non-fusogenic complex (Wang et al., 2017). Moreover, tethers stabilize SNARE proteins by inhibiting their degradation.

Tethering factors comprise two distinct groups, long coiled-coil proteins and MTCs (Cai et al., 2007; Chia and Gleeson, 2014).

Long coiled-coil proteins predominantly regulate vesicle fusion at the Golgi apparatus and early endosomes. Due to their great length, coiled-coil proteins are capable of bridging membranes at a long distance of more than 200 nm (Lürick et al., 2018). Golgin proteins are important tethers associated with the Golgi apparatus, where they are crucial for the protein transport, maintenance of the Golgi organization, and positioning of the Golgi apparatus within the cells. EEA1 is an essential tethering factor at early endosomes, where it interacts with active Rab5, the membrane lipid PI(3)P, and SNAREs, such as Syntaxin13 (McBride et al., 1999; Gillingham and Munro, 2003). The multiple interactions of EEA1 ensure that all essential factors are gathered for efficient and specific fusion events.

In contrast to long coiled-coil proteins, MTCs can only span membranes at a distance of about 30 nm. MTCs can be divided into exocytic complexes associated with tethering containing helical rods (CATCHR), endolysosomal class C VPS complexes, and transport protein particle (TRAPP) complexes.

Exocytic CATCHR complexes include the Golgi-associated retrograde protein (GARP), endosome-associated recycling protein (EARP), conserved oligomeric Golgi (COG), exocyst, and DSL1 complexes (Cai et al., 2007; Chia and Gleeson, 2014). GARP and EARP complexes are structurally related and share three subunits comprising VPS51, VPS52, and VPS53. The fourth subunit varies between the complexes and consists of VPS54 in the GARP complex and VPS50 in the EARP complex (Schindler et al., 2015). These different subunits dictate the intracellular localization of the GARP and EARP complexes at the TGN and recycling endosomes, where they regulate traffic from endosomes to TGN and transport from endosomes to recycling endosomes, respectively (Lürick et al., 2018). The COG complex comprises eight different subunits COG1-8, which are organized in two subcomplexes A (COG1-4) and B (COG5-8) bridged by the interaction between COG1 and COG8 (Cai et al., 2007). The complex is crucial for the homeostasis of the Golgi apparatus and essential for vesicle transport from endosomes to Golgi apparatus (Chia and Gleeson, 2014). The exocyst complex consists of eight subunits, Sec3, Sec5, Sec6, Sec8, Sec10, Sec15, Exo70, and Exo84 and facilitates vesicle tethering at the plasma membrane (Wu and Guo, 2015). The DSL1 complex is formed by only three subunits, Dsl1, Dsl3, and Tip20 and regulates retrograde trafficking from the Golgi apparatus to the ER (Chia and Gleeson, 2014). Endolysosomal class C VPS complexes are represented by CORVET and HOPS complexes. The complexes have four common subunits consisting of VPS11, VPS16, VPS18, and VPS33 (Cai et al., 2007). In addition, each of the complexes possesses two unique

subunits, which comprise the Rab5-binding subunits VPS3 and VPS8 in the CORVET complex and the Rab7-binding subunits VPS39 and VPS41 in the HOPS complex. The CORVET complex promotes the fusion of early endosomal vesicles, whereas the HOPS complex facilitates the fusion of late endosomal vesicles (Chia and Gleeson, 2014; van der Beek et al., 2019). The TRAPP complexes comprise three distinct forms. TRAPPI consists of the six subunits TRAPPC1-6 and is required for tethering of ER-derived vesicles to the Golgi apparatus. TRAPP II additionally contains the subunits TRAPPC7, TRAPPC9, TRAPPC10, and TRAPPC2L and is crucial for vesicle traffic at the TGN. TRAPP III further includes the TRAPPC8 subunit and is essential for the formation of autophagosomes (Sacher et al., 2008; Chia and Gleeson, 2014).

1.5 The importance of membrane trafficking for the immune system

Membrane trafficking has been implicated in multiple processes essential for the immune system, such as antigen presentation, immune receptor internalization, and defense signaling mediated by cytokines and chemokines.

Professional APCs comprise DCs, macrophages, and B cells, whereas DCs are the most potent APCs. DCs process and present antigens to CD4-positive and CD8-positive T cells via major histocompatibility complexes (MHC) II and I, respectively, to induce T cell-dependent immune responses. Exogenous antigens are usually presented by MHC II molecules. These antigens are internalized by either CME, caveolar endocytosis, phagocytosis, or micropinocytosis and transported from early endosomes to late endosomes and lysosomes. They are further processed by lysosomal enzymes, loaded onto MHC II molecules, and presented to CD4-positive T cells at the cell surface. Alternatively, cytoplasmic antigens can enter this pathway by the transport to the endolysosomal compartment. However, cytosolic proteins derived from either the host or pathogens typically follow the class I MHC pathway. This pathway involves cytosolic protein processing by the proteasome and trafficking of the generated peptides to the ER. Upon translocation by the transporter associated with antigen processing (TAP), peptides are loaded onto MHC I molecules. Of note, MHC I molecules can also present exogenous proteins, a process termed cross-presentation. Cross-presentation requires the export of ingested proteins from the phagosomal compartment to the cytosol, followed by the translocation by TAP transporters into the ER. The peptide-loaded MHC I complex is then trafficked to the plasma membrane to activate CD8-positive T cells (Shim et al., 2006; Blum et al., 2013; Rock et al., 2016).

Internalization of immune receptors, such as the B cell receptor (BCR) and the T cell receptor (TCR), has been shown to critically regulate their activation, thus playing an essential role in shaping the immune response. For instance, endocytosis of the TCR/CD3 complexes and the signaling molecules involved in signal transduction affect the amplitude, location, and duration of TCR signaling. TCR endocytosis can either be ligand-induced or ligand-independent and clathrin-dependent or clathrin-independent. Signaling is initiated at the plasma membrane upon TCR engagement, however, sustained signaling is observed from internalized receptors, which use endosomes as signaling platforms. Defects in the internalization of TCRs result in dysregulated signaling. For example, thymocytes of mice deficient in dynamin 2, an essential component of the endocytic machinery, revealed an increased TCR surface expression and decreased signaling as well as perturbed proliferation upon stimulation (Willinger et al., 2015). Also, thymocytes of mice deficient in the ubiquitin ligase Cbl had increased amounts of TCR on the cell surface and showed a hyperactivation of signaling pathways (Murphy et al., 1998; Naramura et al., 1998). In general, TCR internalization can have dual effects on signaling: on the one hand it can promote signaling from internal signaling platforms, such as early endosomes, and on the other hand it can terminate signaling by downregulating TCR levels on the cell surface and facilitating lysosomal degradation of receptors. Besides internalization and degradation, recycling of TCRs from a pool of internalized TCR/CD3 complexes is a crucial trafficking process, which is required for the formation of the immunological synapse (Lou et al., 2016). Notably, defects in TCR endocytosis are associated with severe immunodeficiency defects in humans (Łyszkiewicz et al., 2020).

Cytokines and chemokines are important immunomodulatory factors and crucial mediators of immune cell communication. Like TCR, endocytosis of cytokine and chemokine receptors regulates their signaling. For instance, the internalization of the cytokine receptor tumor necrosis factor receptor 1 (TNFR1) is required for TFN-induced apoptotic signaling (Mahul-Mellier et al., 2008). Besides, clathrin- and dynamin-dependent endocytosis of the cytokine receptor type I interferon receptor (IFNAR) has been shown to be crucial for IFN-α-mediated STAT1 and STAT2 signaling (Marchetti et al., 2006). The endocytosis of the C-C chemokine receptor type 7 (CCR7); a receptor with an essential role in leukocyte homing, is described to be clathrin-dependent and involves dynamin, Eps15, Rab5, and EEA1. Upon internalization, CCR7 is recycled back to the cell surface for another round of chemokine sensing, which is crucial for a rapid and efficient immune response. In contrast, its ligand CCL19 is sorted for lysosomal processing (Otero et al., 2006). The removal and degradation of circulating chemokines and cytokines in the lysosomal compartment are essential to prevent an exaggerated immune response and uncontrolled recruitment of leukocytes.

Aberrant membrane trafficking has been linked to various human genetic disorders and immune dysfunction, which affect different steps of endosomal trafficking, such as vesicle fusion and fission events, cargo sorting, and vesicle transport along the cytoskeleton.

The adaptor protein complex 3 (AP-3) facilitates cargo shuttling from the TGN and endosomes. Mutations in *AP3B1* prevent proper assembly of the complex and cause Hermansky-Pudlak syndrome type 2 (HPS2). Affected individuals present with albinism, bleeding diathesis, impaired cytotoxic activity, and neutropenia (Jung et al., 2006; Hauck and Klein, 2013). Pearl mice harbor mutations in the β3A subunit of the AP-3 complex and are murine equivalents to human HPS2. The phenotypes of mice and humans partly overlap, since mice also display hypopigmentation, defective lysosomal secretion, and abnormal platelet-dense granules. However, pearl mutant mice do not show decreased neutrophil counts (Feng et al., 1999; Vallejo et al., 2013). Another rare disorder with defective intracellular trafficking is the Chediak-Higashi syndrome (CHS), which is caused by mutations in the lysosomal trafficking regulator (*LYST*) gene (Barbosa et al., 1996). Lyst controls lysosomal trafficking and biogenesis and its absence results in enlarged lysosomal vesicles and impaired phagolysosomal formation (Westphal et al., 2017). Patients are neutropenic and suffer from persistent and recurrent infections. Moreover, they present with partial albinism, bleeding tendency, and progressive neurological dysfunction (Kaplan et al., 2008; Dame et al., 2019). Mutant beige mice correspond to human CHS and their phenotypes resemble the disease in humans. Beige mice are characterized by enlarged vesicles resulting from defective vesicle fusion (Barbosa et al., 1996). In addition, beige mice show an increased susceptibility to infections, enhanced bleeding tendency, hypopigmentation, as well as decreased neutrophil chemotaxis and bactericidal activity (Gallin et al., 1974; Saxena et al., 1982; Nagle et al., 1996; Jackson, 1997). In contrast to humans, beige mice do not display neutropenia (Gallin et al., 1974). Like Lyst, the late endosomal/lysosomal adaptor and MAPK and mTOR activator 2 (LAMTOR2) protein is essential for the structural maintenance and function of the lysosomal compartment. Patients with loss-of-function mutations in *LAMTOR2* manifest with partial albinism, small stature and immune dysfunctions including neutropenia, reduced T cell-mediated cytotoxicity, and impaired B cell development (Bohn et al., 2007; Łyszkiewicz et al., 2019). LAMTOR2-deficient mice die early in embryonic development (Teis et al., 2006).

Since Rab proteins are crucial for the efficiency and specificity of vesicle fusion events, it is not surprising that dysfunctional Rab proteins lead to various human diseases. Rab27a is crucial for targeting and docking of exocytic vesicles to the PM and loss-of-

function mutations in the *RAB27A* gene cause Griscelli syndrome type 2 (GS2). Clinical manifestations of affected individuals include hypopigmentation, neurologic abnormalities, and immunodeficiency with periodic neutropenia and reduced NK cell as well as T cell cytotoxicity (van Gele et al., 2009; Ohbayashi et al., 2010; Meeths et al., 2010). Ashen mice have mutations in *Rab27a* and exhibit similar phenotypes as patients with GS2, including pigmentary dilution and impaired cytotoxic activity (Wilson et al., 2000; Stinchcombe et al., 2001; Haddad et al., 2001). Moreover, mutations in *RAB7* affect endolysosomal vesicle traffic and cause Charcot-Marie-Tooth disease type 2B neuropathy. Patients suffer from distal muscle weakness, sensory loss, and motor abnormalities (Cherry et al., 2013; BasuRay et al., 2013). Mice with a loss of Rab7 are embryonic lethal at an early stage of E7-8 (Kawamura et al., 2012).

Like Rab proteins, VPS proteins are crucial regulators of the endocytic pathway and mutations in distinct *VPS* genes are associated with various human diseases. VPS13 is localized at the Golgi apparatus, where it plays an important role in vesicle fusion and maintaining the morphology of the Golgi complex. Patients with loss-of-function mutations in *VPS13B* suffer from the Cohen syndrome, a disease characterized by a developmental delay, short stature, obesity, psychomotor retardation, and severe neutropenia (Kolehmainen et al., 2003; Schäffer and Klein, 2007). VPS13B deficiency causes motor deficits in mice and infertility in male mice. Apart from that, VPS13B-deficient mice do not show any apparent phenotypes (Kim et al., 2019; Da Costa et al., 2020). *VPS33B* is another *VPS* gene, which is implicated in a severe disease. VPS33B is described to promote endosome maturation in the degradation pathway and loss of *VPS33B* expression in macrophages of Drosophila results in excessive inflammatory responses upon microbial stimulation (Akbar et al., 2016). Mutations in the *VPS33B* gene cause arthrogryposis-renal dysfunction-cholestasis (ARC) syndrome in patients, a disorder with a poor prognosis and a high death rate in infancy. Patients further display a failure to thrive, ichthyosis, osteopenia, and kidney as well as liver dysfunctions (Zhou and Zhang, 2014; del Brío Castillo et al., 2019). Mice with a complete lack of VPS33B are early embryonic lethal (Perez-Garcia et al., 2018). In contrast, timed tamoxifen-induced knockout (KO) of *Vps33b* results in an increased platelet count and deficiency in α-granules in mice (Bem et al., 2015). The VPS protein VPS45 is a crucial regulator of vesicle trafficking through the endosomal compartment. Patients with pathogenic variants in *VPS45* are severely neutropenic and suffer from recurrent and life-threatening mutations. Moreover, they present with hepatomegaly, splenomegaly, thrombocytopenia, extramedullary hematopoiesis, and bone marrow fibrosis (Stepensky et al., 2013; Vilboux et al., 2013; Meerschaut et al., 2015; Shah et al., 2017). Rabenosyn-5 is a binding partner of VPS45 and patients with loss-of-function mutations in *RBSN* show a phenotypic overlap with VPS45-deficient patients, as they

present with severe neutropenia, extramedullary hematopoiesis, and bone marrow fibrosis (Magoulas et al., 2018). Rabenosyn-5-deficient mice are lethal at the preweaning stage (Phenotyping center, Wellcome Trust Sanger Institute). The generation and characterization of VPS45-deficient mouse models are described for the first time in this thesis.

These defects in membrane trafficking highlight the importance of proper endocytic trafficking. Importantly, they show that the slightest disturbances in membrane trafficking contribute to the pathogenesis of severe immunological disorders.

1.6 Human VPS45 deficiency

1.6.1 Neutrophil granulocytes

Neutrophil granulocytes are the predominant leukocytes in the peripheral blood, roughly accounting for 70% of all white blood cells. Every day more than 10^{11} neutrophils are generated in the bone marrow (Strydom and Rankin, 2013; Lahoz-Beneytez et al., 2016). During maturation in the bone marrow from myeloid lineage progenitor cells, neutrophils progress through five different stages, comprising myeloblasts, promyelocytes, metamyelocytes, band neutrophils, and segmented neutrophils. Once matured and released from the bone marrow to the blood, mature neutrophils lose their proliferative capacity and have a short life span of about 24 hours (Hidalgo et al., 2019). To exert defense against pathogens at extravascular sites of infection, neutrophils exit the blood circulation and enter tissues by adhesion and transmigration through the blood vessels. Important regulators of these processes comprise adhesion molecules, such as the L-selectin CD62 and integrins, including the lymphocyte function-associated antigen-1 (LFA-1) and Mac-1, chemokines, such as CXCL8 (IL-8), and cytokines, including TNF and IL-1 (Subramanian et al., 2016; Teng et al., 2017). Neutrophils are essential for the efficient defense against invading pathogens by carrying out various functions, such as the phagocytosis and phagolysosomal destruction of pathogens with the aid of reactive oxygen species (ROS) and proteolytic enzymes, such as cathepsin G, the release of cytotoxic granule compounds, neutrophil extracellular traps (NETs), as well as the production and secretion of chemokines and cytokines (Nguyen et al., 2017). A multitude of receptors are involved in the recognition of pathogens and activation of neutrophils, including opsonin receptors, such as Fc and C3 receptors, pattern recognition receptors, such as toll-like receptors (TLRs), and cytokine receptors, such as the G-CSFR and INFGR (Futosi et al., 2013).

Neutrophil granulocytes are readily packed with four distinct types of granule subsets, which can be immediately released to carry out various immune functions, such as the

destruction of pathogens, initiation of inflammatory responses, or wound healing. The four granule subtypes comprise azurophilic or primary granules, specific or secondary granules, gelatinase or tertiary granules, and granules, which are enriched in the microbial lectin ficolin-5. Azurophilic granules typically contain hydrolases, such as the neutrophil elastase or myeloperoxidase, whereas the specific granules have an increased abundance of the antibacterial protein lactoferrin. Gelatinase granules are characterized by the presence of matrix metalloproteinases. Besides, neutrophils contain secretory vesicles, which are markedly smaller in size and enriched in cytokines and transmembrane receptors (Subramanian et al., 2016; Teng et al., 2017; Lawrence et al., 2018). To date, the precise processes involved in the formation of the distinct granule subtypes and protein sorting in neutrophil granulocytes are largely unknown. It is under debate, whether protein sorting occurs in neutrophils at all (Lawrence et al., 2018). However, studies point towards an active biosynthetic pathway (1.2), as proteins involved in the transport of newly synthesized proteins are expressed in neutrophils, such as the proteoglycan serglycin and the multisubunit adaptor protein complexes AP-1, AP-3, and AP-4 (Lemansky et al., 2003; Niemann et al., 2007; Sheshachalam et al., 2014).

1.6.2 Severe congenital neutropenia (SCN)

SCN is a group of rare diseases with a prevalence of 3-8.5 cases per million individuals and a type of congenital neutropenia characterized by an absolute neutrophil count of less than 500 per microliter of peripheral blood (Donadieu et al., 2011; Skokowa et al., 2017). In comparison, the neutrophil count ranges from 500 to 1000 in individuals with moderate neutropenia and from 1000 to 1500 in individuals with mild neutropenia. In healthy individuals, the neutrophil count is considered to range from 1500 to 7500. Insufficient amounts of neutrophil granulocytes predispose the affected individuals to persistent and recurrent bacterial and fungal infections. In general, the risk of severe infections increases with decreasing neutrophil counts (Klein, 2011; Donadieu et al., 2011; Hauck and Klein, 2013).

Genetic defects underlying SCN

The majority of SCN subtypes show a halt in the maturation of neutrophil granulocytes at the promyelocyte stage in the bone marrow and an increased susceptibility of neutrophil precursors to undergo apoptosis. For instance, the functions of neutrophil granulocytes are hampered by an impaired cell adherence, defective migration, and inefficient killing of bacteria. Mechanistic defects include protein mistrafficking, dysregulation of mitochondrial homeostasis, aberrant actin polymerization, and impaired glycosylation. Overall, various intracellular pathways are affected and a multitude of monogenetic defects with different modes of inheritance are ascribed to the pathogenesis of

SCN, highlighting the heterogeneity of the disorder (Klein, 2011; Hauck and Klein, 2013).

Mutations in *ELANE* were identified as a cause for SCN (Horwitz et al., 1999; Dale et al., 2000). ELANE encodes the protein neutrophil elastase, which is a serine protease expressed in azurophilic granules of polymorphonuclear neutrophils during granulopoiesis. It is released in response to inflammation to exert various functions: the protein is, inter alia, responsible for the destruction of bacterial proteins and crucial for efficient host defense against invading pathogens (Belaaouaj, 2002). More than 100 distinct mutations, which are usually inherited in an autosomal dominant fashion, were found in the *ELANE* gene over time and they account for roughly 60% of all SCN cases (Germeshausen et al., 2013; Makaryan et al., 2015). Pathomechanisms underlying neutropenia-associated mutations include mislocalization and misfolding of the protein inducing an unfolded protein response in the ER, which results in a maturation arrest at the promyelocyte stage and an increased susceptibility of neutrophil progenitors to undergo apoptosis (Köllner et al., 2006; Grenda et al., 2007).

Historically, patients lacking mature neutrophil granulocytes were first described in 1950 by Rolf Kostmann (KOSTMANN, 1956). The underlying genetic defects causing the Kostmann syndrome were identified in 2007 when mutations were found in the HCLS1-associated protein X-1 (*HAX1*) gene (Melin et al., 2007; Klein et al., 2007). Thus, the Kostmann syndrome refers to a subform of SCN, in which patients carry mutations in *HAX1*. HAX1-deficient neutrophils are characterized by a maturation arrest at the promyelocyte stage and elevated levels of apoptosis. Studies suggest that HAX1 is crucial for mitochondrial homeostasis, as the protein is predominantly localized in mitochondria and biallelic variants in *HAX1* cause a disturbance of the inner mitochondrial membrane potential (Suzuki et al., 1997; Klein et al., 2007). Apart from its role in mitochondrial homeostasis, a multitude of functions are ascribed to HAX1, such as mRNA processing, protein transport between the nucleus and the cytoplasm, regulation of the cytoskeleton, and cell motility (Sarnowska et al., 2007; Burnicka-Turek et al., 2010; Cavnar et al., 2011; Grzybowska et al., 2013; Klein, 2017). To date, the exact function of the protein remains unclear.

Apart from *ELANE* and *HAX1*, biallelic loss-of-function mutations in *CSF3R* encoding the G-CSFR were identified to cause SCN (Triot et al., 2014; Klimiankou et al., 2015). The cytokine receptor is crucial for the survival, proliferation, and differentiation of neutrophil granulocytes. Analysis of the patient's bone marrow revealed a normal maturation of neutrophil granulocytes (Triot et al., 2014; Klimiankou et al., 2015). Cellular studies showed an aberrant glycosylation pattern of the G-CSFR. In addition, the mu-

tant receptor was retained in the ER and inefficiently targeted to the cell surface. Importantly, phosphorylation levels of STAT3 and STAT5 were reduced, demonstrating abrogated downstream signaling (Triot et al., 2014). These studies highlight the importance of proper trafficking and signaling of the G-CSFR for neutrophil homeostasis.

Further genes implicated in SCN include *G6PC3*, G*FI1*, *JAGN1*, *VPS45* and *WAS* (Devriendt et al., 2001; Person et al., 2003; Ancliff et al., 2006; Boztug et al., 2009; Boztug et al., 2014). The underlying genetic variants of large numbers of SCN patients remain unknown.

Treatment of SCN

The majority of SCN patients responds to the mainstay of treatment with recombinant human G-CSF (rhG-CSF), resulting in increased levels of neutrophil granulocytes in the blood circulation, reduced incidences of severe infections, and an overall improved quality of life. Some patients, however, are refractory to an even high-dose therapy with rhG-CSF, leaving hematopoietic stem cell transplantation as the only treatment option.

Patients with loss-of-function mutations in *CSF3R* do not respond to the treatment with rhG-CSF (Triot et al., 2014; Klimiankou et al., 2015). Moreover, all identified VPS45-deficient patients are refractory to the therapy with G-CSF, even in high doses (Stepensky et al., 2013; Vilboux et al., 2013; Meerschaut et al., 2015; Shah et al., 2017). Thus, hematopoietic stem cell transplantation is the only treatment option for these patients to date.

SCN patients generally harbor an increased risk to acquire somatic *CSF3R* mutations and to develop myelodysplastic syndrome (MDS) or acute myeloblastic leukemia (AML). These mutations cause a truncation of the G-CSFR resulting in an increased half-life of the mutant protein and prolonged downstream signaling, thus supporting the proliferation of these clones (Hermans et al., 1999; Liu et al., 2008; Hauck and Klein, 2013; Skokowa et al., 2017). It is still under debate which effect G-CSF therapy has on the progression of the diseases. Thus, a regular clinical monitoring is indispensable for all SCN patients.

1.6.3 Identification and function of the SM protein VPS45

Vacuolar protein sorting (*vps*) genes were first identified and characterized through the screening and characterization of genetically manipulated yeast, which exhibit aberrant sorting of vacuolar hydrolases, such as proteinase A, proteinase B, and carboxypepti-

dase Y (Rothman and Stevens, 1986; Bankaitis et al., 1986; Banta et al., 1988; Rothman et al., 1989). Overall, more than 40 *vps* genes have been found to mediate efficient sorting and targeting of vacuolar resident hydrolases, emphasizing the complexity of the vacuolar pathway. Based on their vacuolar structures, yeast *vps* deletion mutants are grouped into six different classes A-F (Raymond et al., 1992). Class A mutants have one to three vacuoles and do not show any morphological deviation from WT yeast. In contrast, class B mutants have a fragmented vacuole, and class C mutants lack any apparent vacuolar structures. Class D mutants contain a single, slightly enlarged vacuole and fail to inherit vacuoles to daughter cells. Class E mutants have a WT resembling vacuole in addition to novel prevacuolar compartments, and class F mutants possess a single normal-looking vacuole besides smaller fragmented vacuoles (Raymond et al., 1992).

Vps45p was identified in such a yeast genetic screen and its function was first studied in *vps45* null mutants, which are assigned to class D *vps* mutants (Raymond et al., 1992; Cowles et al., 1994). The evolutionary conserved Vps45p protein is about 64 kD and belongs to the SM family. The analysis of the *vps45* deletion allele revealed that Vps45p is crucial for the delivery of vacuolar enzymes to the vacuolar compartment (Piper et al., 1994; Cowles et al., 1994; Bryant and James, 2001). In addition, *vps45* mutants have longer doubling times and their growth is temperature-sensitive (Piper et al., 1994; Shanks et al., 2012). Moreover, loss of Vps45p causes an accumulation of vesicles, which form large clusters in proximity to the vacuole (Piper et al., 1994; Cowles et al., 1994). Subcellular fractionation studies showed that the Vps45p protein is likely associated with peripheral membranes of transport vesicles, endosomes, and the Golgi apparatus, suggesting a role in trafficking from the Golgi apparatus to endosomes (Piper et al., 1994; Cowles et al., 1994; Bryant and James, 2001). Furthermore, Vps45p directly interacts with the t-SNARE Tlg2p and the PI(3)P binding protein Vac1p, which are functional homologues of mammalian Syntaxin16 and Rabenosyn-5, respectively (Nichols et al., 1998; Peterson et al., 1999; Tall et al., 1999; Bryant and James, 2001). Notably, Vps45p impacts on the expression levels of Tlg2p, as loss of Vps45p results in reduced amounts of Tlg2p, whereas increased Vps45p expression results in an elevated Tlg2p abundance (Bryant and James, 2001; Shanks et al., 2012; Stepensky et al., 2013).

A role in endocytic membrane trafficking is ascribed to VPS45 in Drosophila and *C. elegans* (Gengyo-Ando et al., 2007; Morrison et al., 2008). Deletion of VPS45 affects cargo internalization and causes an accumulation of small endosomal vesicles in both organisms, which is in line with results obtained in yeast and suggests a role of Vps45 in the formation of endosomes (Cowles et al., 1994; Piper et al., 1994; Gengyo-Ando et al., 2007; Morrison et al., 2008). Additionally, VPS45 is essential for the development

of Drosophila, as inactivation of Vps45 results in early lethality at larval stages (Morrison et al., 2008). Moreover, temperature sensitivity was observed in the absence of VPS-45 in *C. elegans* strains, resulting in a developmental arrest and lethality (Gengyo-Ando et al., 2007).

Studies of the mammalian homologue of Vps45p showed that the protein is ubiquitously expressed with the highest expression in rat brain, testis, and kidney (Bock et al., 1997; El-Husseini et al., 1997; Tellam et al., 1997). In line with results obtained in yeast studies, fractionation and immunofluorescence analyses revealed an association of mammalian VPS45 with endosomal membranes and the Golgi apparatus (Bock et al., 1997; Tellam et al., 1997). Moreover, mammalian VPS45 directly binds to Syntaxin16 and Rabenosyn-5 (Nielsen et al., 2000; Dulubova et al., 2002), which is in agreement with previous studies performed in yeast. These interactions seem to be conserved throughout eukaryotic evolution, as VPS45 binds to Rabenosyn-5 and Syntaxin16 in Drosophila and *C. elegans*, respectively (Gengyo-Ando et al., 2007; Morrison et al., 2008). In addition, mammalian VPS45 stabilizes the protein levels of its binding partners, since the downregulation of VPS45 expression results in reduced levels of Rabenosyn-5 and Syntaxin16 (Rahajeng et al., 2010; Vilboux et al., 2013). In human cells, VPS45 was further described to play a role in the recycling of β1 integrins as well as cell migration (Rahajeng et al., 2010).

1.6.4 Human VPS45 deficiency is associated with SCN

Since 2013, *VPS45* is known as a gene implicated in the pathogenesis of SCN (Vilboux et al., 2013; Stepensky et al., 2013). Two distinct biallelic mutations, p.Thr224Asn (exon 7) and p.Glu238Lys (exon 8), have been identified in children of eight families with severe and recurrent infections. Clinically, the affected individuals presented with a poor weight gain, bone marrow fibrosis, nephromegaly, hepatomegaly, splenomegaly, thrombocytopenia, and extramedullary hematopoiesis. Patients carrying the p.Glu238Lys mutation additionally had neurological defects, including a delay in development and hearing loss.

Blood analysis of patients carrying the p.Thr224Asn mutation revealed the presence of immature forms of neutrophil granulocytes (Vilboux et al., 2013). Furthermore, peripheral blood cells, fibroblasts, and a lymphoblastic cell line derived from these patients showed markedly reduced levels of the VPS45 protein (Stepensky et al., 2013; Vilboux et al., 2013). Besides, a decreased expression of its known interaction partners Rabenosyn-5 and Syntaxin16 was observed in patient fibroblasts (Vilboux et al., 2013). Moreover, the p.Thr22Asn mutation seemed to affect the intracellular localization of

the VPS45 protein. Whereas control cells showed a perinuclear staining, patient neutrophils and fibroblasts revealed a diffuse distribution throughout the cytoplasm. Patient cells carrying the p.Thr224Asn mutation further had a reduced cell surface expression of β1 integrin, reduced migration capacity, impaired superoxide production, and aberrant chemotaxis. A decreased capacity to migrate towards a scratch introduced in a wound-healing assay was also observed for fibroblasts carrying the p.Glu238Lys mutation (Vilboux et al., 2013). P.Thr224Asn-mutated patient platelets contained fewer α granules and fibroblasts were negative for the staining with LysoTracker (Stepensky et al., 2013). In general, an increased susceptibility to undergo apoptosis was observed in patient bone marrow cells and neutrophils (Vilboux et al., 2013; Stepensky et al., 2013).

In 2015, the same p.Glu238Lys biallelic mutation described by Vilboux et al. (Vilboux et al., 2013) was found in a child with SCN and similar clinical manifestations, including bone marrow fibrosis, anemia, and thrombocytopenia (Meerschaut et al., 2015). Notably, this patient also showed neurologic abnormalities, which have been described for patients with the p.Glu238Lys mutation before. No neurological manifestations were observed for patients carrying biallelic p.Thr224Asn mutations, suggestive of a phenotype-genotype correlation (Meerschaut et al., 2015).

In 2017, a distinct biallelic mutation, p.Pro468Leu, was found in *VPS45* in a newborn with SCN (Shah et al., 2017). The patient had similar clinical manifestations, comprising bone marrow fibrosis, thrombocytopenia, and extramedullary hematopoiesis. Peripheral blood analysis revealed a maturation of neutrophil granulocytes up to the band form. In contrast to patients described by Stepensky et al. (Stepensky et al., 2013), the patient carrying the p.Pro468Leu mutation did not have a lack of α granules in platelets. However, the affected child had neurological defects and a delay in development, which had been observed for patients with the p.Glu238Lys mutation.

All above-mentioned VPS45-deficient patients were refractory to the therapy with G-CSF, even in high doses (Vilboux et al. 2013a; Stepensky et al. 2013; Shah et al. 2017; Meerschaut et al. 2015). To date, hematopoietic stem cell transplantation is the only treatment option for such patients.

Of note, all distinct mutated VPS45 residues comprising threonine 224, glutamate 238, and proline 468 are highly conserved throughout evolution (Stepensky et al., 2013; Vilboux et al., 2013; Shah et al., 2017). Previous computational analysis proposed an instability and aberrant functions of both p.Thr224Asn and p.Glu238Lys mutants (Vilboux et al., 2013). Further structural three-dimensional modeling of the protein showed that the three known VPS45 mutations are close to each other in a hinge region, which

presumably is crucial for the binding of SNARE proteins. Thus, the mutants likely share structural and functional defects (Shah et al., 2017).

Notably, homozygous mutations in *RBSN*, encoding the VPS45 binding protein Rabenosyn-5, have been identified in three siblings with SCN (Magoulas et al., 2018). Clinical manifestations resembled those of VPS45 deficiencies and included anemia, thrombocytopenia, myelofibrosis, hepatomegaly, splenomegaly, and extramedullary hematopoiesis. Moreover, patients had a developmental delay and showed a severe intellectual disability. Analysis of bone marrow cells did not reveal a maturation arrest of neutrophil granulocytes. Two of the siblings did not respond to G-CSF therapy, whereas one sibling showed a transient response (Magoulas et al., 2018).

2 Aims of the thesis

To date, little is known about the biology of VPS45 in the contexts of the immune system and neutropenia. The protein has been implicated in intracellular membrane trafficking through the endosomal system, yet the precise function of VPS45 in vesicle transport remains unknown. In humans, VPS45 deficiency is associated with SCN and such patients are susceptible to persistent, life-threatening bacterial infections. Mutations in *VPS45* severely affect the function of neutrophil granulocytes and result in a lack of response to the standard therapy with G-CSF, thus limiting curative options of affected patients (Stepensky et al., 2013; Vilboux et al., 2013; Meerschaut et al., 2015; Shah et al., 2017).

VPS45 is a member of the SM protein family, which is involved in intracellular vesicle fusion events. Moreover, previous studies in distinct model organisms showed that VPS45 interacts with Rabenosyn-5, which is an early endosomal protein and Rab5 effector (Peterson et al., 1999; Nielsen et al., 2000; Gengyo-Ando et al., 2007; Morrison et al., 2008). In addition, depletion of VPS45 affects the recycling of receptors (Rahajeng et al., 2010; Vilboux et al., 2013). Based on these findings, it was hypothesized that VPS45 plays a role in the fusion of early endosomes.

The overall goal of this thesis was to unravel the molecular mechanisms underlying VPS45 deficiencies. To achieve this goal, the following specific aims were pursued.

The first aim was to get insights into VPS45-driven vesicle fusion processes. In particular, *in vitro* human cell lines were utilized to reveal the roles of VPS45 in endocytosis, recycling, and degradation pathways.

Patients are refractory to the therapy with G-CSF. Upon ligand binding, the G-CSFR is internalized and follows the endocytic route. Thus, the second aim was to analyze whether VPS45 deficiency has a direct impact on the trafficking and signaling of the G-CSFR.

The third aim was to investigate the effects of disease-related mutations on the function of the VPS45 protein. Patient-associated mutations result in a reduced abundance of the VPS45 protein (Vilboux et al., 2013). However, it is unclear, whether those mutations also affect the function of VPS45.

All previously identified patient-associated mutations result in decreased amounts of VPS45 but leave the basic function of the protein possibly intact. Thus, it is plausible that a homozygous KO is not compatible with life. Therefore, the fourth aim was to verify the impact of VPS45 deficiency on mammals by generating and characterizing a mouse model with a complete KO of *VPS45*.

As the main manifestation of VPS45 deficiency in humans is severe neutropenia, the fifth aim was to study the role of VPS45 in the context of neutrophil granulocytes. To this end, conditional mouse models with a tissue-specific lack of VPS45 in the myeloid and the hematopoietic compartments were generated and characterized.

3 Materials and methods

3.1 Molecular biology

3.1.1 Polymerase chain reaction (PCR)

The DNA for the generation of expression vectors was amplified using the Q5 high-fidelity DNA Polymerase (New England BioLabs). The standard PCR reaction setup and thermocycling conditions for cloning are shown in Table 3-1 and Table 3-2.

Table 3-1: Standard PCR reaction setup used for cloning.

Component	25µl reaction volume
5x Q5 reaction buffer	5 µl
10 mM dNTPs	0.5 µl
10 µM forward primer	1.25 µl
10 µM reverse primer	1.25 µl
Template DNA	30 ng
Q5 high-fidelity DNA polymerase	0.25 µl
5x Q5 high GC enhancer	5 µl
Nuclease-free water	to 25 µl

Table 3-2: Standard PCR thermocycling conditions used for cloning.

Step	Temperature	Time
Initial denaturation	95 °C	30 seconds
35 cycles	95 °C	5 seconds
	*50-72 °C	10 seconds
	72 °C	30 seconds/kb
Final extension	72 °C	10 minutes
Hold	4 °C	Forever

*The cycling conditions, including annealing temperature and extension time, were adjusted to different primers and templates.

3.1.2 Site-directed mutagenesis

VPS45 mutations were introduced by standard PCR mutagenesis using the respective *VPS45*^{WT} plasmids as templates. The Q5 high-fidelity DNA Polymerase (New England BioLabs) and oligonucleotides containing the *VPS45* mutations were used to synthe-

size mutant strands. The PCR product was treated with the DpnI endonuclease to digest the parental DNA template and was transformed into competent *E. coli* (DH5α, New England BioLabs). Primers used for mutagenesis are listed in Table 3-6.

3.1.3 Plasmids

All plasmids used in this study are shown in Table 3-3.

Table 3-3: Plasmids used in this study.

Name	Backbone	Tag	Antibiotic	Reference
pCMV6-AC-GFP-VPS45	pCMV6-AC-GFP	TurboGFP (C-terminal)	Ampicilin	OriGene (RG206027, NM_007259)
pRRL.cPPT.SF	pRRL	-	Ampicilin	(Schambach et al., 2006)
pRRL-VPS45WT-GFP	pRRL	TurboGFP (C-terminal)	Ampicilin	This thesis
pRRL-VPS45Thr224Asn-GFP	pRRL	TurboGFP (C-terminal)	Ampicilin	This thesis
pRRL-VPS45Glu238Lys-GFP	pRRL	TurboGFP (C-terminal)	Ampicilin	This thesis
pRRL-VPS45WT-FLAG-IRES-GFP	pRRL	FLAG-IRES-TurboGFP (C-terminal)	Ampicilin	This thesis
pRRL-VPS45Thr224Asn-FLAG-IRES-GFP	pRRL	FLAG-IRES-TurboGFP (C-terminal)	Ampicilin	This thesis
pRRL-VPS45Glu238Lys-FLAG-IRES-GFP	pRRL	FLAG-IRES-TurboGFP (C-terminal)	Ampicilin	This thesis
pRRL-VPS45WT-IRES-RFP	pRRL	IRES-RFP (C-terminal)	Ampicilin	This thesis
pRRL-VPS45WT-IRES-RFP	pRRL	IRES-RFP (C-terminal)	Ampicilin	This thesis
pRRL-VPS45WT-IRES-RFP	pRRL	IRES-RFP (C-terminal)	Ampicilin	This thesis
pRRL-mCherry-Rab5	pRRL	mCherry (N-terminal)	Ampicillin	This thesis

pRRL-mCerulean-Rab7	pRRL	mCerulean (N-terminal)	Ampicillin	This thesis
pRRL-mCerulean-Rab4	pRRL	mCerulean (N-terminal)	Ampicilin	This thesis
pRRL-mCerulean-Rab11	pRRL	mCerulean (N-terminal)	Ampicilin	This thesis
mCherry-Rab5	mCh-alpha tubulin (Addgene 49149)	mCherry (N-terminal)	Kanamycin	Addgene (49201)
mCherry-Rab7a	pAcGFP1-C1	mCherry (N-terminal)	Kanamycin	Addgene (61804)
mCerulean3-Rab4a-7	mCerulean3	mCerulean3 (N-terminal)	Kanamycin	Addgene (55443)
mCerulean-Rab11a-7	mCerulean	mCerulean (N-terminal)	Kanamycin	Addgene (55390)
pMMP-G-CSFR-eGFP	pMMP	eGFP (C-terminal)	Ampicilin	(Triot et al., 2014)
pCAG-Cre-IRES2-GFP	pCAG	IRES2-GFP (C-terminal)	Ampicilin	Addgene (26646)
MIGR1-Cre-IRES2-GFP	MSCV	IRES2-GFP (C-terminal)	Ampicilin	This thesis
MIGR1-IRES-GFP	MSCV	IRES-GFP (C-terminal)	Ampicilin	Provided by Prof. A. Krueger (Goethe Universität, Frankfurt am Main)
pCL-Eco	CMV-LXSN	-	Ampicilin	Provided by Prof. A. Krueger (Goethe Universität, Frankfurt am Main)
pSpCas9(BB)-2A-GFP	PX458	GFP (C-terminal)	Ampicilin	Addgene (48138)
pcDNA3.GP.4xCTE	pcDNA3	-	Ampicilin	(Dull et al., 1998)
pRSV-Rev	pRSV-Rev	-	Ampicilin	Addgene (12253)
pMD2.G	pMD2.G	-	Ampicilin	Addgene (12259)

3.1.4 Oligonucleotides

Oligonucleotides used for cloning are listed in Table 3-4.

Table 3-4: Oligonucleotides used for cloning.

Name	Sequence (5‘-3‘)
Cre-IRES2-GFP_F	GAATTCGAATTCGCCACCATGGGCCCAAAGAAGAAGAG
Cre-IRES2-GFP_R	GTCGACGTCGACTTACTTGTACAGCTCGTCCAT
NheIAgeIVPS45_F	GCTAGCACCGGTGCCACCATGAACGTGGT
SpeISalIVPS45_R	GTCAGCACTAGTTTAAACTCTTTCTTCACCGGC
VPS45StopMluI_R	ACGCGTACGCGTTTTATCTTCTGCTCGCTGACCTT
AgeIVPS45_F	ACCGGTACCGGTGCCACCATGAACGTGGTTTTTGCTGTGAA-GCAGTACATTTCC
VPS45CFLAGStopMluI_R	ACGCGTACGCGTCTACTTGTCGTCATCGTCTTTGTAG-TCTCTTCTGCTCGCTGA
mCherry-Rab5AgeI_F	GCACCGGTTCAGATCCGCTAGCATGGTG
mCherry-Rab5MluI_R	GAACGCGTCCGCGGTACCTCAGTTGCTA
mCherry-Rab7AgeI_F	GCACCGGTTACCGGTCGCCACCATGGTG
mCherry-Rab7MluI_R	GAACGCGTCGGTGGATCCCGGGCCCGCG
mCeruleanAgeI_F	GCACCGGTTACCGGTCGCCACCATGGTGAGCAAG
mCeruleanRab4MluI_R	GAACGCGTGATCCGGTGGATCCCTAACAAC
mCeruleanRab11MluI_R	GAACGCGTCTGATTATGATCAGTTATCTA
Cre-IRES2-GFP_F	GAATTCGAATTCGCCACCATGGGCCCAAAGAAGAAGAG
Cre-IRES2-GFP_R	GTCGACGTCGACTTACTTGTACAGCTCGTCCAT

Oligonucleotides used for sequencing are shown in Table 3-5.

Table 3-5: Oligonucleotides used for sequencing.

Name	Sequence (5‘-3‘)
pRRL_F	GCTTCTGCTTCCCGAGCTCTA
pRRL_R	TACGCTATGTGGATACGCTGC
pRRL_IRES_R	GCCTTATTCCAAGCGGCTTC
VPS45CtermSeq_F	CGAAGCAAGGAGAGCTCTCA
VPS45CtermSeq_R	TGAGAGCTCTCCTTGCTTCG
mCherry_F	CCCCGTAATGCAGAAGAAGA
CMV_F	CGCAAATGGGCGGTAGGCGTG
Rab5_7_F	TTGCCAAAGAGTGAACCCCAGAAT
Rab5_7_R	GAGGTGTGGGAGGTTTTTTAAAGCAAGTA
MIGR1seq_F	ATCCTCCCTTTATCCAGCCCTCA
MIGR1seq_R	CCCCCCTTTTTCTGGAGACTA

Oligonucleotides used for site-directed mutagenesis are listed in Table 3-6.

Table 3-6: Oligonucleotides used for site-directed mutagenesis.

Name	Sequence (5‘-3‘)
VPS45Thr224Asn_F	GATGCCATCAACCCATTGCTA
VPS45Thr224Asn_R	TAGCAATGGGTTGATGGCATC
VPS45Glu238Lys_F	CATGGTCCACAAACTACTAGG
VPS45Glu238Lys_R	CCTAGTAGTTTGTGGACCATG

Oligonucleotides used for qRT-PCR are listed in Table 3-7.

Table 3-7: Oligonucleotides used for qRT-PCR.

Name	Sequence (5‘-3‘)
mVps45_F	TTGGTCAGTGAGCGGAATCT
mVps45_R	CGGATTCTGCAGGAGTCTCT
mActin_F	CATTGCTGACAGGATGCAGAAGG
mActin_R	TGCTGGAAGGTGGACAGTGAGG

3.1.5 Agarose gel electrophoresis

Agarose gels were prepared by heating 1% (w/v) agarose in 100 ml of TBE buffer (90 mM Tris, 90 mM boric acid and 2 mM EDTA) and supplementing with 0.2% ethidium bromide solution. DNA samples were mixed with 6x loading dye (30% (v/v glycerol, 0.01% (w/v) bromophenol blue) prior to loading the samples on the gel in a wide Mini-Sub cell GT cell (Bio-Rad). 10 µl of mid-range DNA ladder (Jena Bioscience) was loaded as a reference. The gels were visualized using the ChemiDoc XRS+ system (Bio-Rad).

3.1.6 Recovery of DNA from agarose gels

PCR products were purified from agarose gels using the Zymoclean Gel DNA Recovery kit (Zymo Research) according to the manufacturer’s instructions.

3.1.7 Restriction enzyme digestion

Purified PCR products or plasmids were digested with fast digest restriction enzymes (Thermo Fisher Scientific) for 1 hour at 37 °C according to manufacturer’s manuals. Plasmids were treated with 1 U/ml alkaline phosphatase (Thermo Scientific) to prevent re-ligation of the vector. DNA restriction fragments were purified from agarose gels.

3.1.8 Ligation

Ligation reactions were set up in a molar ratio of 1:3 vector:insert using the T4 DNA Ligase (New England BioLabs) for 2 hours at room temperature or overnight at 16 °C according to the manufacturer's instructions. Following, 10 µl of the ligation mix was used for bacterial transformation.

3.1.9 Transformation of chemically competent *E. coli*

Competent *E. coli* (DH5α, New England BioLabs) were transformed by heat shock. 25 µl of bacteria was mixed with either 30 ng of plasmid DNA or 10µl of ligation reaction and kept on ice for 20 minutes. Bacteria were transformed by heat shock for 45 seconds at 42 °C on a ThermoMixer (Eppendorf), recovered on ice for 2 minutes, and incubated in 1 ml of LB medium for 1 hour at 37 °C. Following incubation, bacteria were pelleted for 1 minute at 21,130 x g at room temperature, resuspended in 100 µl of LB medium, streaked on LB plates containing appropriate antibiotics (100 µg/ml Ampicilin or 50 µg/ml Kanamycin), and kept for 12-18 hours at 37 °C to form colonies. Single bacterial colonies were picked to inoculate 3 ml of LB medium containing appropriate antibiotics. After 12 to18 hours of incubation, bacteria were pelleted for 10 minutes at 21,130 x g at room temperature and plasmid DNA was isolated using the Zyppy Plasmid Miniprep Kit according to the manufacturer's manual. Larger quantities of DNA were obtained by inoculating 100 ml LB medium containing appropriate antibiotics with glycerol stocks. Glycerol stocks were prepared by mixing 500 µl of glycerol (Sigma-Aldrich) and 500 µl of bacterial culture.

3.1.10 Isolation of plasmid DNA

Plasmid DNA was purified using the Zyppy Plasmid Miniprep Kit or the Qiagen Plasmid Maxi Kit according to the manufacturer's manuals. Primers used for sequencing are indicated in Table 3-5.

3.1.11 Cloning of expression vectors

All expression vectors cloned in this study were verified by sequencing (Table 3-4) and are listed in Table 3-3.

VPS45 and Rab gene constructs were cloned into the 3rd generation lentiviral backbone pRRL.cPPT.SF (Schambach et al., 2006; Warlich et al., 2011). The multiple cloning site of this backbone was modified by a colleague, Benjamin Marquardt, to provide additional restriction sites (5' to 3': BamHI, AgeI, SpeI, MluI, BsiWI, ApaI, NdeI, NsiI, and SalI).

The Cre sequence was cloned into the retroviral MigR1 backbone (Pear et al., 1998).

pRRL-VPS45-GFP

Human VPS45^{WT} was amplified from the pCMV6-AC-GFP plasmid obtained from Origene (Table 3-3) using the NheIAgeIVPS45_F and SpeISalIVPS45_R primers (Table 3-4) to introduce 5' NheI and AgeI restriction sites followed by the Kozak sequence (GCCACC) and 3' SpeI and SalI restriction sites. The amplified fragment and the empty pRRL backbone were digested using AgeI and SpeI restriction enzymes and ligated as described in 3.1.8. The patient mutations Thr224Asn and Glu238Lys were introduced by site-directed mutagenesis as described in 3.1.2.

pRRL-VPS45-IRES-RFP

Human VPS45 was amplified from WT and mutant pRRL-VPS45-GFP plasmids (Table 3-3) using the NheIAgeIVPS45_F and VPS45StopMluI_R primers (Table 3-4) to introduce 5' NheI and AgeI restriction sites followed by the Kozak sequence (GCCACC), 3' MluI restriction sites, and a stop codon at the end of the open reading frame. The amplified fragments and the empty pRRL backbone were digested using AgeI and MluI restriction enzymes and ligated as described in 3.1.8. The newly generated vector was linearized using SalI restriction enzyme and SalI-digested IRES-RFP was inserted as described in 3.1.8.

pRRL-VPS45-FLAG-IRES-GFP

Human VPS45 was amplified from WT and mutant pRRL-VPS45-GFP plasmids (Table 3-3) using the AgeIVPS45_F and VPS45CFLAGStopMluI_R primers (Table 3-4) to introduce a 5' AgeI restriction site followed by the Kozak sequence (GCCACC) and a 3' MluI restriction site. The AgeI- and MluI-digested WT or mutant fragments were ligated with the backbone of the AgeI- and MluI-digested pRRL-VPS45-IRES-RFP plasmid as described in 3.1.8.

pRRL-mCherry-Rab5

MCherry-Rab5 was amplified from the mCherry-Rab5 plasmid obtained from Addgene (49201, Table 3-3) using the mCherry-Rab5AgeI_F and mCherry-Rab5MluI_R primers (Table 3-4) to introduce 5' AgeI and 3' MluI restriction sites. The AgeI- and MluI-digested fragment and the AgeI- and MluI-digested backbone of the pRRL-VPS45-GFP plasmid were ligated as described in 3.1.8.

pRRL-mCerulean-Rab7

Rab7 was cut from the mCherry-Rab7 plasmid obtained from Addgene (61804, Table 3-3) using XhoI and BamHI restriction enzymes. Rab4 was removed from the mCerulean-Rab4 plasmid obtained from Addgene (55443) using XhoI and BamHI restriction

enzymes and replaced by Rab7, which was ligated as described in 3.1.8. MCerulean-Rab7 was extracted by digestion with AgeI and SpeI restriction enzymes and ligated into the AgeI- and SpeI-digested empty pRRL backbone.

pRRL-mCerulean-Rab4

MCerulean-Rab4 was amplified from the mCerulean-Rab4 plasmid obtained from Addgene (55443, Table 3-3) using the mCeruleanAgeI_F and mCeruleanRab4MluI_R primers (Table 3-4) to introduce 5' AgeI and 3' MluI restriction sites. The AgeI- and MluI-digested fragment were ligated with the AgeI- and MluI-digested backbone of the pRRL-VPS45-GFP plasmid as described in 3.1.8.

pRRL-mCerulean-Rab11

MCerulean-Rab11 was amplified from the mCerulean-Rab11 plasmid obtained from Addgene (55390, Table 3-3) using the mCeruleanAgeI_F and mCeruleanRab11MluI_R primers (Table 3-4) to introduce 5' AgeI and 3' MluI restriction sites. The AgeI- and MluI-digested fragment and the backbone of the AgeI- and MluI-digested pRRL-VPS45-GFP plasmid were ligated as described in 3.1.8.

MIGR1-Cre-IRES2-GFP

Cre-IRES2-GFP was amplified from the pCAG-Cre-IRES2-GFP plasmid obtained from Addgene (26646, Table 3-3) using the Cre-IRES2-GFP_F and Cre-IRES2-GFP_R primers (Table 3-4) to introduce EcoRI and SalI restriction sites. The EcoRI- and SalI-digested fragments were ligated with the EcoRI- and SalI-digested backbone of the MIGR1-IRES-GFP plasmid as described in 3.1.8.

3.1.12 Quantitative real-time PCR

Total RNA was extracted from cells using the RNeasy Mini Kit (Qiagen) according to the manufacturer's protocol. CDNA was synthesized from total RNA using the High Capacity cDNA Reverse Transcription Kit (Applied Biosystems) according to the manufacturer's instructions. Quantitative real-time PCR was carried out with the StepOne System (Applied Biosystems) using the SYBR Select Master Mix (Applied Biosystems). MRNA was normalized to the expression of a housekeeping gene and the data was analyzed by the comparative cycle threshold (CT) method. The primers were designed using the online tools Primer3 and BLAST (National Center for Biotechnology Information, NCBI) and are listed in Table 3-7.

3.2 Cell biology

3.2.1 Cell culture

All cell lines were maintained in incubators with 5% (v/v) CO_2 at 37 °C and passaged at 70%-80% confluency. Adherent cells were detached using Trypsin-EDTA (Gibco).

Adherent cell lines used in this study comprised the human cervical cancer cell line HeLa, the human embryonic kidney 293 cell line containing the SV40 T-antigen (HEK293T), the 293-derived retroviral packaging cell line (293GPG), and the murine bone-marrow-derived stromal cell line OP9. HeLa, HEK293T, and 293GPG cells were grown in Dulbecco's modified Eagle medium (DMEM; Gibco) supplemented with 10% (v/v) fetal bovine serum (FBS; Gibco), 2 mM L-glutamine (Gibco), 1% (v/v) Penicillin-Streptomycin (10000 U/ml; Gibco), and 20 mM HEPES (Gibco). The growth medium of 293GPG cells was additionally supplemented with 1 µg/ml tetracycline (Sigma Aldrich), 2 µg/ml puromycin (Sigma-Aldrich), and 0.3 mg/ml G418 (Sigma-Aldrich). OP9 cells were maintained in Minimum Essential Medium α (MEMα with L-glutamine, without ribonucleosides and deoxyribonucleosides, Gibco) and supplemented with 10% (v/v) FBS, 1% (v/v) Penicillin-Streptomycin (10000 U/ml; Gibco), and 20 mM HEPES (Gibco).

PLB-985 is a suspension cell line that was established from a patient with acute myeloid leukemia. The cells were cultured in Roswell Park Memorial Institute 1640 Medium (RPMI 1640, GlutaMax Supplement; Gibco) supplemented with 10% (v/v) FBS (Gibco), 1% (v/v) Penicillin-Streptomycin (10000 U/ml; Gibco), and 20 mM HEPES (Gibco).

All cell lines were regularly tested for mycoplasma using the PlasmoTest (InvivoGen) and were confirmed to be mycoplasma-negative throughout this work.

3.2.2 Cryopreservation of cells

Cells were washed with phosphate-buffered saline (PBS, Gibco) and centrifuged at 300 x g for 5 minutes at 4 °C. The pellet was resuspended in 1 ml freezing medium (10% DMSO (v/v) in FBS), transferred to cryogenic storage tubes (Greiner Bio-One), and stored in Mr. Frosty Freezing Containers (Thermo Fisher Scientific) at -80 °C until permanent storage in a liquid nitrogen tank.

3.2.3 Transfection of adherent cell lines

All transfections were carried out using polyethylenimine (PEI) in a 1:2 ratio of total DNA (µg) and PEI (µg) in the cell culture medium. The PEI solution was added to the

DNA solution and vortexed. The DNA/PEI mix was incubated for 20 minutes at room temperature to enable the formation of transfection complexes and added dropwise to the cells. The culture medium was replaced after 18 hours of incubation at 37 °C and the expression was monitored after 24-48 hours by fluorescent microscopy.

3.2.4 Production of lentiviral and retroviral particles

Lentiviral particles were produced by transfection of HEK293T cells, which were grown to a confluency of 70% in 10 cm tissue culture dishes. Prior to transfection, the growth medium was replaced by 10 ml of complete DMEM containing 25 µM chloroquine (Sigma-Aldrich). The transfection solution for one dish was prepared by mixing 15 µg of the lentiviral vector of interest, 10 µg of pcDNA3.GPx4xCTE (expressing HIV-1 Gag-Pol), 5 µg of pRSV-REV, 2 µg of pMD.G (expressing VSV-G), and 73.5 µl of 2.5 M $CaCl_2$ (Sigma-Aldrich) in up to 600 µl of low TE buffer (1 mM Tris-HCl pH 7.5, 0.05 mM EDTA pH 8). The DNA mix was added dropwise to 600 µl of 2x HBS (Gibco) while bubbling with a 2 ml serological pipette (Sarstedt). The transfection mix was incubated for 30 minutes at room temperature and added dropwise to the cells. After 16 hours the culture medium was changed and the supernatant containing viral particles was collected 48 hours and 72 hours post-transfection, respectively. Viral particles were filtered through a 0.22 µm polyvinylidene difluoride PVDF membrane (Millipore) and aliquots were stored at -80 °C.

Retroviral particles encoding Cre-IRES2-GFP were produced by cotransfecting HEKT293T cells with the retroviral MIGR1 plasmid containing Cre-IRES2-GFP and the pCL-Eco packaging plasmid as described above.

Retroviral particles encoding the G-CSFR-GFP fusion protein were generated by transfection of human-derived packaging 293GPG cells, which were grown in 10 cm tissue culture dishes to a confluency of 70% prior to transfection. The transfection solution for one dish was prepared by mixing 12.5 µg of the retroviral vector of interest and 73.5 µl of 2.5 M $CaCl_2$ (Sigma-Aldrich) in up to 600 µl of low TE buffer (1 mM Tris-HCl pH 7.5, 0.05 mM EDTA pH 8). The DNA mix was added dropwise to 600 µl of 2x HBS (Gibco) while bubbling with a 2 ml serological pipette (Sarstedt). The transfection mix was incubated for 30 minutes at room temperature and added dropwise to the cells. After 16 hours the growth medium was replaced by 10 ml of tetracycline-free DMEM (Gibco) containing 10% (v/v) fetal bovine serum (FBS; Gibco), 2 mM L-glutamine (Gibco), 1% (v/v) Penicillin-Streptomycin (10000 U/ml; Gibco), and 20 mM HEPES (Gibco) to initiate the production of virus particles. The supernatant was collected 24 hours, 48 hours, and 72 hours post-transfection, respectively, and filtered through a 0.22 µm PVDF

membrane (Millipore). Aliquots were stored at -80°C after ultracentrifugation (Optima L-80 XP, SW 41 Ti rotor, Beckman Coulter) for 2.5 hours at 20.000 rpm at 4°C.

3.2.5 Transduction

Prior to transduction, the culture medium was replaced by fresh growth medium containing 10 µg/ml polybrene (Sigma-Aldrich). Cells were transduced with viral particles ranging in ratios from 1:5 to 1:100. The growth medium was replaced the following day and gene expression was monitored after 72 hours.

3.2.6 Western blot

Cells were collected in ice-cold PBS and centrifuged for 3 minutes at 300 x g at 4 °C Cell pellets were lysed in cold lysis buffer (Cell Signaling) supplemented with proteinase inhibitor cocktail (PIC, Sigma-Aldrich) and phenylmethanesulfonylfluoride (PMSF, Alpha Diagnostic International) for 30 minutes on ice. Cell lysates were centrifuged for 15 minutes at 21,130 x g at 4 °C to remove insoluble matter and supernatants were collected. Protein concentrations were determined in a Bradford assay (Roti-Quant, Carl Roth) using a Synergy H1 microplate reader. Equal amounts of proteins were boiled with Laemmli buffer (750 mM Tris pH 6.8, 6% (w/v) sodium dodecylsulfate (SDS), 25% (v/v) glycerol, 0.05% (w/v) bromophenol blue) for 10 minutes at 95 °C. Samples and a pre-stained protein marker (Jena Bioscience) were resolved using polyacrylamide gels (Table 3-8) and transferred on a PVDF membrane (Amersham Hybond P 0.45, GE Healthcare) using the Mini Trans-Blot Electrophoretic Transfer Cell system (Bio-Rad) according to the manufacturer's instructions. Membranes were blocked in either 5% low-fat milk (Carl Roth) in PBS or 5% bovine serum albumin (BSA, Applichem) in PBS for 1 hour at room temperature. Primary antibodies were diluted in either 5% low-fat milk in PBS or 5% BSA (Table 3-9) in PBS and incubated overnight at 4 °C. Following three washes with PBS containing 0.1% Tween (PBS-T, Sigma-Aldrich) for 10 minutes each, membranes were incubated with secondary antibodies coupled to horseradish peroxidase (Table 3-10) diluted in either 5% low-fat milk in PBS or 5% BSA in PBS for 1 hour at room temperature. Membranes were washed four times with PBS-T for a total of 60 minutes and signal was detected using the ECL substrate (SuperSignal West Dura, Thermo Scientific) and the ChemiDoc XRS+ Imaging System (Bio-Rad). Prior to incubation with further antibodies, membranes were stripped using the Restore Western Blot Stripping buffer (Thermo Fisher Scientific).

Table 3-8: Composition of SDS-PAGE gels.

Separating gel (%)	**8**	**10**	**12**	**15**	**Stacking gel (%)**	**5**
dH_2O (ml)	9.3	7.9	6.6	4.8	dH_2O (ml)	5.5
30% Acrylamide (ml)	5.3	6.7	8.0	10.0	30% Acrylamide (ml)	1.3

1.5 M Tris pH 8,8 (ml)	5.0	5.0	5.0	5.0	1.5 M Tris pH 8,8 (ml)	1.0
10% SDS (µl)	200	200	200	200	10% SDS (µl	80
10% APS (µl)	200	200	200	200	10% APS (µl)	80
TEMED (µl)	12	8	8	8	TEMED (µl)	8

Table 3-9: Primary antibodies used for Western Blot.

Antigen	Host	Dilution	Source
VPS45	Rabbit	1:1000	Synaptic Systems (137002)
Cathepsin D	Mouse	1:1000	R&D Systems (MAB1014, clone 185111)
Cathepsin E	Mouse	1:1000	R&D Systems (MAB1294, clone 212211)
EGFR	Rabbit	1:1000	Cell Signaling Technology (4267, clone D38B1)
FLAG	Mouse	1:1000	Sigma-Aldrich (F1804, clone M2)
Phospho-Stat3 (Tyr705)	Rabbit	1:1000	Cell Signaling Technology (9145, clone D3A7)
Total Stat3	Mouse	1:1000	BD Biosciences (610190, clone 84/Stat3)
Rab4	Rabbit	1:1000	Cell Signaling Technology (2167)
Rab11	Rabbit	1:2000	Cell Signaling Technology (5589, clone D4F5)
Syntaxin6	Rabbit	1:2000	Cell Signaling Technology (2869, clone C34B2)
Syntaxin16	Mouse	1:1000	Proteintech (66775-1-Ig, clone 4A9D8)
Rabenosyn-5	Rabbit	1:1000	Proteintech (22218-1-AP)
EEA1	Mouse	1:1000	BD Transduction Laboratories (610457, clone 14/EEA1))
LAMP2	Mouse	1:1000	Abcam (ab25631, clone H4B4)
LAMP1	Rabbit	1:1000	Cell Signaling Technology (9091, clone D2D11)
Rab5	Rabbit	1:1000	Cell Signaling Technology (3547, clone C8B1)
Rab7	Rabbit	1:1000	Cell Signaling Technology (9367)
LC3B	Rabbit	1:1000	Cell Signaling Technology (2775)
GAPDH	Rabbit	1:1000	Santa Cruz Biotechnology (sc-32233, clone 6C5)
Actin (HRP-coupled)	Mouse	1:5000	Santa Cruz Biotechnology (sc-47778, clone C4)

Table 3-10: Secondary antibodies used for Western Blot.

Antigen	Conjugate	Dilution	Source
Mouse	HRP	1:5000	Santa Cruz Biotechnology (sc-2064)
Rabbit	HRP	1:5000	Cell Signaling Technology (7074)

3.2.7 Immunoprecipitation

$5x10^6$ HEK293T cells were seeded per 10 cm tissue culture plate and transfected with FLAG constructs (Table 3-3) the following day as described in 3.2.3.. 48 hours post-transfection, cells were washed with PBS and harvested using Nunc Cell Scrapers (Thermo Fisher Scientific). A fraction of cells was used to determine the transfection efficiency by flow cytometry. Cell pellets were lysed in 500 µl RIPA buffer (150 mM NaCl, 25 mM Tris HCl pH 7.5, 1 mM EDTA, 2.5 mM sodium pyrophosphate, 50 mM sodium fluoride, 1% NP40, 5% glycerol) supplemented with PIC (Sigma-Aldrich) and PMSF (Alpha Diagnostic International) for 30 minutes on ice and the lysate was centrifuged for 15 minutes at 21,130 x g at 4 °C. 10% of the cleared lysate was used for the input fraction. Per sample, 30 µl of FLAG beads (ANTI-FLAG M2 Affinity Gel, Sigma-Aldrich) were washed three times with RIPA buffer, centrifuged for 3 minutes at 250 x g at 4 °C, and added to the lysate. The lysate/bead mixture was incubated for 4 hours on a rotating wheel at 4 °C. Subsequently, beads were washed three times with RIPA buffer to remove unbound material. Beads were boiled in 80 µl of 2x Laemmli buffer for 10 minutes at 95 °C and samples were analyzed by Western Blot.

3.2.8 Flow cytometry and cell sorting

Flow cytometry analysis of samples was performed using the LSRFortessa (BD Biosciences) and the FlowJo v9 software. Cells were sorted using the BD FACS Aria (BD Biosciences). For flow cytometry and sorting, cells were typically stained with indicated antibodies (Table 3-11) for 30 minutes on ice. Prior to analysis, cells were filtered through a 50 µm nylon filter (Sysmex, CellTrics).

Table 3-11: Antibodies used for flow cytometry and cell sorting.

Antigen	Conjugate	Dilution	Source
CD19	biotinylated	1:200	BioLegend (clone 6D5)
Gr-1	biotinylated	1:500	eBioscience (clone RB6-8C5)
CD11b	biotinylated	1:500	eBioscience (clone M1/70)
CD117	PE	1:200	BD Biosciences (clone 2B8)

Sca-1	PE-Cy7	1:200	eBioscience (clone D7)
Gr-1	PE	1:200	BioLegend (clone RB6-8C5)
CD11b	e450	1:200	Thermo Fisher Scientific (clone M1/70)
Phospho-Stat3 (Tyr705)	Alexa Fluor 647	1:50	BioLegend (651008, clone 13A3-1)

3.2.9 Immunofluorescence

Cells were seeded on 0.13-0.16 mm glass cover slips (Karl Hecht) in a 24-well plate and cultured for 18 hours in order to attach to the plate. Cells were washed twice with PBS and fixed with 3% formaldehyde (Electron Microscopy Sciences) for 12 minutes at room temperature. Subsequently, cells were washed twice with PBS and autofluorescence was quenched by incubating cells with 50 mM NH_4Cl/PBS for 15 minutes at room temperature. After quenching, cells were permeabilized and blocked with PBS containing 0.05% (w/v) saponin (Sigma Aldrich) and 1% (w/v) BSA (Sigma Aldrich) for 1 hour at room temperature. After washing with PBS containing 0.05% (w/v) saponin (Sigma Aldrich), cells were incubated with primary antibodies (Table 3-12) for either 1.5 hours at room temperature or overnight at 4 °C. Following three washes for 5 minutes each with PBS, the staining was visualized using a secondary fluorophore-coupled antibody (Table 3-13). DNA was counterstained with 300 nM 4',6-diamidino-2-phenylindole (DAPI, Applichem) for 2 minutes at room temperature before mounting the cover slips on glass slides (Thermo Fisher Scientific) using the fluorescent mounting medium (Dako). Samples were visualized by using either Leica TCS SP5 or Zeiss LSM 800 confocal microscopes with a 63x oil-immersion objective. Colocalization coefficients and Pearson correlation were analyzed using the Zeiss Zen Blue 2.6 software (blue edition).

Table 3-12: Primary antibodies used for immunofluorescence.

Antigen	Host	Dilution	Source
EEA1	Mouse	1:400	BD Transduction Laboratories (610457)
LAMP2	Mouse	1:400	Abcam (ab25631)
LAMP1	Rabbit	1:400	Cell Signaling Technology (9091, clone D2D11)
EGFR	Rabbit	1:200	Cell Signaling Technology (4267, clone D38B1)
GM130	Mouse	1:100	BD Biosciences (610822, clone 35/GM130)

Table 3-13: Secondary antibodies used for immunofluorescence.

Antigen	Conjugate	Dilution	Source
Goat anti-mouse IgG	Alexa Fluor 488	1:800	Thermo Fisher Scientific (A-11001)
Goat anti-mouse IgG1	Alexa Fluor 633	1:800	Thermo Fisher Scientific (A-21126)
Goat anti-Rabbit IgG	Alexa Fluor 488	1:800	Thermo Fisher Scientific (A-27034)
Goat anti-Rabbit IgG	Alexa Fluor 633	1:800	Thermo Fisher Scientific (A-21070)

3.2.10 Live cell imaging of endosome maturation

Cells coexpressing mCherry-Rab5 and mCerulean-Rab7 (Table 3-3) were sorted to express comparable amounts of both proteins and were seeded into glass bottom dishes (ibidi, 35 mm # 1.5H) the day before imaging. Prior to imaging (Zeiss, LSM800), cells were incubated with dark red fluorescent microspheres (FluoSpheres Carboxylate-modified Microspheres, 0.02 µm, Thermo Fisher Scientific) for 10 minutes at 37 °C to allow uptake. Subsequently, cells were washed twice with PBS and analyzed in growth medium by imaging on a microscope stage at 37 °C, 5% CO_2, and a humidified atmosphere using a 63x/1.40 oil DIC M27 objective. Sequences were recorded as 16-bit 1155 x 1025 frames every 12 seconds for up to 90 minutes, using bidirectional scanning and 1x line averaging. Images were analyzed as described in 3.4.1.

3.2.11 Propidium iodide (PI) staining

PI staining was performed according to the protocol of Riccardi and Nicoletti (Riccardi and Nicoletti, 2006). 500 000 HeLa cells were washed with PBS and gently resuspended in 250 µl Nicoletti buffer (0.1% sodium citrate, 0.1% Triton X-100, 50 µg/ml PI in distilled water). Cells were incubated in the dark for 2 hours at 4 °C, centrifuged at 400 x g for 5 minutes, resuspended in PBS, and analyzed by flow cytometry.

3.2.12 Generation of *VPS45* knockout (KO) clones using CRISPR/Cas9 genome editing

The sgRNAs targeting exon 7 of the *VPS45* gene were designed using the online CRISPR Guide Design tool provided by Feng Zhang's lab. Two targets with the lowest predictions to have off-target effects (Table 3-15) were inserted into the pSpCas9(BB)-

2A-GFP (Addgene, PX458, 48138) plasmid according to Feng Zhang's protocol. Co-transfection of both targets were predicted to generate an out-of-frame deletion of around 58 bp resulting in a non-functional VPS45 protein.

To generate *VPS45* KO clones, HeLa cells were transfected with both vectors using jetPEI (Polyplus) according to the manufacturer's protocol. The suspension cell line PLB-985 was transfected using the Nucleofector Technology (Lonza) according to the manufacturer's suggestions. 48 hours after transfection, GFP-positive cells were single-sorted in 96-well plates using BD FACS Aria (BD Bioscience) and grown for approximately 3 weeks. Clones were validated for VPS45 disruption by PCR analysis (Table 3-15). Targeted gene regions were amplified, and deletions were detected as shifts in band sizes using agarose gel electrophoresis. Modifications of potential KO clones were analyzed by Sanger sequencing. The absence of VPS45 was further validated by immunoblotting.

Table 3-14: Sequences targeted by CRISPR/Cas9-mediated genome editing.

Name	Sequence (5'-3')
VPS45-Target1	CACCGTTTGAATTCCGTCGGACAG
VPS45-Target2	AAACCATTGCTAAACCAGGTACAC

Table 3-15: Oligonucleotides used for sequencing of CRISPR/Cas9-edited clones.

Name	Sequence (5'-3')
VPS45-CRISPR_F	ATGGTTGCACAAACCATCTTTCTCTC
VPS45-CRISPR_R	GAAGCAGAAGAGTTATGATGACAGTGGA

3.2.13 Endocytosis of fluorescent ovalbumin (OVA)

HeLa cells were incubated with 32.5 µg/ml OVA-488 (Ovalbumin, Alexa Fluor 488 Conjugate, Thermo Fisher Scientific) for various time points at 37 °C. The uptake of fluorescent OVA was stopped by transferring cells to ice-cold PBS. After washing cells twice with ice-cold PBS, the rate of uptake was determined by flow cytometry as a change in MFI from the baseline (fluorescence at 4°C).

3.2.14 Uptake and processing of cargo proteins in HeLa cells

HeLa cells were incubated with either 65 µg/ml of DQ OVA (DQ Ovalbumin, Thermo Fisher Scientific), 65 µg/ml DQ Green BSA (Thermo Fisher Scientific), or 65 µg/ml pHrodo Green dextran (Thermo Fisher Scientific) for various time points at 37 °C. Cargo uptake and processing were stopped by transferring aliquots of cells to ice-cold

PBS. Cells were washed twice with ice-cold PBS and the rate of cargo processing was determined by flow cytometry as a change in MFI from the baseline (fluorescence at 4 °C). Cells were additionally treated with 25 µM chloroquine (CQ).

3.2.15 Epidermal growth factor receptor (EGFR) trafficking

HeLa cells were grown on coverslips (Karl Hecht) and starved in plain DMEM for a minimum of 6 hours. To induce EGFR trafficking, cells were stimulated with 100 ng/ml EGF (Thermo Fisher Scientific) for various time periods at 37 °C. Cells were washed twice with ice-cold PBS, fixed, and processed for confocal microscopy as described in 3.2.9. Quantitative analysis was performed as specified in 3.4.1.

3.2.16 Granulocyte colony-stimulating factor receptor (G-CSFR) trafficking

HeLa cells expressing G-CSFR-GFP fusion proteins were grown on coverslips and starved in serum-free DMEM overnight. G-CSFR trafficking was triggered by stimulating cells with 100 ng/ml G-CSF (PeproTech) for various time periods at 37 °C. Cells were washed twice with ice-cold PBS, fixed, and processed for confocal microscopy as described in 3.2.9. Analysis of colocalization was performed as outlined 3.4.1.

3.2.17 G-CSFR-mediated signaling

PLB-985 cells were starved in plain RPMI overnight. G-CSFR-mediated signaling was induced by stimulating cells with 100 ng/ml G-CSF (PeproTech) for various time periods at 37 °C. Following stimulation, cells were washed with ice-cold PBS and processed for analysis by western blot (3.2.6) or flow cytometry. For flow cytometry, cells were fixed in 4% formaldehyde for 15 minutes at room temperature and incubated in methanol for 30 minutes on ice prior to staining with antibodies for 30 minutes at room temperature.

3.2.18 Transferrin recycling

HeLa cells were detached using PBS supplemented with 10 mM EDTA and starved in serum-free DMEM for 30 minutes at 37 °C. Cells were incubated with 25 µg/ml Tf-633 (Thermo Fisher Scientific) for 30 minutes at 37 °C and washed with ice-cold PBS. Recycling of Tf was facilitated at 37 °C for various time points and stopped by transferring cells to ice-cold PBS. Surface-bound Tf was removed (PBS supplemented with 100 mM Glycine and 100 mM NaCL). Cell-associated Tf was measured by flow cytometry and expressed as the percentage of initial Tf present at time=0.

3.3 Transgenic mouse models

3.3.1 Mouse husbandry and breeding

Mice were maintained and bred in “Zentrale Versuchstierhaltung” (ZVH, Ludwig-Maximilians-Universität München) under specific pathogen-free conditions. All experiments were conducted according to the German animal welfare law.

3.3.2 Generation of VPS45-deficient mouse models

Engineered ES clones HEPD0764_7_D04 targeting exon 4 of *Vps45* were obtained from the European Mouse Mutant Cell Repository (EuMMCR, Helmholtz Zentrum München). ES clones were microinjected into C57BL/6 blastocysts and transplanted into pseudopregnant female mice in cooperation with Prof. Eckhard Wolf at the Gene Center Munich (Ludwig-Maximilians-Universität München). Chimeric mice were identified by PCR analysis and germline transmission of the targeted tm1a allele (*Vps45*$^{tm1a(EUCOMM)Hmgu}$) was verified by genotyping of tail DNA. Mice heterozygous for the targeted allele were either intercrossed to obtain *Vps45* KO mice or bred to mice expressing the FLP transgene to obtain *Vps45* floxed mice. Homozygous *Vps45* floxed mice were then bred to heterozygous LysM-Cre or Vav-Cre transgenic mice to induce the deletion of loxP-flanked regions in the myeloid or hematopoietic compartments, respectively.

3.3.3 Genotyping of mice

At the time of weaning, small tail tips were cut from mice. Tail tips were incubated in 100 µl of DirectPCR Lysis Reagent (Mouse Tail, Viagen Biotech) supplemented with 0.2 mg/ml Proteinase K (PEQLAB) overnight with an agitation of 900 rpm at 56 °C (ThermoMixer, Eppendorf). Proteinase K was inactivated for 1 hour at 85 °C and supernatants were used for genotyping. The genotyping strategy is depicted in Figure 4-27 and oligonucleotides used for genotyping are listed in Table 3-16. The Vps45-5’arm and Vps45-3’arm primer pair was used to identify the WT and the floxed allele, whereas the Vps45-5’arm and LAR3 primer pair was used to identify the targeted allele.

Table 3-16: Oligonucleotides used for genotyping of mice.

Name	Sequence (5‘-3‘)
Vps45-5’arm	GTAGGGTATAACTACCGAGCTCAGG
Vps45-3’arm	GCTTGGAAGAAGAGGTCCTACAGG
LAR3	CAACGGGTTCTTCTGTTAGTCC
Flpe_s	CTAATGTTGTGGGAAATTGGAGC
Flpe_as	CTCGAGGATAACTTGTTTATTGC

LysM-Cre_F	TAATCGCCATCTTCCAGCAG
LysM-Cre_R	CAATTTACTGACCGTACAC
Vav-Cre_F	GGTGTTGTAGTTGTCCCCACT
Vav-Cre_R	CAGGTTTTGGTGCACAGTCA

The OneTaq 2X Master Mix with Standard Buffer (New England BioLabs) was used to genotype the mice.

The standard PCR reaction setup and thermocycling conditions used to genotype the mice are shown in Table 3-17 and Table 3-18. PCR products were separated by agarose gel electrophoresis as described in 3.1.5.

Table 3-17: Standard PCR reaction setup used for genotyping of mice.

Component	25µl reaction volume
One Taq 2X Master Mix with Standard Buffer	12.5 µl
10 µM forward primer	1 µl
10 µM reverse primer	1 µl
Template DNA	2 µl of DNA lysate
Nuclease-free water	10 µl

Table 3-18: Standard PCR thermocycling condition used for genotyping of mice.

Step	Temperature	Time
Initial denaturation	95 °C	30 seconds
35 cycles	95 °C	30 seconds
	*50-68 °C	30 seconds
	68 °C	1 minute/kb
Final extension	68 °C	10 minutes
Hold	4 °C	Forever

*The cycling conditions, including annealing temperature and extension time, were adjusted to different primers and templates.

3.3.4 Histological analysis of embryos

Synchronized breeding of heterozygous mice was set up and mating was assessed by checking the vaginal plugs of females, which were designated as day 0.5 post-coitus. Mouse embryos were dissected from the uterus, fixed in 4% formaldehyde (Santa Cruz Biotechnology) for roughly 5 hours at room temperature, and stored in 70% ethanol (Carl Roth) at 4 °C. Embryonic tissues were sequentially dehydrated using a series of

ascending ethanol concentrations and cleared in Xylene (Carl Roth). Embryos were immersed in paraffin and sectioned at 5 µm on a RM 2155 microtome (Leica).

Paraffin slides were incubated twice in dewax (BioGenex Laboratories Biogenex) for 5 minutes respectively and in 1% periodic acid solution for 10 minutes. Slides were further stained with Schiff's reagent (Sigma-Aldrich) for 25 minutes and counterstained with Mayer's Hämalaun solution (Sigma-Aldrich) for 40 minutes. Following a series of ascending ethanol concentrations and Xylene incubation, slides were mounted with the Eukitt mounting medium (Sigma-Aldrich). Slides were prepared at room temperature and rinsed with tap water during the steps.

Images were acquired using an AxioVert (Zeiss) microscope and processed by the Axio Vision software (Zeiss).

3.3.5 Isolation of bone marrow cells

Mice were euthanized with CO_2 and femur and tibia bones were dissected from the hind legs of the mice. After tissue removal, the ends of the bones were cut off and the bone marrow cells were flushed with ice-cold PBS using a 27G needle (B. Braun) attached to a 5 ml syringe (B. Braun). Cell clumps were removed by filtering the bone marrow suspension through a 50 µm filter (CellTrics, Sysmex). Cell pellets were obtained by centrifugation at 300 x g for 5 minutes at 4 °C. Red blood cells were lysed in RBC lysis buffer (155 mM NH_4Cl, 12 mM $NaHCO_3$, 0.1 mM EDTA) for 3 minutes at room temperature and subsequently washed with PBS. Cells were kept on ice and stained with antibodies (Table 3-11).

3.3.6 *Ex vivo* deletion of VPS45 in LSK cells and differentiation into neutrophils using OP9 cocultures

LSK cells (c-Kit+, sca-1+, Gr-1-, CD11b-, CD19-) were sorted from the bone marrow of either *Vps45*$^{WT/WT}$, *Vps45*$^{Flox/WT}$, or *Vps45*$^{Flox/Flox}$ mice and cultured overnight in MEMα (Thermo Fisher Scientific) supplemented with murine cytokines: 50 ng/ml SCF, 25 ng/ml IL-7, 25 ng/ml FLT3L, and 20 ng/ml IL-6 (all from PeproTech). On the following day, viral particles expressing Cre-IRES2-GFP (Table 3-3) were loaded on RetroNectin-coated (50 µg/ml, Takara Bio Inc) 96-well flat-bottom plates (Sarstedt). The spin infection of LSK cells was performed for 45 minutes at 700 x g at 32 °C in the presence of polybrene (8 µg/ml, Sigma-Aldrich) and cells were cultured overnight. The day after, cells were transferred on OP9 monolayers in 24-well plates and cultured in MEMα supplemented with 0.5 ng/ml IL-7, 5 ng/ml FLT3L, and 10 ng/ml SCF. Fresh medium and growth factors were added to the culture every third and the differentiation

of LSK cells into neutrophil granulocytes (CD11b+, Gr-1+) was monitored on different days of coculture by flow cytometry.

3.4 Quantitative analysis

3.4.1 Confocal microscopy analysis

Immunofluorescent images were analyzed using the Zeiss Zen 2.6 (blue edition) software.

Colocalization analysis of fixed samples

Colocalization measurements were performed by drawing a line around cell boundaries and nuclei to include the cytoplasmic region for the analysis. The Pearson coefficients between two channels were determined using the Zeiss Zen 2.6 software.

Image analysis of live cell imaging

Fluorescent intensities of all recorded channels of an acquired image were measured by manually drawing a ring around the vesicle containing the fluorescent cargo (diameter ~1.5 µm). The background intensities of the respective images were determined by drawing circles outside the cells and subtracted from the intensities of the vesicles. Intensities were further normalized using the GraphPad Prism 6.0 software.

3.4.2 Statistics

Statistical analysis of the data was performed using the GraphPad Prism 6.0 software. No method of randomization was applied, and no samples were excluded from the analyses. No statistical method was used to predetermine the sample size for analyses. The number (n) or biological repeats and statistical tests are indicated in the figure description. *, $p<0.05$; **, $p<0.01$; ***, $p<0.001$; ****, $p<0.0001$. $p>0.05$ was considered as not significant (ns).

4 Results

4.1 Generation and characterization of VPS45-deficient cell lines

4.1.1 CRISPR/Cas9-mediated KO of *VPS45*

To investigate the function of VPS45 in the endocytic pathway, endogenous VPS45 was deleted from PLB-985 and HeLa cell lines using the CRISPR/Cas9 system. PLB-985 cells belong to the myeloid lineage and can be differentiated towards mature neutrophils (Tucker et al., 1987; Pedruzzi et al., 2002). PLB-985 are suspension cells and possess a low cytoplasm to nucleus ratio, thus impeding comprehensive microscopy-based analyses of cargo trafficking through various endocytic compartments. For this purpose, VPS45-deficient HeLa cell lines were generated. Most of the modifications introduced by CRISPR/Cas9 resulted in a frameshift and the KO of the *VPS45* gene. The loss of the VPS45 protein was validated by immunoblotting (Figure 4-1).

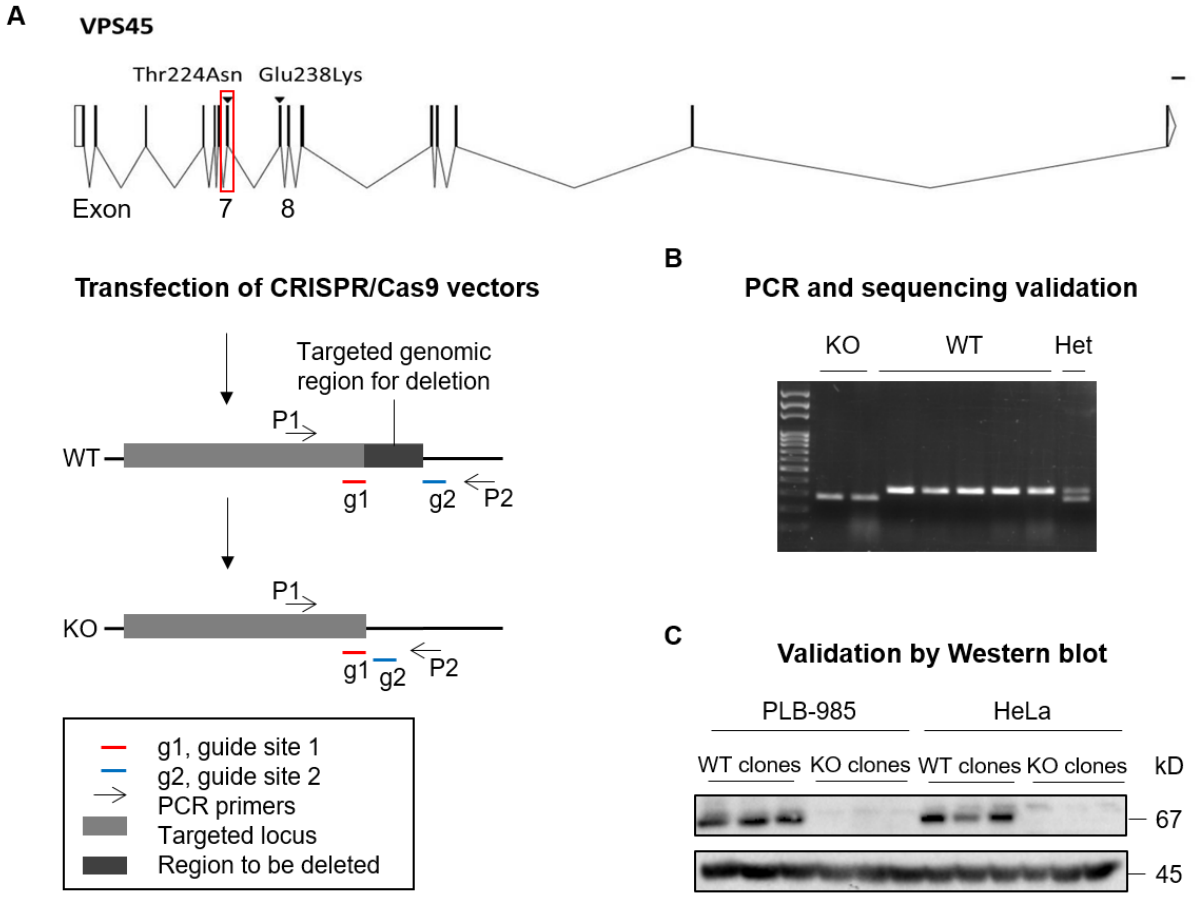

Figure 4-1 Generation of *VPS45* KO HeLa and PLB-985 cell clones by CRISPR/Cas9 engineering.

(A) Exon 7 of *VPS45* was targeted by the cotransfection of Cas9 and specific guide RNAs. (B) Single cells were screened for deletions in the targeted region by PCR and potential KO clones were sequenced. (C) Western blot analysis confirming the absence of the VPS45 protein in CRISPR/Cas9-edited *VPS45* KO HeLa and PLB-985 clones.

4.1.2 VPS45 affects the expression of its binding partners

VPS45 interacts with the dual Rab4 and Rab5 effector Rabenosyn-5 and binds the SNARE protein Syntaxin16 (Nielsen et al., 2000; Dulubova et al., 2002). To investigate, whether the loss of VPS45 affects the expression of both interaction partners, their protein levels were analyzed in WT and *VPS45* KO HeLa and PLB-985 cells by immunoblotting. VPS45-depleted HeLa clones showed markedly reduced abundances of both binding partners Rabenosyn-5 and Syntaxin16 as compared to control clones. Similarly, loss of *VPS45* expression resulted in decreased protein levels of Rabenosyn-5 and Syntaxin16 in PLB-985 cells (Figure 4-2). These results demonstrate that VPS45 affects the expression of its binding partners.

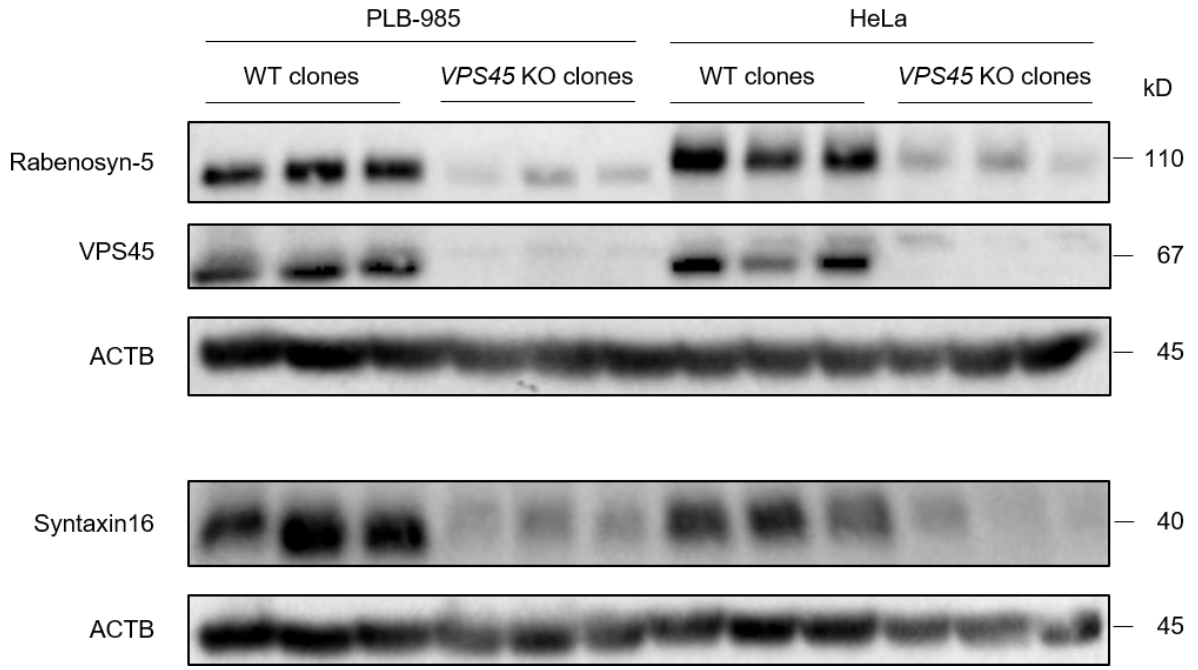

Figure 4-2 VPS45 impacts on the protein levels of its binding partners Rabenosyn-5 and Sytnaxin16.

Immunoblot analysis of expression levels of VPS45 binding partners Rabenosyn-5 and Syntaxin16 in WT and *VPS45* KO HeLa and PLB-985 clones. The blots are representative of at least two independent experiments.

4.1.3 Loss of VPS45 disrupts the intracellular organization of endosomal and lysosomal vesicles

Next, the morphology and distribution of various types of intracellular vesicles were examined in the presence and absence of VPS45 in HeLa cells by confocal microscopy. In control cells, the early endosomal marker EEA1 showed a typical punctate

distribution throughout the cytoplasm, whereas VPS45 deficiency resulted in the aggregation of early endosomes. Furthermore, late endosomes showed an aberrant morphology: LAMP2-positive vesicles were clustered and enlarged in KO cells. Similarly, LAMP1-positive lysosomes were aggregated and some of the lysosomes were enlarged in KO cells (Figure 4-3).

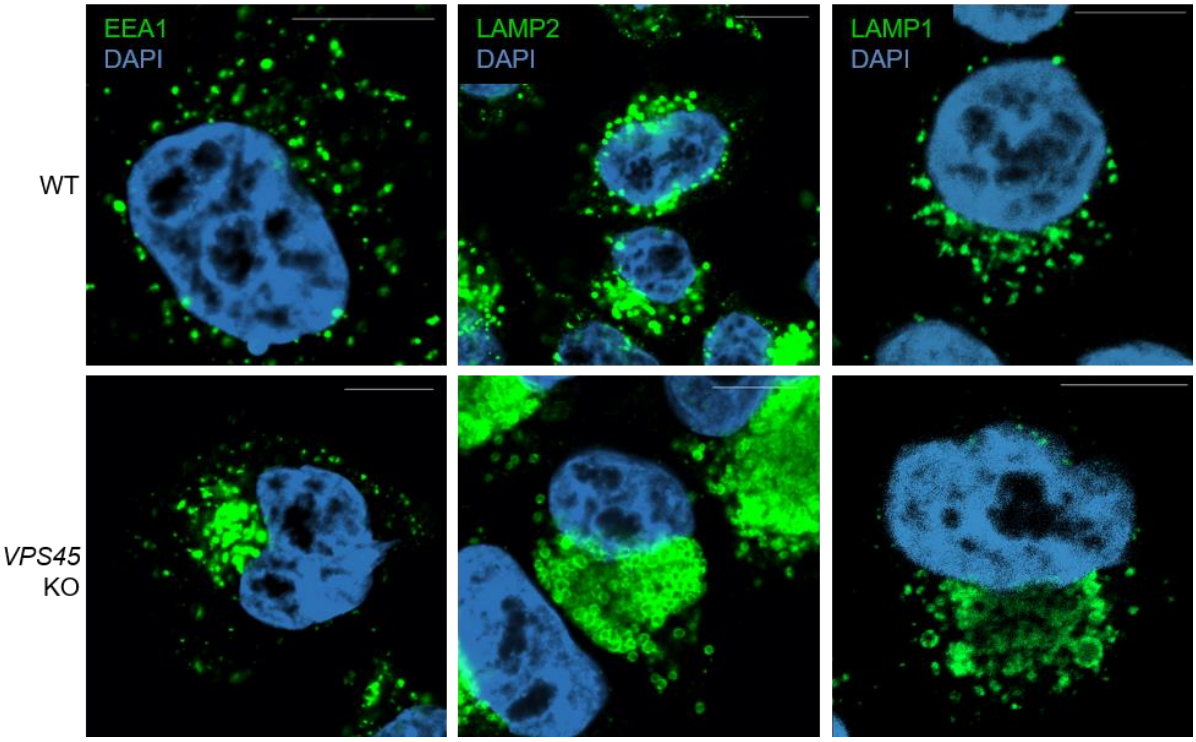

Figure 4-3 VPS45 controls the intracellular organization of endolysosomal vesicles.

WT and *VPS45* KO HeLa clones were stained for early endosomes (EEA1), late endosomes (LAMP2), lysosomes (LAMP1), and the nucleus (DAPI). Confocal microscopy images are representative of at least three independent experiments. Scale bars, 10 µm.

Despite the aggregation of endolysosomal vesicles, the overall protein levels of EEA1, LAMP2, and LAMP1 were not affected in neither HeLa nor PLB-985 cells in the absence of VPS45, as revealed by immunoblotting (Figure 4-4).

In sum, VPS45 plays an essential role in maintaining the intracellular organization of endosomal and lysosomal vesicles.

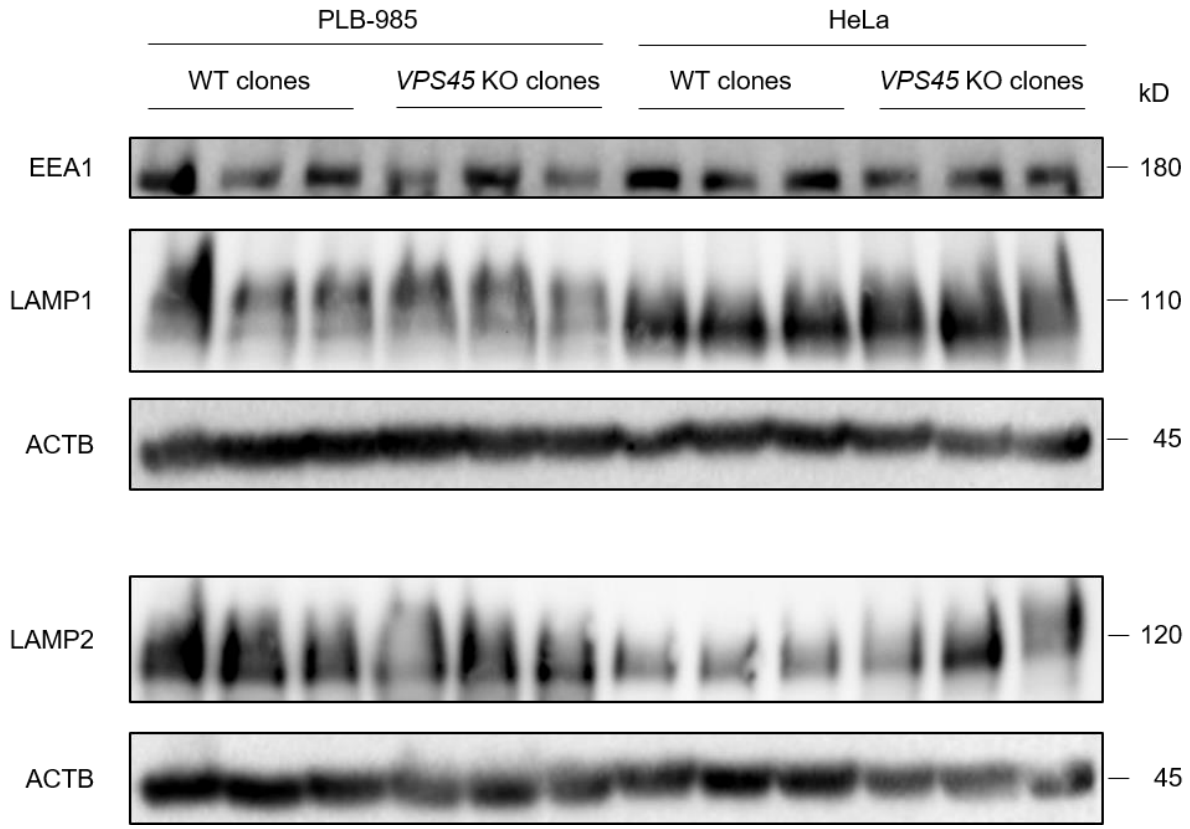

Figure 4-4 Depletion of VPS45 does not affect expression levels of EEA1, LAMP2, and LAMP1.

Western blot analysis of expression levels of EEA1, LAMP2, and LAMP1 in WT and *VPS45* KO HeLa and PLB-985 clones. Blots are representative of at least two independent experiments.

4.1.4 Endocytosis is not affected in VPS45-deficient HeLa cells

To further investigate the role of VPS45 in endosomal trafficking, the internalization, recycling, and degradation of cellular cargo proteins were assessed. Based on the hypothesis, a defect in the fusion of early endosomes rather than cargo internalization was expected in the absence of VPS45. To test the impact of VPS45 on the first step of the endocytic pathway, WT and *VPS45* KO HeLa clones were incubated with Alexa Fluor 488-conjugated ovalbumin (OVA) for various time periods at 37 °C and the rate of cargo internalization was determined by flow cytometry. Both VPS45-sufficient and VPS45-deficient cells internalized ovalbumin at comparable rates over time (Figure 4-5). Thus, as expected, VPS45 is not required for the uptake of cargo.

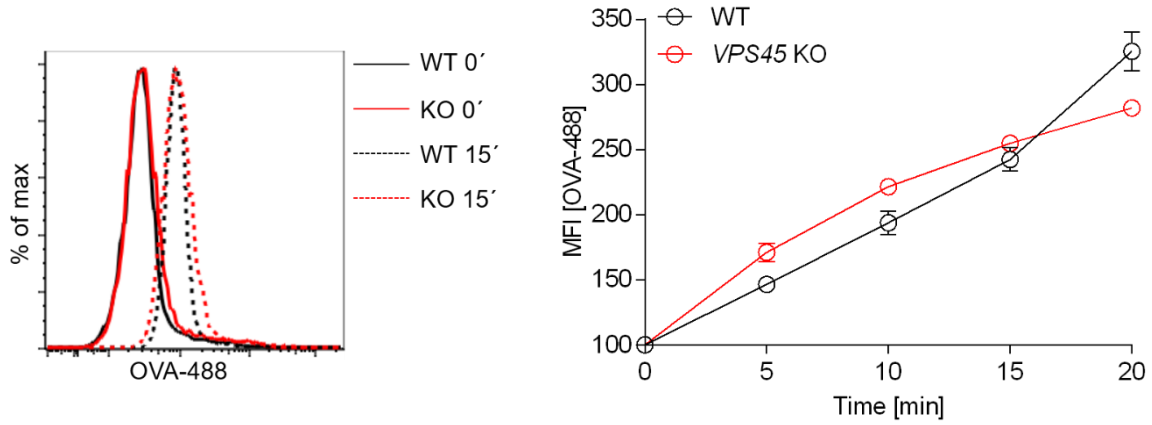

Figure 4-5 VPS45 is not required for the internalization of cargo.

WT and *VPS45* KO HeLa clones were incubated with 32.5 µg/ml fluorescent ovalbumin (OVA) for indicated periods at 37 °C and the rate of cargo uptake was analyzed as a change in MFI from the baseline (fluorescence at 4 °C). Representative histograms of one WT and one *VPS45* KO clone are shown. The chart shows one representative of four independent experiments using four WT clones and four *VPS45* KO clones. Error bars indicate the mean ± SD. Statistical analysis of significance using one-way ANOVA followed by Tukey´s multiple comparison test revealed no significant difference in OVA uptake between WT and *VPS45* KO HeLa clones.

4.1.5 VPS45 depletion results in delayed cargo recycling

VPS45 interacts with the dual Rab4 and Rab5 effector Rabenosyn-5, which plays a role in Tf recycling (Renzis et al., 2002; Navaroli et al., 2012). Since expression levels of Rabenosyn-5 were reduced in the absence of VPS45 (Figure 4-2), the recycling of cargo was expected to be affected in *VPS45* KO HeLa cells.

To assess the role of VPS45 in the recycling pathway, the trafficking of the TfR and its ligand Tf was analyzed. Upon ligand binding, the complex is internalized via CME and recycled via either the Rab4-mediated fast route or the Rab11-mediated slow route. WT and *VPS45* KO HeLa clones were incubated with Tf coupled to Alexa Fluor 647 for 30 minutes at 37 °C to saturate the endocytic and recycling systems. Subsequently, recycling kinetics were determined by flow cytometry as the loss of fluorescence from intracellular stores.

In control cells, a fast decline of the Tf signal was observed, indicating that Tf was efficiently recycled back to the cell surface and released. After 10 minutes of recycling 60% of the loaded Tf and after 20 minutes 75% of the initial Tf was released from WT cells. In contrast, Tf recycling was less efficient in VPS45-deficient cells. Although the loss of VPS45 did not completely abrogate Tf recycling, a significant delay in recycling rates was observed. After 10 minutes roughly 30% of loaded Tf was released and only after 60 minutes 75% of initial Tf was released from *VPS45* KO cells (Figure 4-6).

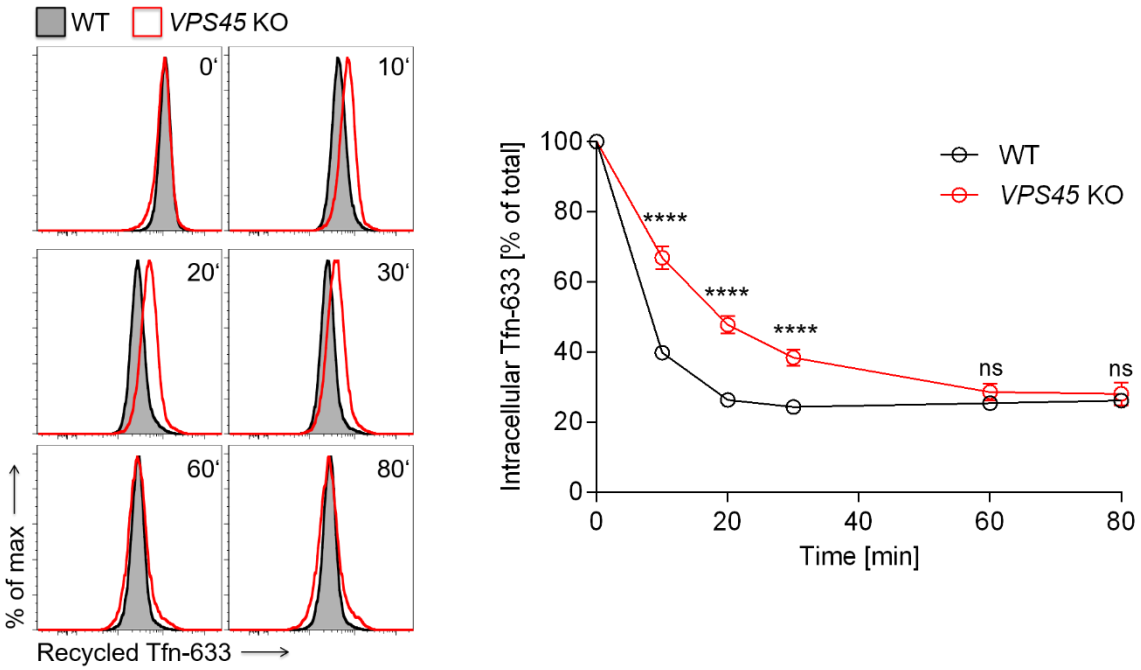

Figure 4-6 VPS45 depletion leads to delayed recycling of Tf.

Flow cytometric analysis of Tf recycling in WT and *VPS45* KO HeLa cells. Cells were incubated with 25 µg/ml of fluorescent Tf for 30 minutes at 37°C, followed by a chase for the indicated periods and removal of surface-bound Tf. Representative histograms of one WT clone and one *VPS45* KO clone are shown on the left. The chart on the right shows cell-associated Tf as a percentage of initial Tf present at time t=0 and summarizes one representative experiment of four independent experiments using four WT and five *VPS45* KO clones. Error bars indicate the mean ± SD. Statistical analysis of significance was performed using one-way ANOVA followed by Tukey´s multiple comparison test. ns: not significant; ****, p<0.0001.

To get insights into the spatio-temporal distribution of Tf, recycling was further examined by confocal microscopy. WT and *VPS45* KO HeLa cells transduced with mCerulean-Rab4 or mCerulean-Rab11 were incubated with fluorescent Tf and receptor-ligand complexes were followed over time. In agreement with the flow cytometry data, intracellular Tf accumulated after 10 and 30 minutes in VPS45-deficient cells as compared to control cells. VPS45 depletion did not prevent the association of Tf with Rab4- and Rab11-positive recycling vesicles, however, the Tf accumulation at early timepoints indicates a delayed transit of Tf to Rab4-positive recycling vesicles and transfer to the plasma membrane (Figure 4-7).

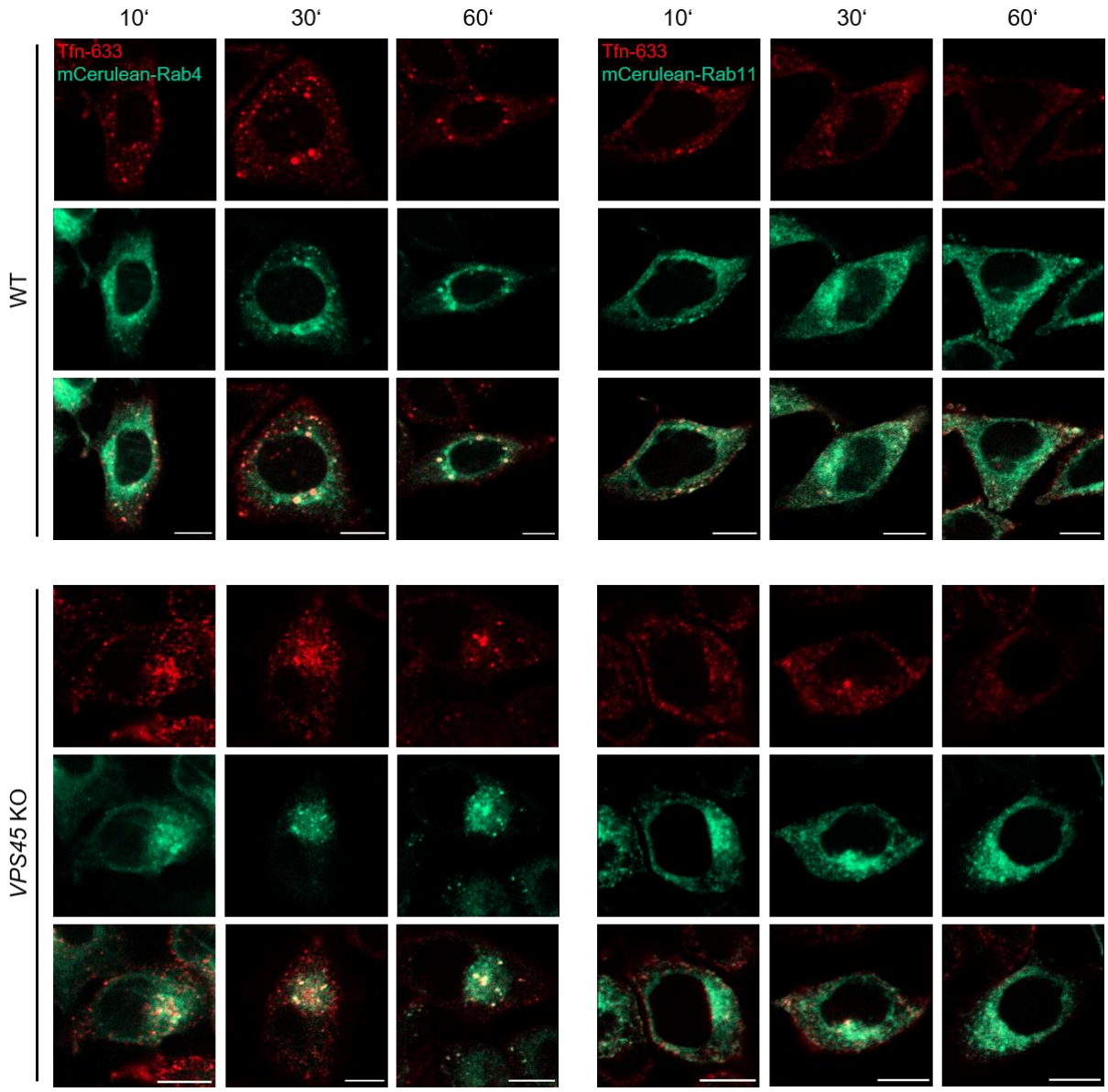

Figure 4-7 Loss of VPS45 does not prevent the association of Tf with Rab4- and Rab11-positive vesicles.

WT and *VPS45* KO HeLa clones expressing either mCerulean-Rab4 or mCerulean-Rab11 were incubated with 25 µg/ml of fluorescent Tf for 30 minutes at 37°C, followed by a chase for the indicated periods. Representative confocal microscopy images of Tf recycling are shown. Pictures are representative of two independent experiments. Scale bars, 10 µm.

In HeLa cells, which do not overexpress Rab4 or Rab11, the endogenous expression of Rab4 was not affected in the absence of VPS45. Rab11 expression, however, was slightly elevated in VPS45-depleted HeLa cells (Figure 4-8).

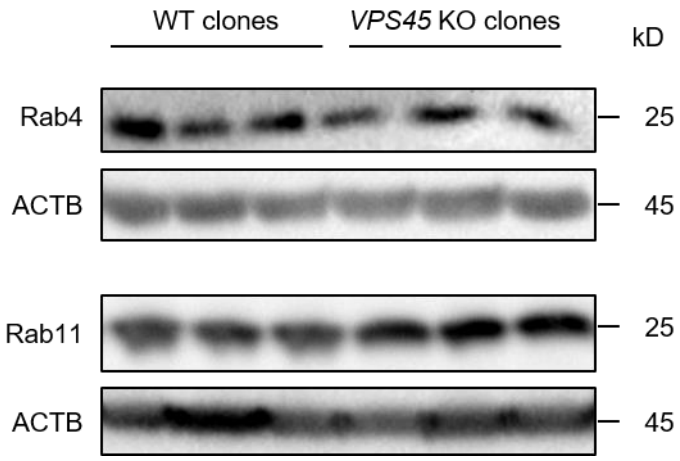

Figure 4-8 Comparable abundance of endogenous Rab4 and Rab11 proteins in the absence of VPS45.

Western blot analysis of Rab4 and Rab11 expression in WT and *VPS45* KO HeLa clones. The blot is representative of two independent experiments.

4.1.6 Lysosomal degradation of cargo is disrupted in *VPS45* KO cells

To further investigate how the degradation pathway is affected by the absence of VPS45, the transport of cargos destined for processing in the lysosomal compartment was analyzed using three different compounds: DQ Ovalbumin (DQ OVA), DQ Green BSA, and pHrodo Green dextran. These cargo proteins differ in their size, route of uptake, and mode of fluorescence release. Whereas DQ OVA has a molecular weight of around 45 kD, the size of DQ Green BSA is roughly 66 kD, and the size of pHrodo Green dextran is approximately 10 kD. The uptake of DQOVA is mainly mediated through the mannose receptor pathway, whereas the main route of uptake of DQ Green BSA and pHrodo Green Dextran is macropinocytosis (Burgdorf et al., 2006; Tejeda-Muñoz et al., 2019). Both DQ OVA and DQ Green BSA are heavily labeled with the self-quenched BODIPY dye, which is pH insensitive and gains fluorescence upon proteolytic processing in lysosomes. In contrast, pHrodo Green dextran is pH sensitive and gains fluorescence with decreasing pH.

To investigate the cargo processing capacity, WT and *VPS45* KO clones were incubated with respective compounds for indicated time periods and the production of fluorescent peptides was measured by confocal microscopy or flow cytometry.

Bright DQ OVA signals were apparent after 90 minutes of incubation in control cells by confocal microscopy. These signals were mainly associated with LAMP2-positive late endosomes, indicating an efficient processing of DQ OVA in the degradative compartment. In contrast, these signals were significantly less in KO cells, showing that the processing of DQ OVA is perturbed in the absence of VPS45.

Cargo processing was assessed in a quantitative manner using flow cytometry. A steady increase in fluorescence in WT cells was observed for all tested compounds over time, demonstrating efficient lysosomal processing. In striking contrast, VPS45-deficient cells revealed lower fluorescent intensities. These results are in line with the reduced degradative capacity of *VPS45* KO cells observed before. Since the internalization of cargo was efficient in *VPS45* KO HeLa cells, it is likely that post-endocytic steps are perturbed in the degradative pathway, such as the fusion of endolysosomal vesicles, resulting in an inefficient cargo delivery to the lysosomal compartment. To test this hypothesis, cells were additionally treated with chloroquine (CQ), a lysosomotropic compound that blocks lysosomal acidification and affects vesicle fusion (Poole and Ohkuma, 1981; Pless and Wellner, 1996; Pryor et al., 2000). Whereas CQ treatment of WT cells reduced the DQ OVA fluorescence to the level of *VPS45* KO cells, it did not affect cargo processing in the absence of VPS45 (Figure 4-9).

These results demonstrate a reduced capacity of *VPS45* KO cells to degrade cellular cargo, consistent with an impaired fusion of endolysosomal vesicles and inefficient routing of cellular cargo to the lysosomal compartment.

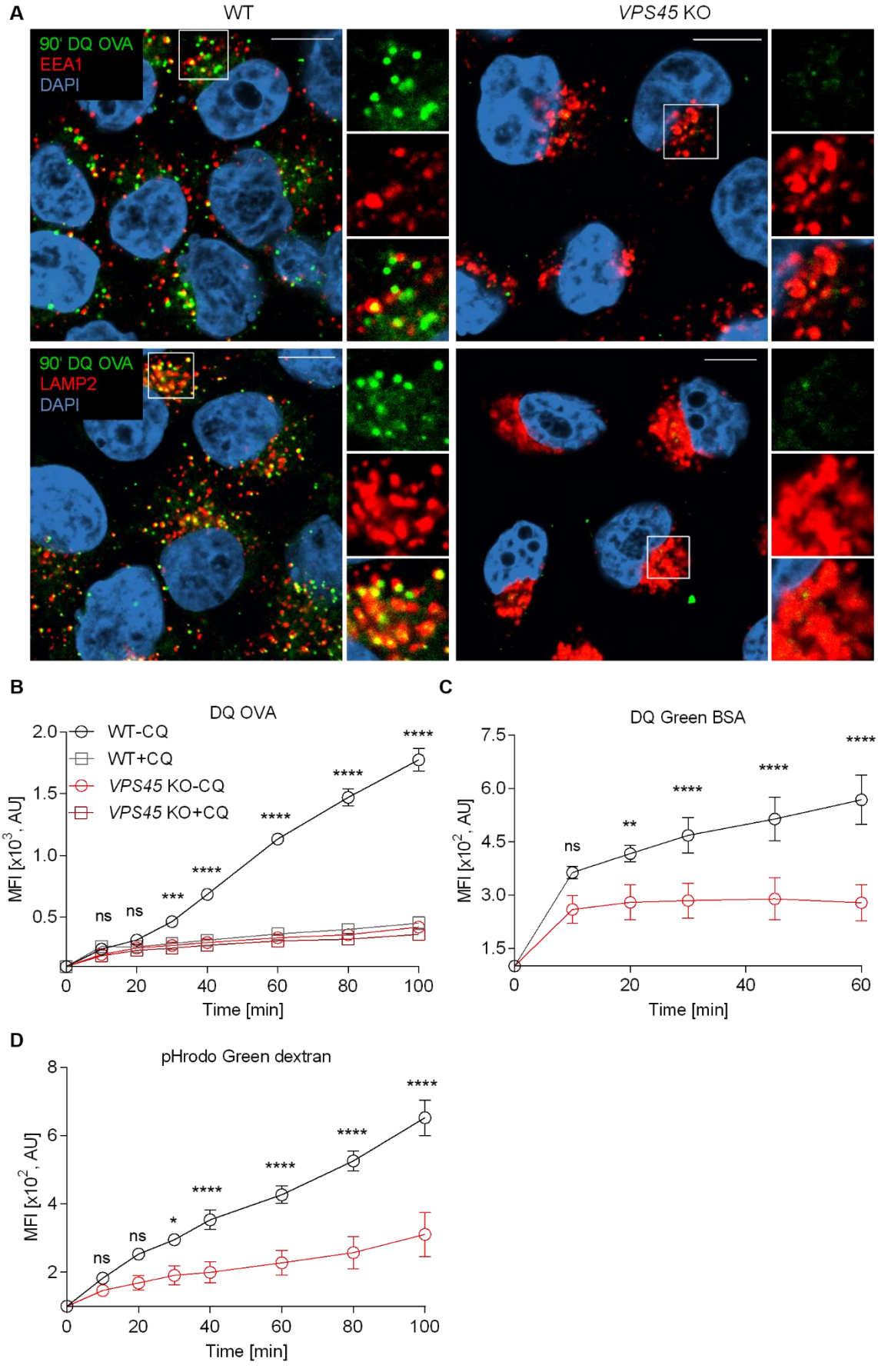
A
WT
VPS45 KO
90' DQ OVA
EEA1
DAPI
90' DQ OVA
LAMP2
DAPI
B
DQ OVA
WT-CQ
WT+CQ
VPS45 KO-CQ
VPS45 KO+CQ
MFI [x10^3, AU]
Time [min]
C
DQ Green BSA
MFI [x10^2, AU]
Time [min]
D
pHrodo Green dextran
MFI [x10^2, AU]
Time [min]

Figure 4-9 Loss of VPS45 leads to an inefficient processing of cargo proteins.

WT and *VPS45* KO HeLa clones were incubated with (A-B) 65 µg/ml DQ OVA, (C) 65 µg/ml DQ Green BSA or (D) 65 µg/ml pHrodo Green dextran for indicated time periods at 37°C. (A) Representative confocal microscopy images of DQ OVA processing in WT and *VPS45* KO HeLa clones are shown. After incubation with DQ OVA for 90 minutes, cells were fixed and stained for early endosomes (EEA1 – upper panel) and late endosomes (LAMP2 – lower panel). DAPI was used to visualize the nucleus. Zoom images represent magnified views of boxed areas (8 µm x 8 µm). Images are representative of two independent experiments. Scale bars, 10 µm. (B-D) The rate of cargo processing was determined by flow cytometry as the change in MFI from baseline (fluorescence at 4°C). (B) WT and *VPS45* KO cells were additionally treated with 25 µM chloroquine (CQ). (B-C) Data are representative of at least four independent experiments and three WT and three *VPS45* KO clones were used in each experiment. (D) Data are pooled from three independent experiments. (B-D) Error bars indicate the mean ± SD. Statistical analysis was performed using one-way ANOVA followed by Tukey´s multiple comparison test. ns: not significant; *, $p<0.05$; **, $p<0.01$; ***, $p<0,001$; ****, $p<0.0001$.

4.1.7 VPS45 is crucial for efficient maturation of cathepsin D

Besides mistrafficking, the reduced degradation rates of the tested compounds could result from a lower overall degradative capacity of *VPS45* KO cells due to an increased lysosomal pH. The expression of the mature form of cathepsin D is widely used as an indicator of the lysosomal pH and proteolytic capacity. Cathepsin D is synthesized as pre-pro-cathepsin D at the rough endoplasmic reticulum and post-translationally modified. The glycosylated inactive 53-kD precursor is transported mainly by mannose 6-phosphate receptors from the Golgi apparatus to the early endocytic compartment and late endosomes, where cathepsin D is further processed into a 47-kD intermediate form. The conversion into the fully active mature 31-kD form occurs in the acidic environment of lysosomes and is dependent on other proteases (Kurt von Figura and Andrej Hasilik; Gieselmann et al., 1983; Gieselmann et al., 1985; Richo and Conner, 1994). Analysis of the distinct cathepsin D maturation stages by immunoblotting revealed a markedly reduced abundance of the 31 kD mature forms, whereas immature forms of the lysosomal protease accumulated in the absence of VPS45 (Figure 4-10). An impaired maturation of cathepsin D might reflect either a mislocalization of the protease due to impaired vesicle fusion and defective targeting to the lysosome or a lower overall degradative capacity due to an increased lysosomal pH in *VPS45* KO cells.

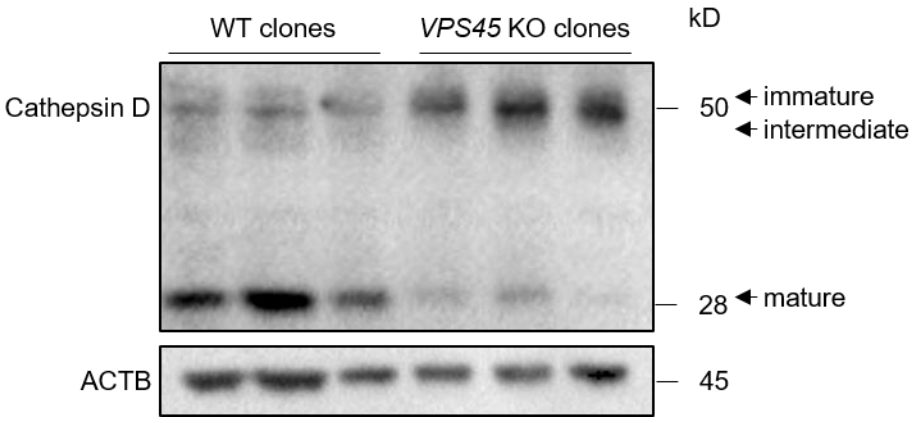

Figure 4-10 Maturation of cathepsin D is delayed in the absence of VPS45.

Expression levels of immature (50 kD), intermediate (46 kD), and mature (28 kD) forms of cathepsin D were analyzed in WT and *VPS45* KO HeLa clones by immunoblotting. Results are representative of three independent experiments.

4.1.8 VPS45 depletion results in endosomal trapping and impaired degradation of EGFR

The EGFR is widely used to assess vesicle transport along the degradative route. Stimulation with EGF results in the internalization of the receptor-ligand complex to early endosomes. Endosome maturation facilitates its transport from early endosomes to late endosomes and subsequent fusion with lysosomes induces its degradation. Thus, this receptor was used to study the impact of VPS45 on the cargo transport along the degradation pathway. To investigate EGFR trafficking and processing, WT and *VPS45* KO HeLa cells were serum-starved prior to stimulation with 100 ng/ml EGF for various time periods.

Immunoblotting revealed a substantial degradation of EGFR over time in control cells, in which most receptors were degraded after 50 minutes. In contrast, the loss of VPS45 impeded the efficient processing of EGFR (Figure 4-11).

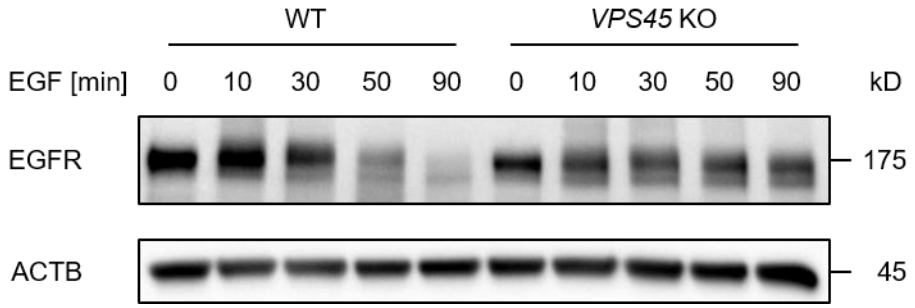

Figure 4-11 VPS45 depletion results in the inefficient degradation of EGFR.

Serum-starved WT and *VPS45* KO HeLa cells were stimulated with 100 ng/ml EGF for indicated time periods and EGFR levels were analyzed by immunoblotting. The blot is representative of three independent experiments.

To further analyze the trafficking of EGFR through the endosomal system, the fate of the receptor was visualized by confocal microscopy. Prior to stimulation with EGF, receptors localized to the cell surface in both WT and *VPS45* KO cells. After 10 minutes of EGF-mediated stimulation, receptors associated with EEA1-positive early endosomes in both WT and *VPS45* KO cells, showing an efficient endocytosis of the receptor-ligand complex. After 90 minutes, EGFR dissociated from EEA1 and signals decreased in control cells, demonstrating efficient processing in the degradative compartment. In line with the western blot studies (Figure 4-11), a minor overall decrease of EGFR signals was detected in the absence of VPS45 over time. In addition, the association of EGFR with EEA1-positive vesicles was prolonged, indicating trapping of the receptor in early endosomes (Figure 4-12).

In sum, these results indicate that VPS45 facilitates cargo transfer from early endosomes to the degradative compartment.

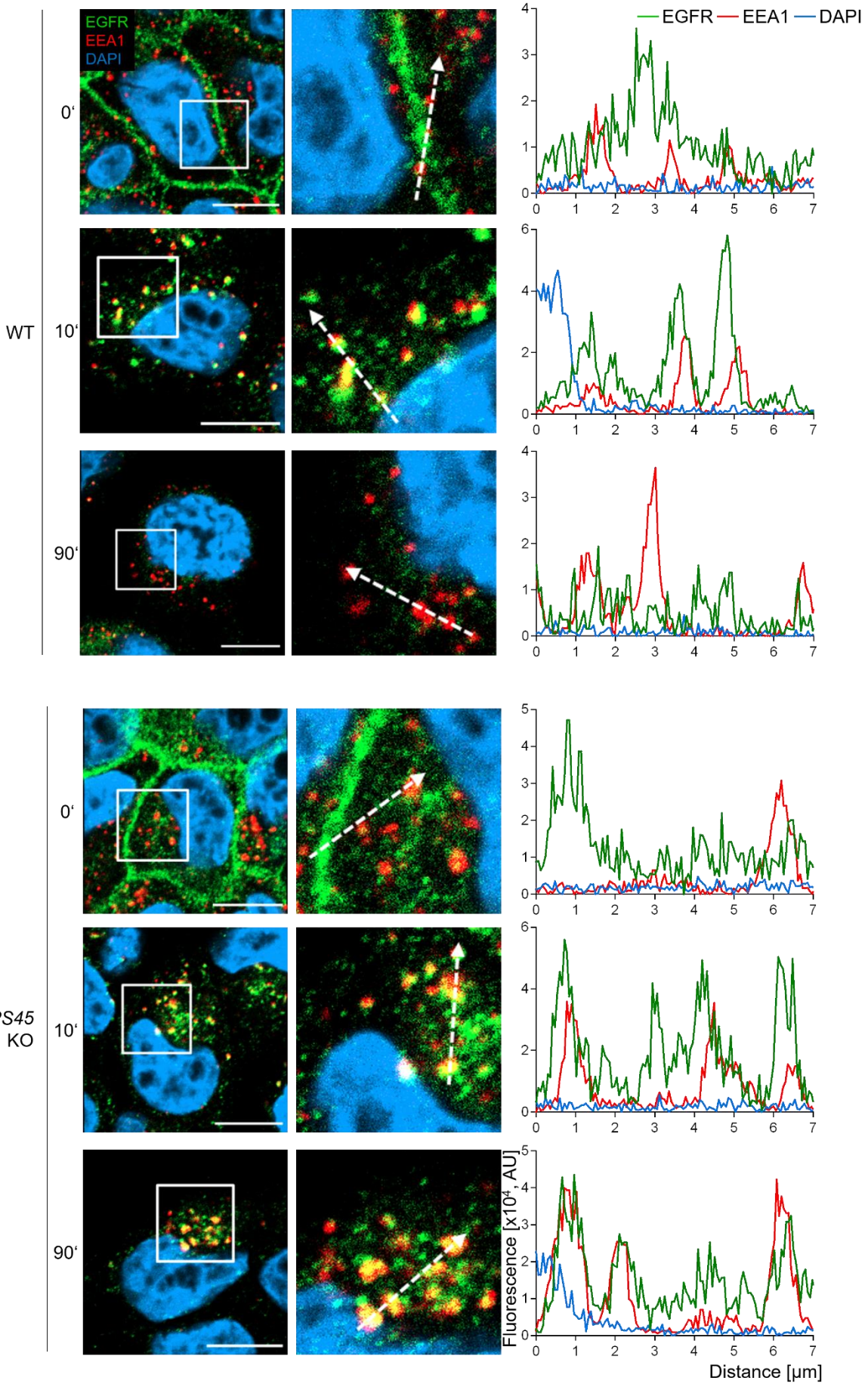
EGFR
EEA1
DAPI
0‘
10‘
90‘
WT
VPS45
KO
EGFR
EEA1
DAPI
Fluorescence [x10⁴, AU]
Distance [µm]

Figure 4-12 Loss of VPS45 leads to trapping of EGFR in early endosomes.

Serum-starved WT and *VPS45* KO HeLa cells were stimulated with 100 ng/ml EGF for indicated time periods, fixed, and costained with anti-EGFR and anti-EEA1 antibodies. Nuclei were visualized using DAPI. Zoom images represent magnified views of boxed areas (10 µm x 10 µm). Profile blots along the dashed arrow (7 µm) are shown on the right. Confocal microscopy images are representative of three independent experiments. Scale bars, 10 µm.

4.1.9 VPS45 deficiency leads to the prolonged association of G-CSFR with early endosomes and disturbed delivery to late endosomes

VPS45-deficient patients are neutropenic and do not respond to the treatment with G-CSF, even in high doses (Stepensky et al., 2013; Vilboux et al., 2013). Upon ligand-binding, G-CSFR is internalized and routed to early endosomal vesicles. Whereas only a few receptors are recycled to the cell surface, most of the receptor-ligand complexes are degraded in lysosomes (Irandoust et al., 2007). Since the EGFR trafficking in VPS45-deficient cells was aberrant, likely due to the defective fusion of endolysosomal vesicles, the hyporesponsiveness of VPS45-deficient patients to the therapy with G-CSF might be attributed to impaired trafficking of G-CSFR.

To test this hypothesis, WT and *VPS45* KO HeLa cells were transduced with G-CSFR-GFP fusion constructs and sorted to obtain equal G-CSFR expression levels. In both WT and *VPS45* KO cells comparable amounts of receptors accumulated at the cell surface and some of the cytoplasmic G-CSFR were associated with EEA1-positive early endosomes prior to stimulation with G-CSF. After 30 minutes of G-CSF stimulation, the association of G-CSFR with early endosomes was more prominent, particularly in VPS45-deficient cells. The difference was further strengthened over time, as receptors kept accumulating in early endosomes of *VPS45* KO cells after 90 minutes of stimulation, whereas this association decreased to the level prior to stimulation in WT cells. In accordance with previous results, G-CSFR colocalized with LAMP2-positive vesicles after 30 minutes of stimulation in control cells and further accumulated in late endosomes after 90 minutes. In striking contrast, routing of G-CSFR to late endosomes was impaired in VPS45-deficient cells: the receptor remained associated with EEA1-positive early endosomes instead (Figure 4-13). Hence, VPS45 depletion causes mistrafficking of the G-CSFR, which potentially explains the hyporesponsiveness of VPS45-deficient patients to the treatment with G-CSF.

These results further strengthen the notion that VPS45 is a critical regulator of receptor trafficking through the endosomal system and loss of VPS45 results in hampered delivery of cargos from endosomes to lysosomes.

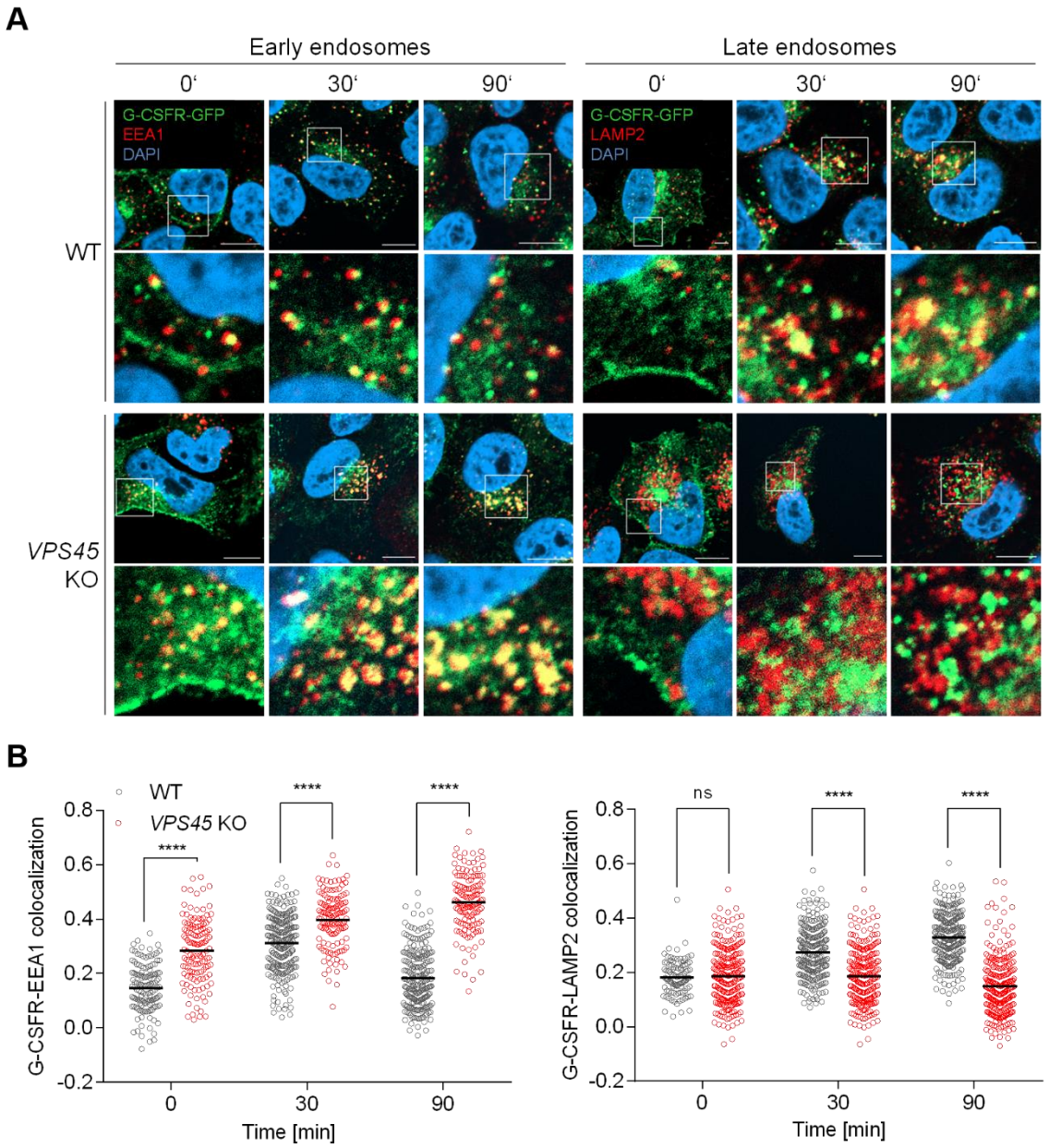

Figure 4-13 Loss of VPS45 results in the prolonged association of G-CSFR with early endosomes and impaired delivery to late endosomes.

(A) Serum-starved WT and *VPS45* KO HeLa clones stably expressing G-CSFR-GFP fusion proteins were stimulated with 100 ng/ml G-CSF for 10 minutes, followed by a chase for the indicated periods. Stimulated cells were fixed and stained with anti-EEA1 and anti-LAMP2 antibodies. DAPI was used as a nuclear stain. Zoom images represent magnified views of boxed areas (10 µm x 10 µm). Confocal microscopy images are representative of two independent experiments and two WT and two *VPS45* KO clones were used in each experiment. Scale bars, 10 µm. (B) Quantification of the G-CSFR-EEA1 and G-CSFR-LAMP2 colocalization of data shown in (A). Pearson‘s correlation coefficient is plotted on the y-axis. >100 cells were scored per genotype. Horizontal lines indicate the means. Statistical analysis was performed using one-way ANOVA with Tukey‘s multiple comparison test.

4.1.10 G-CSF-mediated phosphorylation of STAT3 is not affected in the absence of VPS45 in PLB-985 cells

Loss of VPS45 resulted in the trapping of G-CSFR in early endosomes and impaired its delivery to the degradative compartment in HeLa cells. Therefore, downstream signaling of G-CSFR might be affected. G-CSF activates multiple tyrosine kinases, of which STAT3 is a crucial regulator of granulopoiesis (Panopoulos et al., 2006; Nguyen-Jackson et al., 2010). Thus, G-CSF-mediated STAT3 signaling was analyzed in serum-starved myeloid PLB-985 cells, which express endogenous G-CSFR.

After 15 minutes of G-CSF stimulation, phosphorylation of STAT3 was induced in comparable amounts in WT and *VPS45* KO cells as shown by both flow cytometry and immunoblotting. Signals declined after 60 minutes of stimulation with G-CSF and were terminated in both VPS45-sufficient and VPS45-deficient cells after 120 minutes of ligand incubation (Figure 4-14).

Thus, the kinetics of STAT3 phosphorylation were comparable in WT and *VPS45* KO PLB-985 cells over time, indicating that G-CSF-mediated STAT3 signaling is intact in the absence of VPS45 in PLB-985 cells.

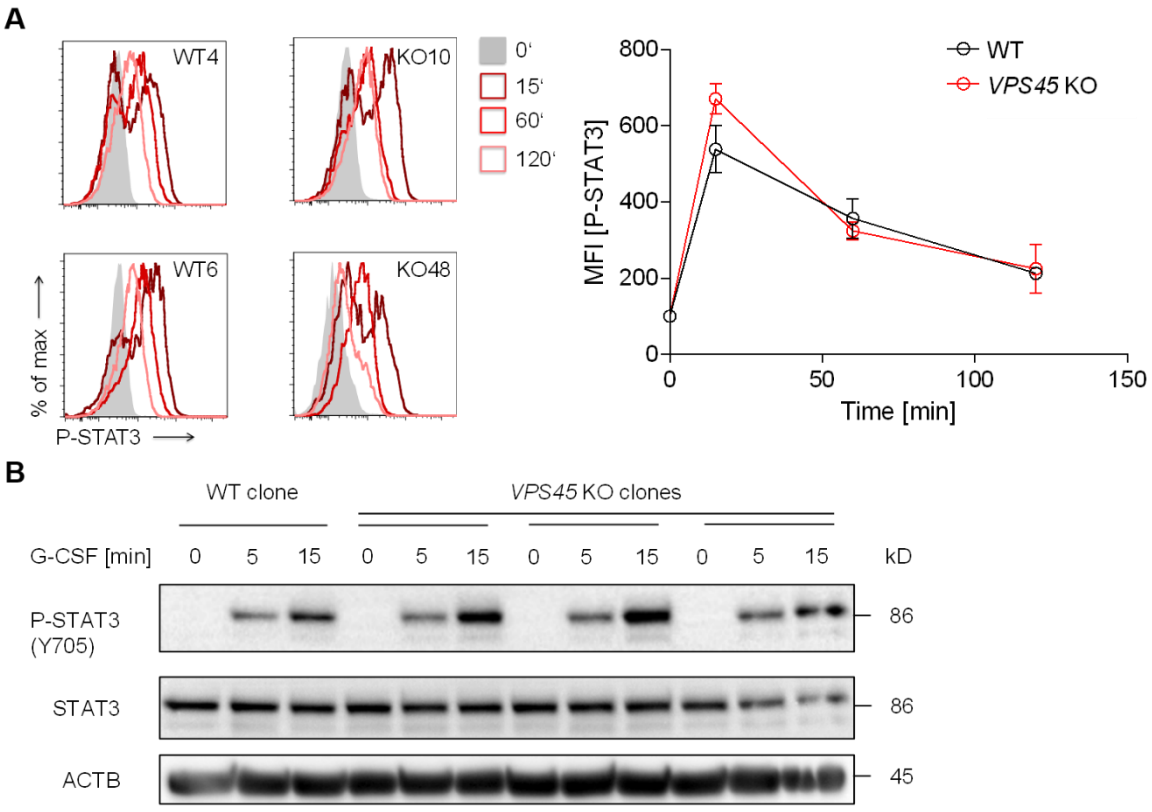

Figure 4-14 G-CSF-mediated phosphorylation of STAT3 is not affected in the absence of VPS45.

(A) Serum-starved WT and *VPS45* KO PLB-985 clones were stimulated with 100 ng/ml G-CSF for indicated periods and the levels of phosphorylated STAT3 were analyzed by flow cytometry. Representative histograms of two WT and two *VPS45* KO clones are shown.

The chart summarizes one representative experiment of four independent experiments using three WT and three *VPS45* KO clones. Error bars indicate the mean ± SD. (B) WT and *VPS45* KO PLB-985 clones were treated as in (A) and phosphorylation of STAT3 was analyzed by western blot. The blot is representative of two independent experiments.

4.1.11 VPS45 depletion results in defective early-to-late endosome maturation

Endosome maturation constitutes an essential step during cargo transport from early endosomes to the degradative compartment. The process of endosome maturation is accompanied by the conversion of early endosomal Rab5 to late endosomal Rab7 (Rink et al., 2005). In previous experiments, internalized cargo proteins were trapped in early endosomes in the absence of VPS45. These cargos failed to traffic to the late endosomal compartment, implying that endosome maturation is perturbed in VPS45-deficient cells. To investigate, whether the switch of Rab5 to Rab7 is affected in VPS45-deficient cells, the fate of fluorescent cargo was followed by live-cell imaging in HeLa cells cotransduced with mCherry-Rab5 and mCerulean-Rab7 fusion constructs.

The shape and distribution of early and late endosomal vesicles differed between control and *VPS45* KO cells. Rab5-positive and Rab7-positive vesicles appeared as ring-shaped structures in control cells, whereas such structures were not found in *VPS45* KO cells. In addition, these vesicles were clustered and disorganized in the absence of VPS45. This finding is in line with the perturbed intracellular organization of endolysosomal vesicles observed in previous experiments (Figure 4-3).

The cargo-containing vesicle revealed a steady decline of Rab5 and continuous increase of Rab7 in control cells over time, indicating that early endosomes were converted into late endosomes. On average, both Rab5 and Rab7 proteins were present at the same vesicle for approximately 7 minutes in control cells. The completed endosome maturation was demonstrated by a complete dissociation of Rab5 and the sole presence of Rab7. In the absence of VPS45, the cargo reached Rab5-positive early endosomes, further showing that there is no deficit in cargo internalization. In striking contrast to control cells, Rab5 remained associated with the cargo-containing vesicle throughout the recording in KO cells, showing that the cargo was trapped in early endosomes and is prevented from its delivery to late endosomes. Over time, Rab7 was recruited to Rab5-positive endosomes, however, this recruitment was slower as compared to control cells. Importantly, Rab5 did not dissociate from the cargo-containing vesicle in KO cells. Consequently, endosome maturation was never completed, demonstrating a defective early-to-late endosome conversion in the absence of VPS45 (Figure 4-15).

These data show that VPS45 is crucial for endosome maturation and cargo delivery to the degradative compartment.

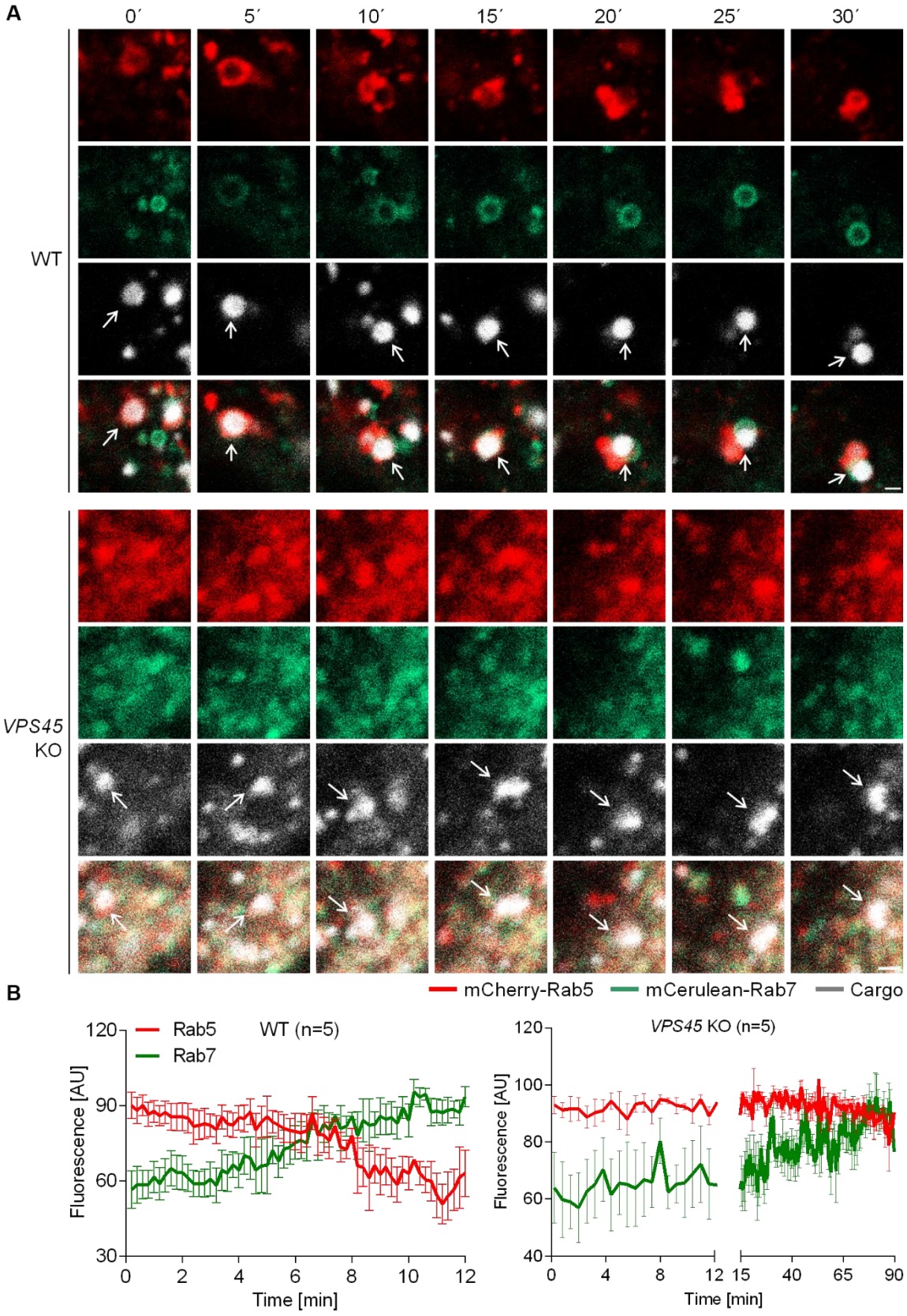

Figure 4-15 Endosome maturation is impaired in the absence of VPS45.

WT and *VPS45* KO HeLa clones were infected with lentiviruses to coexpress mCherry-Rab5 and mCerulean-Rab7. The dynamic changes of Rab5-positive and Rab7-positive

vesicles were imaged during the uptake and intracellular transport of fluorescent cargo (microspheres-633). (A) Representative images of cargo trafficking in WT and *VPS45* KO clones are shown. Images are representative of at least five independent experiments. Scale bars, 1 µm. (B) The corresponding total fluorescence traces of Rab5 (red) and Rab7 (green) over time averaged from five independent experiments are shown. For visualization purposes only every second frame is shown for *VPS45* KO clones for the first 12 minutes. Error bars indicate mean ± SEM.

Notably, endogenous expression levels of Rab5 and Rab7 were not affected in neither HeLa nor PLB-985 cells in the absence of VPS45 (Figure 4-16).

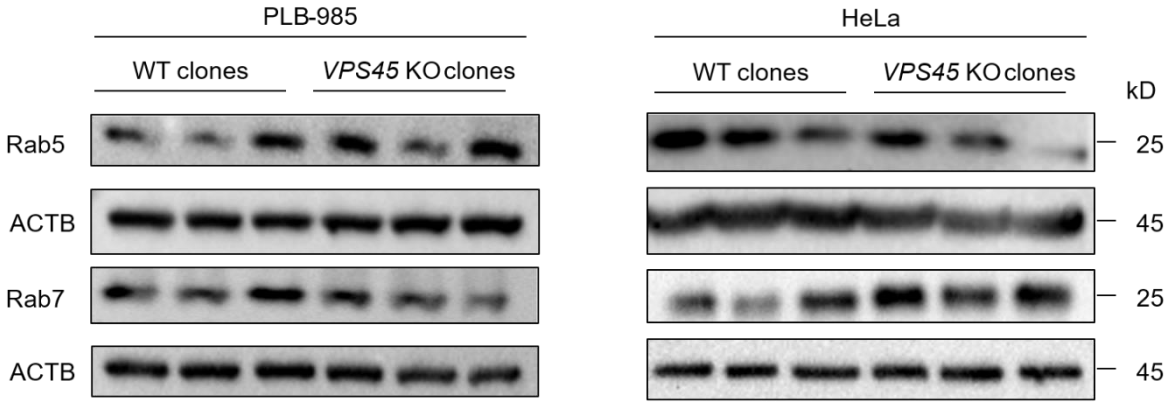

Figure 4-16 Loss of VPS45 does not affect the endogenous expression of Rab5 and Rab7.

Western blot analysis of Rab5 and Rab7 protein levels in WT and *VPS45* KO HeLa and PLB-985 clones. The blots are representative of two independent experiments.

4.1.12 Characterization of endolysosomal vesicles

To further characterize the endolysosomal compartment, cells were costained with vesicle-specific markers in the presence and absence of VPS45. Early endosomes are typically marked by EEA1 and Rab5, late endosomes by LAMP2, and lysosomes by LAMP1. In both WT and *VPS45* KO HeLa clones, the early endosomal markers EEA1 and Rab5 were present on the same vesicles. Some colocalization was observed between EEA1 and LAMP2, whereas EEA1 and LAMP1 stained separate vesicles in both WT and *VPS45* KO HeLa cells (Figure 4-17).

Thus, the loss of VPS45 seems to affect the intracellular organization of the vesicles rather than the identity of endolysosomal vesicles.

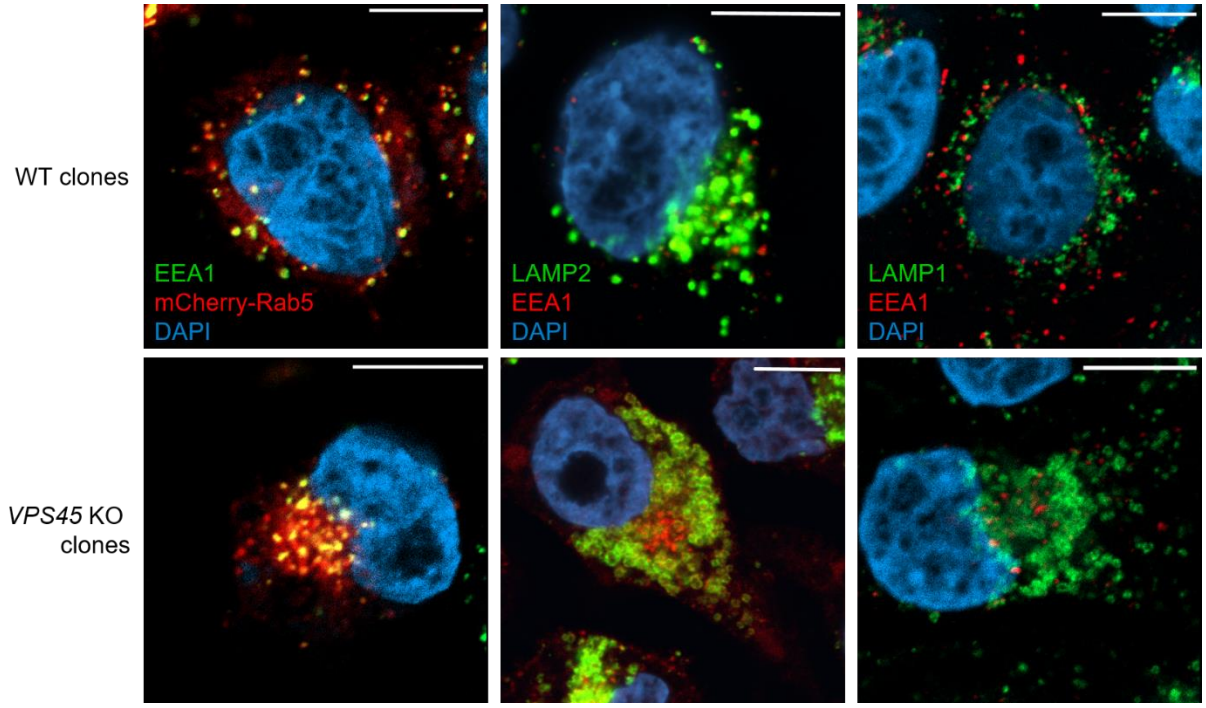

Figure 4-17 Characterization of endosomal vesicles.

Coimmunostaining of early endosomes (endogenous EEA1 and overexpressed mCherry-Rab5), late endosomes (endogenous LAMP2), and lysosomes (endogenous LAMP1) in WT and *VPS45* KO HeLa clones. Nuclei were visualized by DAPI. Confocal microscopy images are representative of two independent experiments. Scale bars, 10 µm.

4.1.13 Loss of VPS45 does not affect the structure of the Golgi apparatus

Studies in yeast propose a function of Vps45p in the transport of cargos from the Golgi apparatus to the prevacuolar compartment (Piper et al., 1994; Cowles et al., 1994; Bryant et al., 1998). Thus, the absence of VPS45 might not only disturb the morphology and distribution of endolysosomal vesicles but also affect the organization of the Golgi apparatus. Accordingly, the Golgi compartment was stained by GM130 and analyzed in the presence and absence of VPS45 in HeLa cells. Confocal microscopy images did not reveal any morphological differences of the Golgi apparatus between WT and VPS45-depleted HeLa cells (Figure 4-18).

This result indicates that the loss of VPS45 specifically affects the endolysosomal compartment.

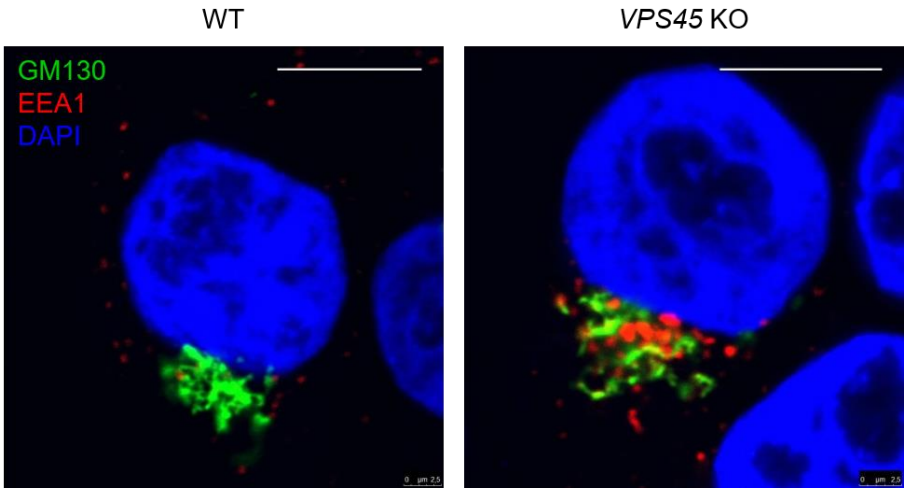

Figure 4-18 The structure of the Golgi apparatus is not affected in the absence of VPS45.

Immunofluorescent staining to visualize the Golgi apparatus (GM130), early endosomes (EEA1), and the nucleus (DAPI). Confocal microscopy pictures are representative of two independent experiments. Scale bars, 10 µm.

4.1.14 Autophagosomal marker LC3-II is enhanced in VPS45-deficient cells

Autophagy constitutes another intracellular degradative pathway, which is crucial for maintaining the cell homeostasis. Cellular components and organelles targeted for disposal are sequestered into double-membrane vesicles in the cytoplasm. These autophagosomes eventually fuse with lysosomes to proteolytically process and clear their content (Eskelinen and Saftig, 2009; Reggiori and Ungermann, 2017). Both degradation pathways do not only share lysosomal degradation as the endpoint, but also rely on the proper function of the Rab5 protein (Ravikumar et al., 2008). Since the loss of VPS45 resulted in decreased expression of the Rab5 effector Rabenosyn-5 and affected the process of endosome maturation, it could also impact on the autophagic equilibrium. Thus, the conversion of LC3-I to LC3-II was examined as an indicator of autophagosome formation.

Immunoblotting revealed significantly increased amounts of LC3-II in the absence of VPS45 (Figure 4-19).

These results indicate that either the synthesis of autophagosomes is elevated in VPS45-silenced conditions or the turnover of autophagosomes is decreased. Thus, VPS45 seems to be a regulator of autophagy, however, more detailed studies are required to define the precise role of VPS45 in autophagy.

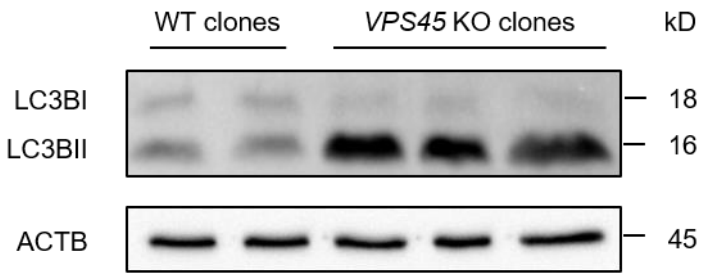

Figure 4-19 Loss of VPS45 results in increased levels of LC3BII.

Western blot analysis of expression levels of LC3BI and LC3BII in WT and *VPS45* KO HeLa cells. One experiment of three independent experiments is shown.

4.1.15 Rate of apoptosis is increased in the absence of VPS45

To investigate whether the overall cell viability is affected by the loss of VPS45, WT and *VPS45* KO HeLa clones were stained with propidium iodide (PI) and analyzed by flow cytometry according to Nicoletti's protocol (Riccardi and Nicoletti, 2006).

Cells lacking VPS45 revealed increased apoptotic fractions in comparison to control cells (Figure 4-20). This is in line with findings in the patient's neutrophils and bone marrow myeloid cells, which showed an elevated apoptosis rate (Stepensky et al., 2013; Vilboux et al., 2013).

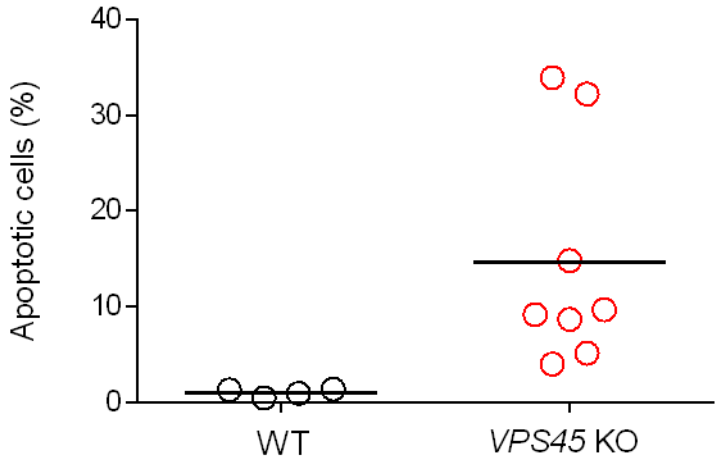

Figure 4-20 Loss of VPS45 results in increased apoptosis.

WT and *VPS45* KO HeLa cells were incubated with Nicoletti buffer for 2 hours at 4° C in the dark and PI-stained cells were analyzed by flow cytometry. Data are pooled from two experiments with two WT and four *VPS45* KO clones, respectively. Horizontal lines indicate the means.

4.2 Characterization of mutant VPS45

Besides generating cell lines with a complete lack of VPS45, a knockin of the patient-associated mutations in HeLa and PLB-985 cells was attempted. However, no correctly modified clones were isolated. Thus, WT and mutant FLAG or GFP fusion proteins were generated to study the functional impact of the patient mutations on the VPS45 protein.

4.2.1 *VPS45* mutations do not alter the subcellular localization of VPS45 proteins

To test whether patient mutations affect the intracellular localization of VPS45, HeLa cells were transduced to express either WT or mutant VPS45 fused to C-terminal GFP. Analysis by confocal microscopy revealed no localization differences between WT and mutant VPS45 proteins, as all variants revealed a network-like distribution throughout the cytoplasm (Figure 4-21). Thus, neither of the patient-associated mutations altered the intracellular localization of VPS45.

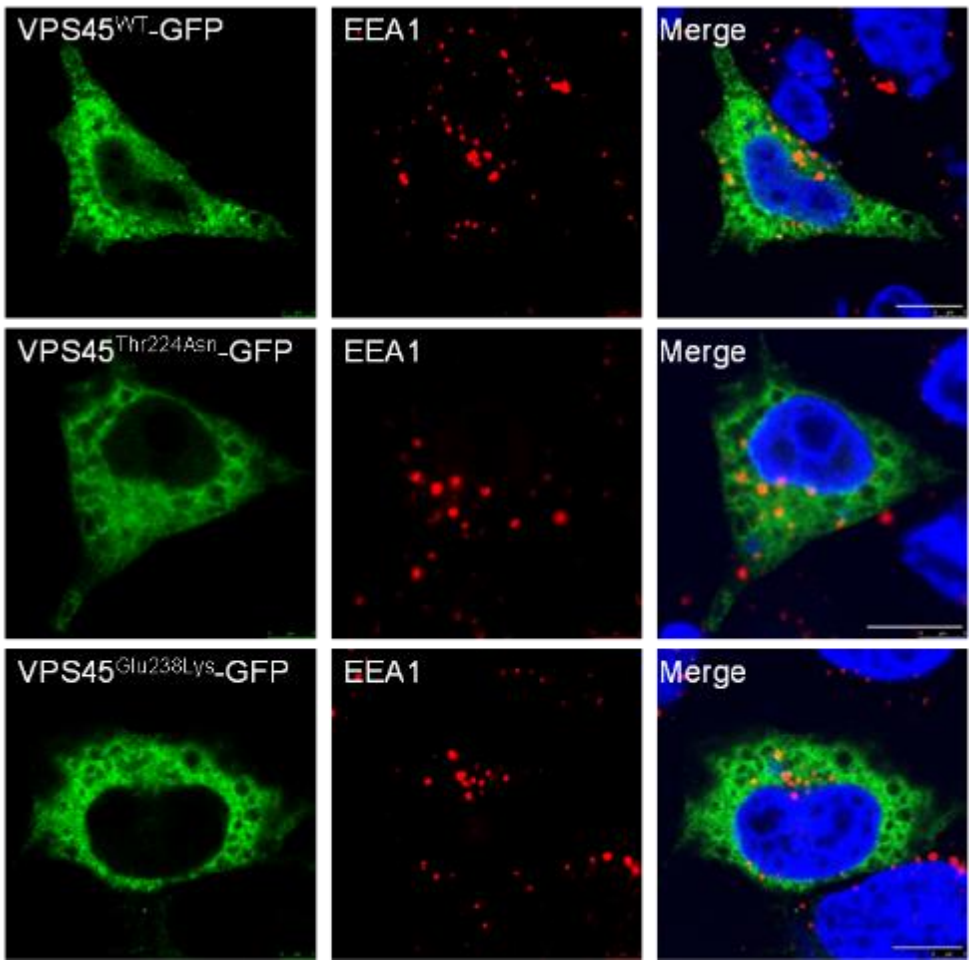

Figure 4-21 Patient-associated mutations do not alter the subcellular localization of VPS45.

HeLa cells were transduced with either *Vps45*^{WT} or the *VPS45*^{Thr224Asn} and *VPS45*^{Glu238Lys} mutants to stably express GFP fusion proteins and stained with anti-EEA1 antibodies. DAPI was used as a nuclear stain. Confocal microscopy images are representative of two independent experiments. Scale bars, 10µm.

4.2.2 Mutations in *VPS45* are hypomorphic

When ectopically expressing WT and mutant VPS45 proteins, significantly lower levels of mutant VPS45 proteins were detected by immunoblotting (Figure 4-22). This result is consistent with studies in patient cells and indicates that both mutations destabilize the VPS45 protein (Stepensky et al., 2013; Vilboux et al., 2013).

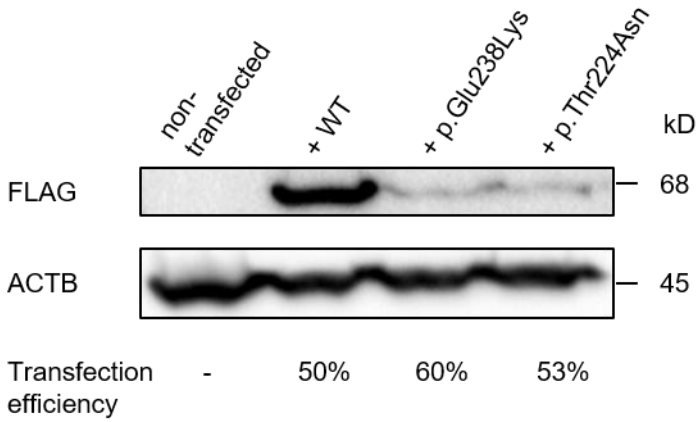

Figure 4-22 Mutated VPS45 proteins are less expressed.

HEK293T cells were transfected with WT or indicated mutant constructs carrying a C-terminal FLAG tag and the expression of proteins was analyzed by immunoblotting using anti-FLAG antibodies. MFI were comparable and transfection efficiencies of FLAG-tagged VPS45 constructs are indicated below. The blot is representative of three independent experiments.

To investigate whether mutated VPS45 proteins are still functional, the interaction with the known binding partners Rabenosyn-5 and Syntaxin16 was analyzed. HEK293T cells were transfected with either C-terminal FLAG-tagged WT or mutant VPS45 constructs and sorted for low and high expression levels. WT and mutant proteins were immunoprecipitated using FLAG beads and the capacity to capture the binding partners Rabenosyn-5 and Syntaxin16 was analyzed by immunoblotting. Copurification results confirmed the interaction of WT VPS45 with Rabenosyn-5 and Syntaxin16, respectively. Moreover, mutant VPS45 proteins were able to pull down both interaction partners, but to a lesser extent (Figure 4-23).

These results indicate that the mutations in *VPS45* do not completely abolish the interaction with its binding partners.

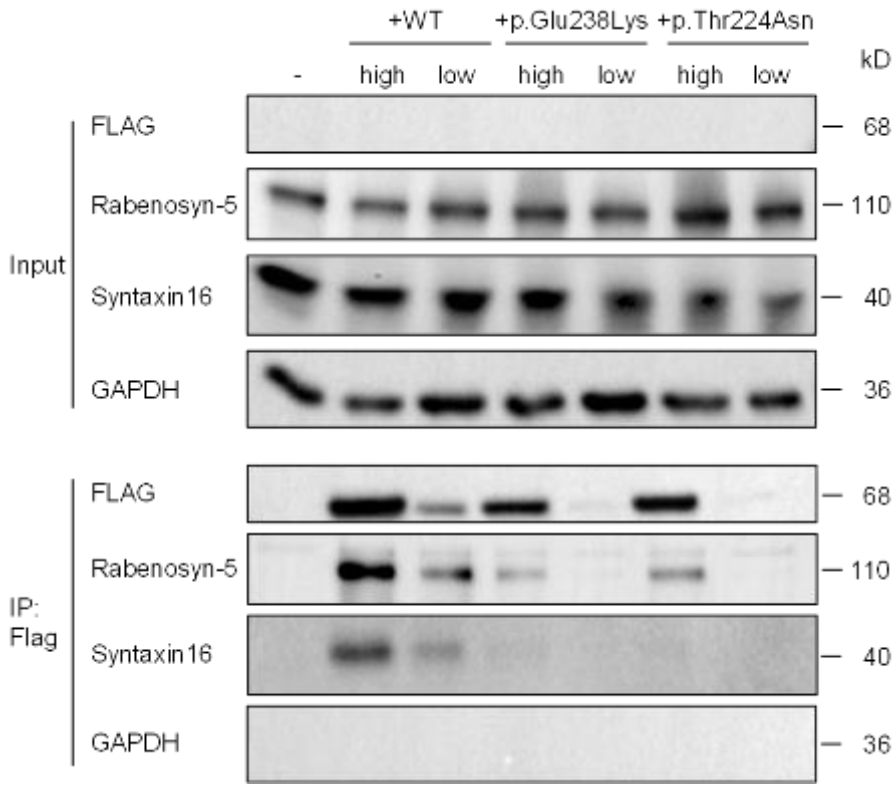

Figure 4-23 Mutant VPS45 binds to interaction partners to a lesser extent.

Non-transfected HEK293T cells or HEK293T cells expressing either low or high levels of C-terminal FLAG-tagged WT or indicated mutant VPS45 proteins were subjected for immunoprecipitation by anti-FLAG beads and western blotting. GAPDH was used as a loading control. Representative data of two independent experiments are shown.

To further analyze the functionality of mutant VPS45 proteins, *VPS45* KO clones were reconstituted with either WT or mutant VPS45 proteins and the capacity to process DQ OVA in the degradative compartment was investigated. As shown in 4.1.6, degradation rates were lower in *VPS45* KO cells as compared to WT cells. Importantly, the processing of DQ OVA into fluorescent peptides was comparable between WT cells and KO cells reconstituted with either WT or mutant VPS45 proteins (Figure 4-24).

These results show that mutant VPS45 proteins retain some functionality. Probably, overexpression provides *VPS45* KO cells with enough amounts of partially functional mutant proteins to recover cargo transport through the endosomal system and degradation in lysosomes.

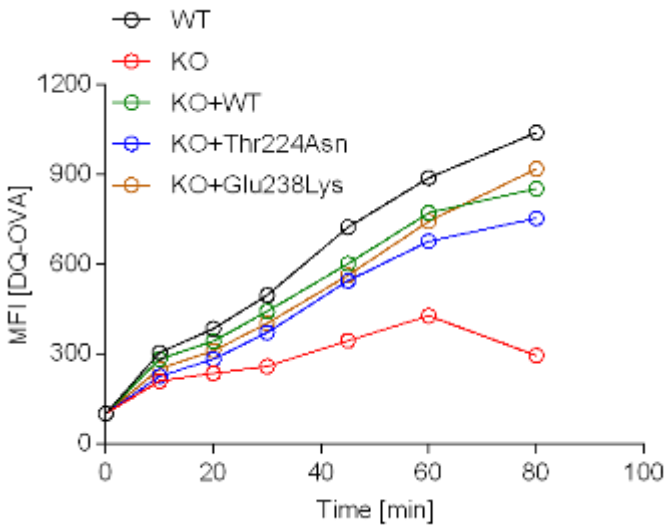

Figure 4-24 Reconstitution of KO cells with WT or mutant VPS45 restores cargo processing.

VPS45 KO HeLa clones were reconstituted with either WT or mutated VPS45 and processing of DQ OVA was analyzed by flow cytometry as the change in MFI from baseline (fluorescence at 4 °C). One representative experiment of three independent experiments is shown.

EEA1-positive early endosomes and LAMP2-positive late endosomes were aggregated in the absence of VPS45. In addition, late endosomal vesicles were enlarged in the absence of VPS45 (Figure 4-3). After reconstitution of *VPS45* KO HeLa cells with either the WT or p.Glu238Lys mutant VPS45, the morphology and distribution of early and late endosomes resembled control cells (Figure 4-25 and Figure 4-3).

Thus, both WT and mutant VPS45 are capable to restore the intracellular vesicle organization.

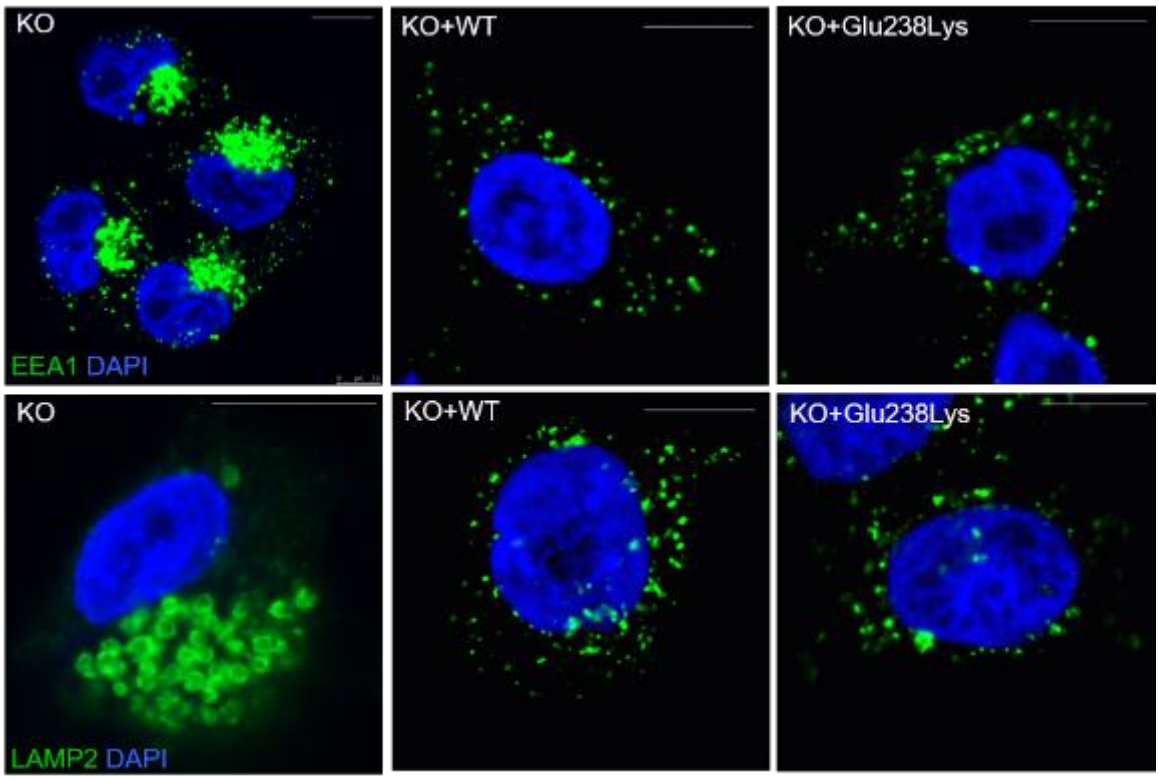

Figure 4-25 Reconstitution of KO cells with WT or mutant VPS45 restores the intracellular organization of endolysosomal vesicles.

VPS45 KO HeLa clones were reconstituted with either WT or the VPS45^{Glu238Lys} mutant and stained for early endosomes (EEA1) and late endosomes (LAMP2). DAPI was used to visualize the nucleus. Confocal microscopy images are representative of two independent experiments. Scale bars, 10 µm.

Noticeably, overexpression of either WT or mutant VPS45 proteins induced the formation of huge vesicles (Figure 4-26). The enlarged structures are likely due to the artificial overexpression resulting in an excess amount of VPS45 proteins.

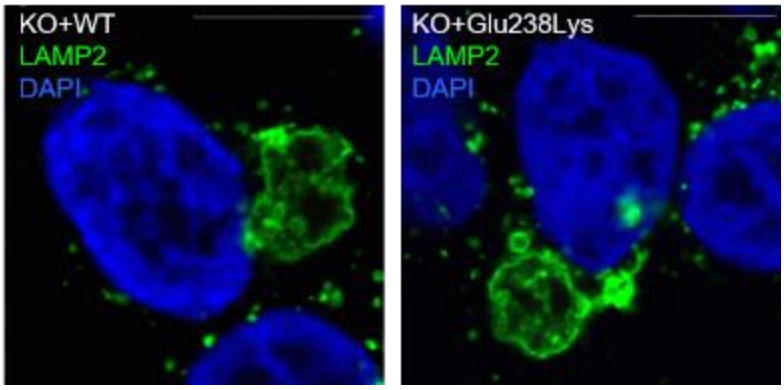

Figure 4-26 Overexpression of WT or mutant VPS45 proteins induces the formation of huge vesicles.

VPS45 KO HeLa clones were reconstituted with either WT or mutated VPS45 and stained for late endosomes (LAMP2). DAPI was used to visualize the nucleus. Confocal microscopy images are representative of two independent experiments. Scale bars, 10 µm.

These results demonstrate that the process of vesicle formation is tightly regulated and interfering with *VPS45* expression results in the disturbed organization of the endolysosomal compartment. Importantly, these results imply that the effects observed in *VPS45* KO cells are not due to off-target effects of CRISPR/Cas9 editing, as the expression of WT and mutant VPS45 selectively reversed the effects of VPS45 depletion.

4.3 Generation and characterization of VPS45-deficient mice

The impact of VPS45 during mammalian development is unknown. To further examine the biological significance of VPS45 in a mammalian model *in vivo*, a KO mouse model was generated using the KO-first strategy provided by the European conditional Mouse Mutagenesis Program (EUCOMM) (Skarnes et al., 2011). This strategy allows the rapid conversion of the KO allele into a conditional KO allele utilizing FLP/FRT and Cre/loxP systems, thus providing flexibility in case the gene of interest plays a critical role during embryo development and loss of gene expression results in embryonic lethality. Since disease-related mutations in *VPS45* are hypomorphic in humans, it was plausible that a homozygous KO of *Vps45* is not compatible with life in mice.

The KO-first construct contains a flippase recognition target (FRT) site followed by an IRES-lacZ cassette and a loxP site. A neomycin resistance cassette is inserted downstream of the first loxP site, followed by a second FRT and loxP site. The targeted exon precedes a third loxP site. The mutagenic KO-first construct is inserted into the intron of a critical exon. The cassette contains a splice acceptor, which results in a null allele (tm1a). By exposing the KO-first construct to the FLP recombinase, the IRES-lacZ and neomycin cassettes, which are flanked by FRT sites, are excised, resulting in the conversion of the tm1a allele into a conditional allele (tm1c). Exposure of the conditional allele to a Cre recombinase results in the excision of the critical exon 4 of *Vps45*, thus creating a frameshift and reverting the conditional allele into a null allele (tm1d) (Figure 4-27).

Another possibility the KO-first strategy offers, is to generate a reporter-tagged deletion allele to study the endogenous expression pattern of the gene of interest. Instead of converting the KO-first allele into a conditional allele using the FLP/FRT system, mice harboring a KO-first allele are crossed with Cre-deleter mice to remove the neomycin resistance cassette and the critical exon, which are flanked by loxP sites. Consequently, these mice are null for the gene of interest and possess a lacZ gene expression reporter. The generation of the reporter-tagged deletion tm1b allele was not implemented in this study.

4.3.1 Generation of a *Vps45* KO mouse model

The presence of the KO-first targeting vector was verified by PCR analysis using a combination of two primer pairs. Primer set 1 amplified the WT allele, whereas primer set 2 amplified the targeting vector (Figure 4-27 and Figure 4-28). Primer sequences, the PCR reaction setup, and thermocycling conditions are specified in Table 3-16, Table 3-17, and Table 3-18, respectively.

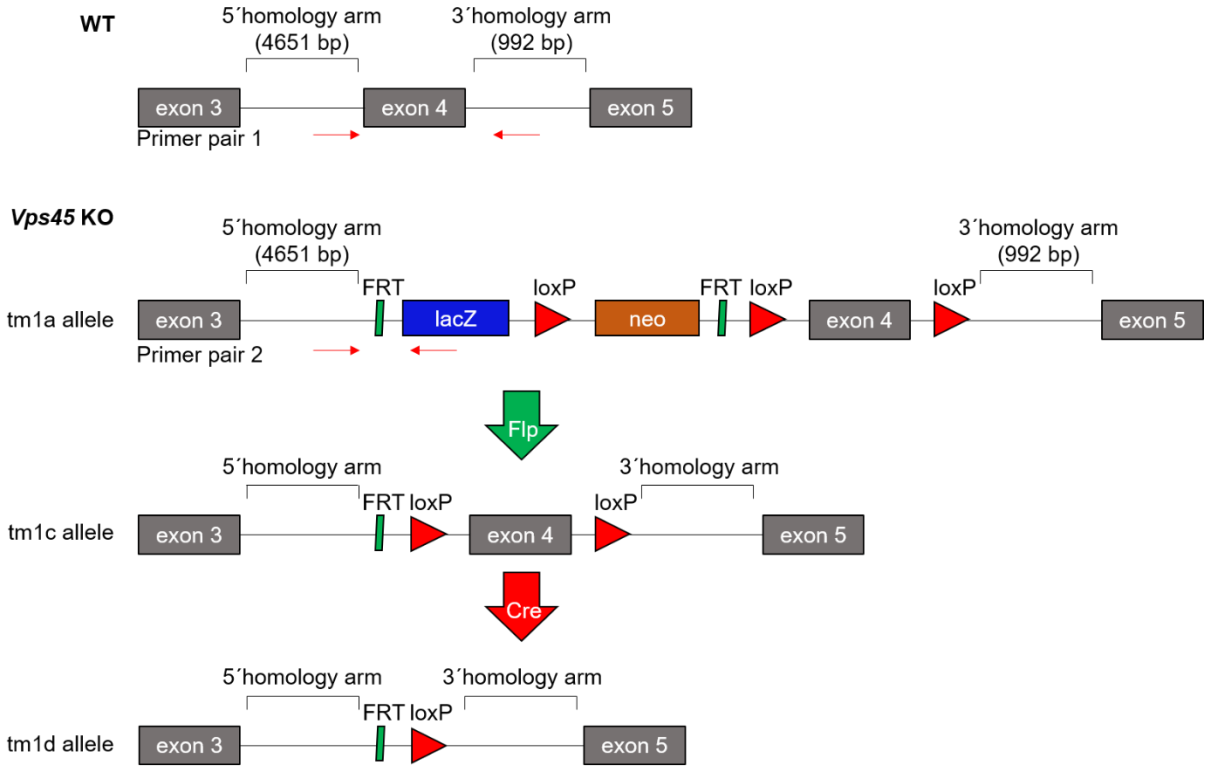

Figure 4-27 KO-first strategy.

Schematic representation of the *Vps45* KO-first strategy, depicting the integration of the targeting cassette in the intron upstream of exon 4 of *Vps45*. Primer sets used to identify wild type (WT) and *Vps45* knockout (KO) alleles are indicated as primer pairs 1 and 2.

4.3.2 VPS45 is essential for mouse embryogenesis

In order to obtain homozygous *Vps45* KO mice, mice heterozygous for the KO-first targeting allele were intercrossed. Genotypes of 148 female and male pups from 24 litters of heterozygous breeding pairs were determined by PCR analysis as described in 4.3.1. Of these pups, 37% (55 mice) were WT and 63% (93 mice) were heterozygous for the *Vps45* null allele. None of the pups was identified as homozygous for the *Vps45* null allele, indicating that the global deletion of VPS45 is embryonic lethal in mice (Figure 4-28).

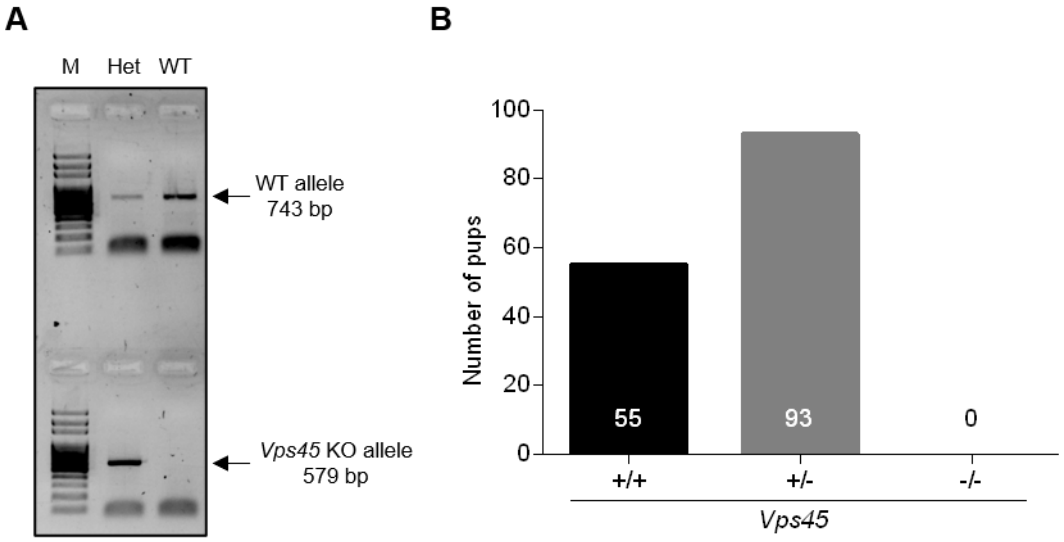

Figure 4-28 Lack of VPS45 causes embryonic death in mice.

(A) Representative PCR-based genotyping results of postnatal progeny derived from *Vps45* heterozygous intercrosses. Primer sets 1 and 2 used to identify WT and heterozygous (Het) mice are shown in Figure 4-27. M: DNA marker. (B) Genotyping results of 148 postnatal pups derived from *Vps45* heterozygous intercrosses.

4.3.3 *Vps45* KO embryos die around E7.5

To define the stage of fetal development in which VPS45 plays an essential role, a timed breeding of heterozygous *Vps45* mice was set up and embryos were dissected from pregnant females at different days post-coitus. Most of the embryos isolated at E11 and E13 showed an age-appropriate development, indicating either WT or heterozygous genotypes. However, some of the E11 and E13 embryos were markedly reduced in size, suggestive of an aberrant development. In contrast, no differences in the outer appearance were observed for E7.5 embryos (Figure 4-29).

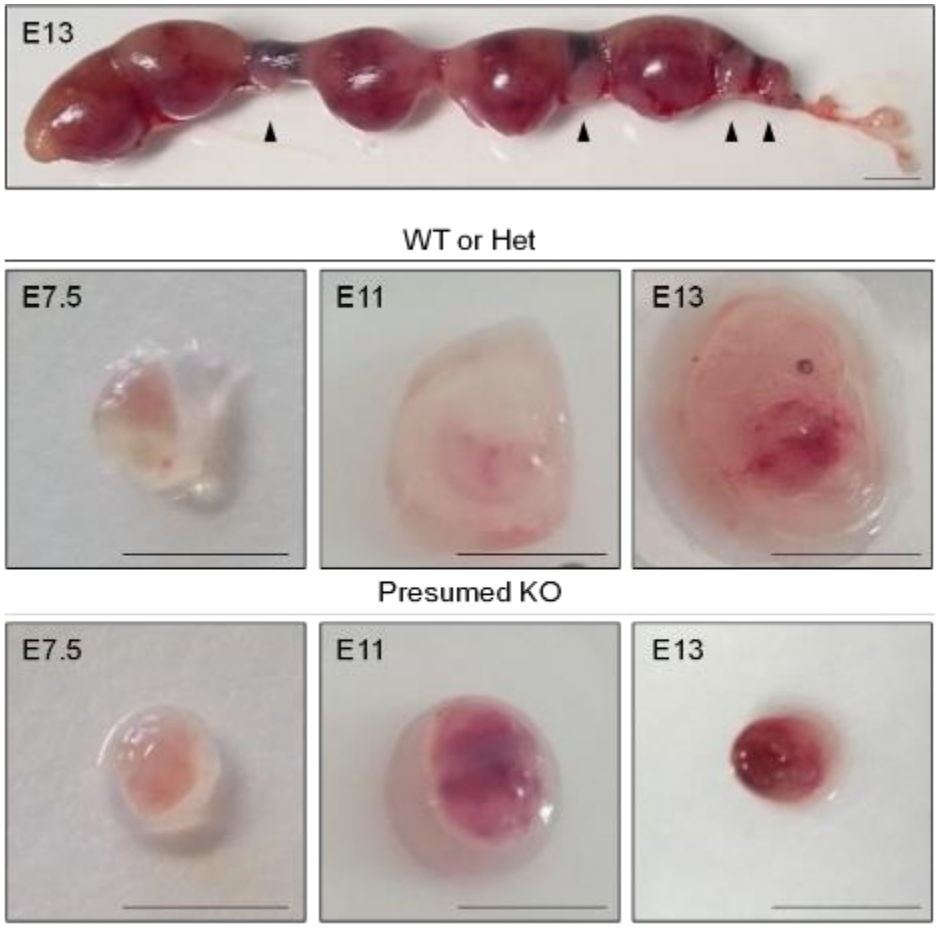

Figure 4-29 VPS45-deficient embryos die at an early stage of embryonic development.

A representative uterus derived from heterozygous intercrosses dissected at E13. Arrowheads show smaller implantation sites, indicating that embryos either died or were severely delayed in development. Scale bar, 5 mm. Representative pictures of excised embryos derived from *Vps45* heterozygous intercrosses at E13, E11, and E7.5 are shown below. Scale bars, 5 mm.

Genotyping of E13 embryos suggested that the non-developing embryos were homozygous for the *Vps45* null allele (Figure 4-30).

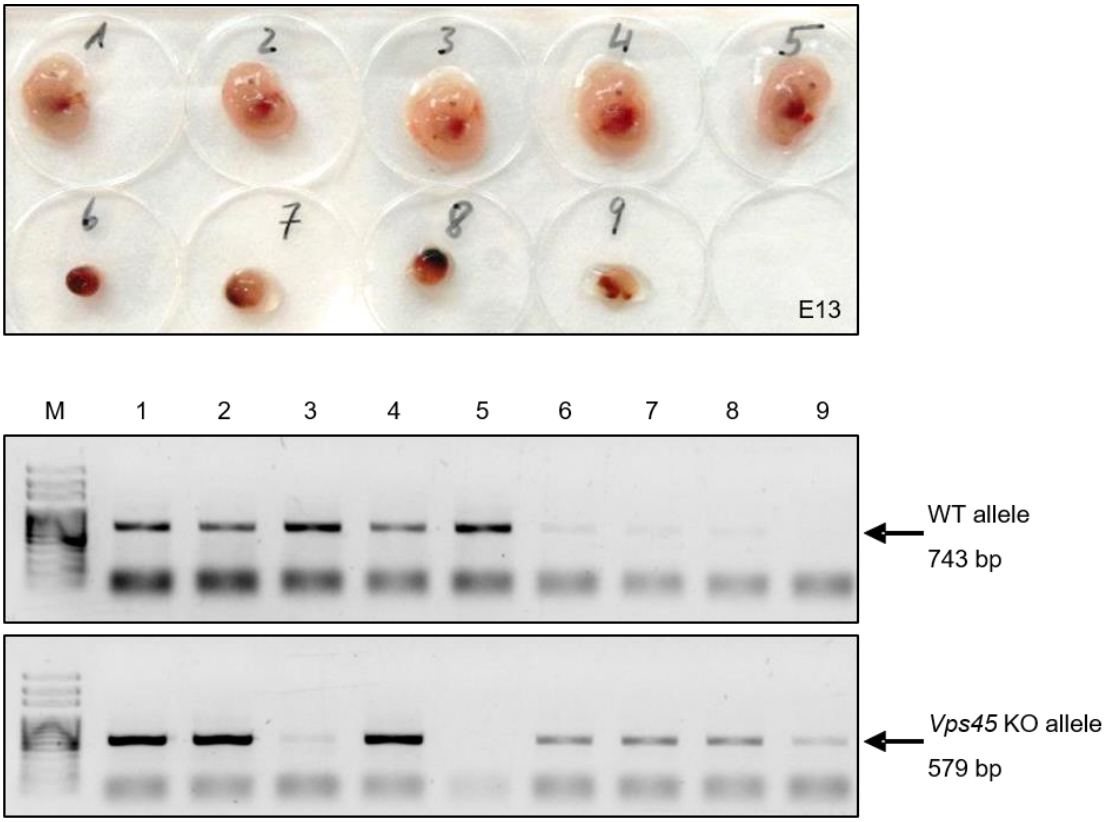

Figure 4-30 Genotyping of VPS45-sufficient and VPS45-deficient embryos.

Genotyping results of E13 embryos derived from *Vps45* heterozygous intercrosses. To remove maternal material, CD45+ cells were depleted from small embryos prior to lysis. Primer sets used to identify WT and *Vps45* KO alleles are shown in Figure 4-27. M: DNA marker.

To further narrow down the stage of fetal development, in which the loss of VPS45 resulted in embryonic death, earlier days of embryogenesis were assessed. At E7.5 no apparent differences in size and shape of embryos were observed (Figure 4-29). Thus, PAS-stained sections of paraffin-embedded E7.5 embryos were analyzed. Some of the embryos displayed organized embryonic ectodermal and endodermal structures. In addition, the formation of the mesoderm, which usually develops between the ectoderm and visceral endoderm (Pereira et al., 2011), was observed, indicating that these embryos were either WT or heterozygous for the *Vps45* null allele. In contrast, cell layers of suspected *Vps45* KO embryos revealed an overall smaller cell mass and appeared as disorganized structures, making the distinction of germ layers difficult (Figure 4-31).

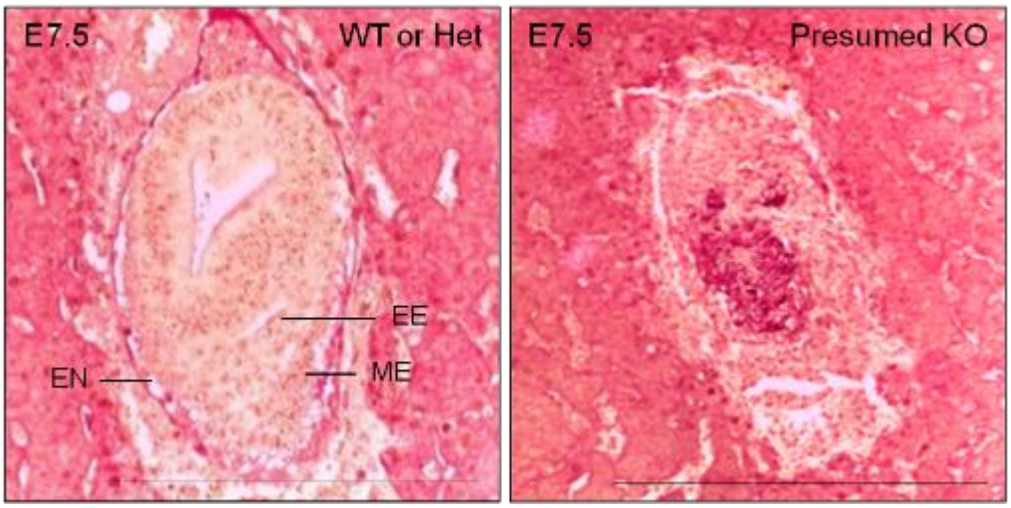

Figure 4-31 VPS45-deficient embryos die at around E7.

PAS-stained cross-sections of paraffin-embedded E7.5 embryos derived from *Vps45* heterozygous intercrosses showing embryonic ectoderm (EE), endoderm (EN), and mesoderm (ME). Scale bars, 1 mm.

These results demonstrate that a complete loss of VPS45 results in embryonic death and affects an early stage of mouse embryogenesis.

4.3.4 Generation of tissue-specific KO mouse models

As VPS45-deficient patients suffer from severe neutropenia, the aim was to investigate the impact of VPS45 on neutrophil granulocytes. The complete loss of VPS45 resulted in an early embryonic lethality in mice and prevented from studying the role of VPS45 for neutrophil differentiation. Thus, two tissue-specific KO mouse lines were generated. The KO-first allele was further converted into a conditional allele (tm1c) by exposure to the FLP recombinase. FLP-mediated recombination of the FRT sites resulted in the removal of the neomycin selection cassette and the splice acceptor. Thus, WT gene expression was restored and the critical exon 4 of *Vps45* was flanked by loxP sites (Figure 4-27). By breeding mice with *Vps45* floxed alleles to LysM-Cre and Vav-Cre mice, the deletion of the critical exon 4 of *Vps45* was induced in the myeloid and hematopoietic compartments, respectively (tm1d; Figure 4-27).

The efficiency of VPS45 depletion in sorted CD11b+Gr-1+ myeloid cells of *Vps45*$^{fl/fl;LysM\text{-}Cre}$ mice and bone marrow cells of *Vps45*$^{fl/fl;Vav\text{-}Cre}$ conditional KO mice was tested by immunoblotting. Surprisingly, both conditional KO mouse lines exhibited an inefficient deletion of VPS45 (Figure 4-32). Thus, a comprehensive analysis of neutrophil differentiation was prevented in these mouse models.

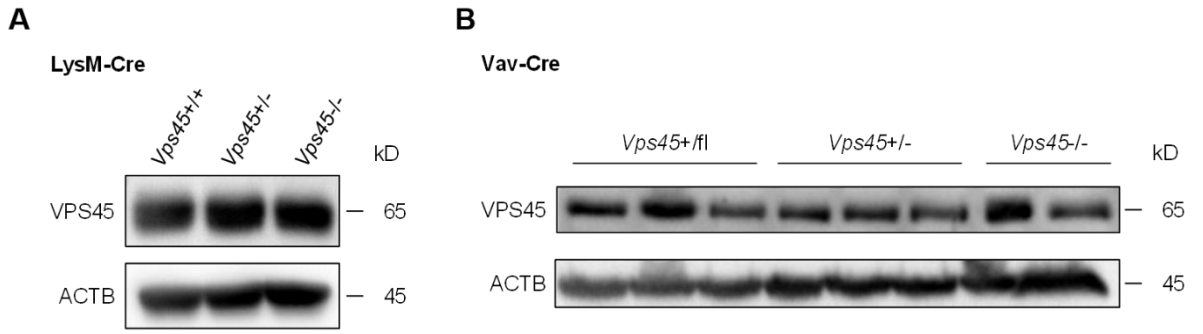

Figure 4-32 Inefficient deletion of VPS45 in conditional KO mouse models.

Immunoblot analysis of VPS45 expression levels in LysM-Cre conditional KO mice. The blot is representative of one independent experiment. (D) Immunoblot analysis of VPS45 expression levels in Vav-Cre conditional KO mice. The blot is representative of four independent experiments.

4.3.5 *Ex vivo* deletion of VPS45 inhibits the differentiation of neutrophils

The inefficient deletion of VPS45 in conditional mouse models impeded investigations of the impact of VPS45 on neutrophils *in vivo*. In order to circumvent this obstacle, VPS45 was depleted *ex vivo* using Cre-expressing retroviruses.

LSK ($Lin^- Sca\text{-}1^+ c\text{-}Kit^+$) cells were sorted from bone marrow cells of either $Vps45^{WT/WT}$, $Vps45^{Flox/WT}$ (controls), or $Vps45^{Flox/Flox}$ mice (Figure 4-33). Control (Cre-IRES-GFP-) or *Vps45* null (Cre-IRES-GFP+) cells were obtained by retroviral transduction with the Cre recombinase and showed comparable transduction efficiencies. LSK cells were cocultured with OP9 bone marrow stromal cells to support granulopoiesis (Lieber et al., 2004). To determine the deletion efficiency, *Vps45* mRNA of sorted CD11b+Gr-1+ myeloid cells was analyzed at day 7 of *in vitro* coculture. As expected, homozygous WT, heterozygous floxed, and homozygous floxed Cre-expressing neutrophils had the highest, intermediate, and lowest *Vps45* mRNA levels, respectively, while *Vps45* mRNA levels were not affected in Cre-negative myeloid cells (Figure 4-33). Generally, the percentage of Cre-positive neutrophils declined over time, reflecting Cre-mediated cellular toxicity (Janbandhu et al., 2014).

Non-transduced cells served as a control and ratios of GFP-positive to GFP-negative cells were compared. Ratio values of 1 indicated equal potential to differentiate into neutrophils, whereas ratio values of less than 1 suggested a disadvantage of Cre-expressing cells over non-transduced cells to differentiate into neutrophils. At day 4 of coculture, flow cytometric analysis showed a markedly reduced abundance of VPS45-depleted CD11b+Gr-1+ neutrophils in comparison to control neutrophils carrying either WT or heterozygous *Vps45* alleles. A further decline in the capacity of VPS45-deficient cells to differentiate into neutrophils was demonstrated at day 7 of coculture. In addition

to Cre-mediated cellular toxicity, insufficient VPS45 abundance may have led to increased cell death or a delay in differentiation. In contrast, control cells efficiently differentiated into CD11b+Gr-1+ neutrophil granulocytes at day 7 of coculture (Figure 4-33). These findings emphasize the importance of VPS45 for neutrophil differentiation.

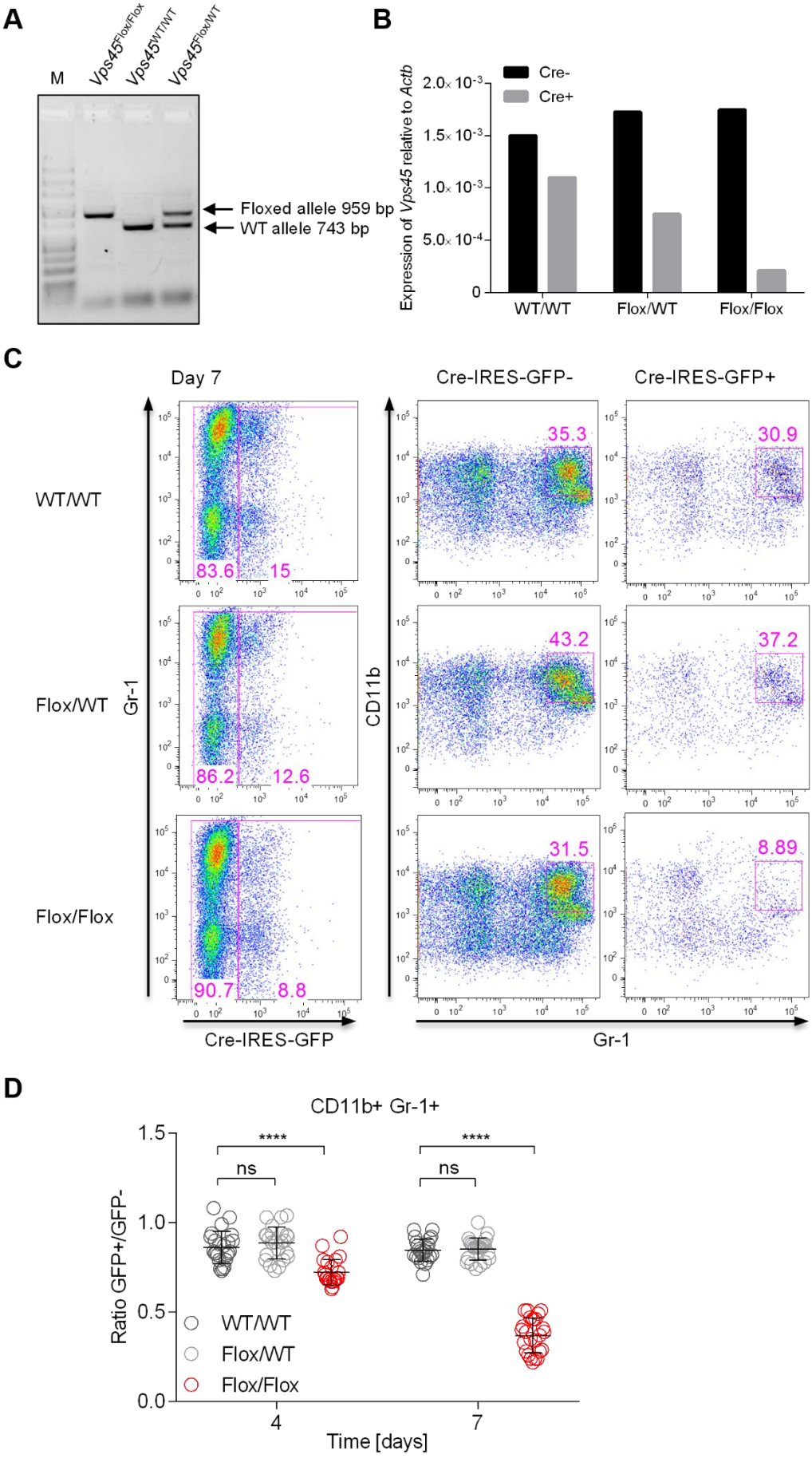
A
M
Vps45Flox/Flox
Vps45WT/WT
Vps45Flox/WT
Floxed allele 959 bp
WT allele 743 bp
B
Cre-
Cre+
Expression of Vps45 relative to Actb
2.0× 10-3
1.5× 10-3
1.0× 10-3
5.0× 10-4
0
WT/WT
Flox/WT
Flox/Flox
C
Day 7
Cre-IRES-GFP-
Cre-IRES-GFP+
WT/WT
Flox/WT
Flox/Flox
Gr-1
CD11b
83.6
15
35.3
30.9
86.2
12.6
43.2
37.2
90.7
8.8
31.5
8.89
Cre-IRES-GFP
Gr-1
D
CD11b+ Gr-1+
Ratio GFP+/GFP-
1.5
1.0
0.5
0.0
****
ns
****
ns
WT/WT
Flox/WT
Flox/Flox
4
7
Time [days]

Figure 4-33 VPS45 depletion impairs the differentiation of neutrophils.

(A) Genotyping results from *Vps45*$^{Flox/Flox}$, *Vps45*$^{WT/WT}$, and *Vps45*$^{Flox/WT}$ mice. (B-D) LSK cells were retrovirally infected with Cre-IRES-GFP and differentiated on OP9 monolayers for up to 7 days. The potential of Cre-expressing (GFP+) and control (GFP-) cells to differentiate into mature neutrophils (CD11b+, Gr-1+) was determined by flow cytometry. (B) Quantitative RT-PCR analysis showing *Vps45* mRNA levels of sorted neutrophils (CD11b+, Gr-1+) at day 7 of OP9 coculture. *Vps45* expression values were normalized to *Actb* expression and data from one experiment is shown. (C) Representative flow cytometry plots show neutrophil differentiation at day 7 of OP9 coculture. (D) Quantification of data shown in (C). Error bars indicate the mean ± SD from two independent experiments with 12 replicate wells for each experiment. Statistical analysis of significance was performed using one-way ANOVA and Tukey´s multiple comparison test. ns: not significant; **, $p<0.01$; ****, $p<0.0001$.

5 Discussion

The role of the evolutionary conserved VPS45 protein is ascribed to the endocytic pathway. The exact molecular mechanisms, in which this protein is involved, remain elusive. VPS45-deficient patients lack neutrophil granulocytes. Therefore, the main goal of this thesis was to elucidate the molecular mechanisms underlying VPS45 deficiencies.

First, the role of VPS45 in trafficking through the endocytic pathway was investigated. This work shows that VPS45 is essential for efficient recycling and degradation of cargos. Moreover, VPS45 regulates the intracellular organization of endolysosomal vesicles.

Besides, this work intended to study the impact of VPS45 on G-CSFR trafficking. Loss of VPS45 leads to aberrant trafficking of G-CSFR, resulting in its trapping in endosomes and impaired delivery to the degradative compartment.

Furthermore, the effects of the disease-related mutations on the function of VPS45 were analyzed. Mutant VPS45 proteins are less expressed and exhibit a reduced capacity to bind to known interaction partners. However, they retain part of their function and thus behave as hypomorphs.

Moreover, the relevance of VPS45 for mouse development was elucidated. This work demonstrates that a complete lack of VPS45 results in embryonic lethality at an early developmental stage.

In addition, the impact of VPS45 on neutrophil granulocytes was investigated. Here, murine VPS45 was shown to be critical for the efficient differentiation of progenitor cells into neutrophil granulocytes.

5.1 Implications of VPS45 in the endocytic pathway

To analyze the relevance of VPS45 in trafficking through the endosomal system, *VPS45* KO HeLa and PLB-985 cells were generated using CRISPR/Cas9 engineering. PLB-985 cells are derived from a patient with acute nonlymphocytic leukemia and can be matured towards granulocytic and monocytic cells (Tucker et al., 1987). These cells have an overall small size and a restricted cytoplasm and are thus not suitable for

detailed microscopic analysis of vesicular trafficking pathways, which was one of the aims of this study. For this purpose, VPS45 was depleted from the cervical cancer cell line HeLa. These cells are widely used to assess intracellular vesicle transport and were a valuable tool to investigate the basic molecular mechanisms in the absence of VPS45 in this study.

So far, effects of VPS45 depletion on the structure of endosomal vesicles have not been investigated in human cells. Early endosomes, late endosomes, and lysosomes were aggregated in the absence of VPS45. In addition, late endosomal and lysosomal vesicles were enlarged. These results accord with studies in yeast, in which vacuoles were enlarged in class D *vps45* mutants (Raymond et al., 1992). Further studies in yeast have shown that loss of Vps45p results in the accumulation of small vesicles, which aggregate in proximity to the nucleus (Piper et al., 1994; Cowles et al., 1994). Likewise, the depletion of VPS45 in cells of Drosophila and *C. elegans* induced the formation of endosomal vesicle clusters (Gengyo-Ando et al., 2007; Morrison et al., 2008). The fact that similar phenotypes are found in distinct organisms upon the loss of VPS45 further points towards an evolutionary conserved role of VPS45 in the maintenance of the endolysosomal compartment and vesicle trafficking through the endosomal system. Notably, the overexpression of either WT or mutant VPS45 proteins in *VPS45* KO HeLa cells resulted in the formation of huge vesicles. These findings indicate that the protein levels of VPS45 are tightly regulated in human cells and either reduced or increased expression severely affects the morphology and distribution of endolysosomal vesicles.

Previous studies in yeast suggest a function of Vps45p in the vesicle transport from the Golgi apparatus to the prevacuolar compartment (Piper et al., 1994; Cowles et al., 1994; Bryant et al., 1998). Moreover, fractionation experiments show an association of Vps45p not only with membranes of endosomes but also with the Golgi apparatus (Cowles et al., 1994). Thus, besides regulating the formation of endolysosomal vesicles, VPS45 might play a role in the maintenance of the structure of the Golgi apparatus. However, the results obtained in this thesis demonstrate that VPS45 depletion does not affect the morphology of the Golgi apparatus. Thus, VPS45 deficiency might specifically impact on the intracellular organization of endolysosomal vesicles. Notably, this result differs from the finding of a previous study, which describes a condensation of the Golgi apparatus in HeLa cells with a siRNA-mediated knockdown of *VPS45* (Rahajeng et al., 2010).

Decreased VPS45 expression resulting from either patient-associated mutations or a siRNA-mediated knockdown has been shown to cause a reduction in protein levels of its binding partners Rabenosyn-5 and Syntaxin16 (Rahajeng et al., 2010; Vilboux et

al., 2013). In the complete absence of VPS45 in both HeLa and PLB-985 cells, the abundance of both binding partners was reduced to an even higher extent, thus confirming that VPS45 affects the expression levels of its interaction partners. It is conceivable that insufficient amounts of VPS45 proteins prevent the proper formation of the vesicle fusion complex and destabilize the direct binding partners. Previous studies indicate that both Rabenosyn-5 and Syntaxin16 are degraded via the proteasomal pathway in the absence of VPS45 (Bryant and James, 2001; Rahajeng et al., 2010). Both binding partners are involved in the fusion of endolysosomal vesicles: Rabenosyn-5 plays a role in early endosomal vesicle fusion as a dual Rab4 and Rab5 effector (Nielsen et al., 2000; Renzis et al., 2002) and the SNARE protein Syntaxin16 is implicated in retrograde trafficking from the TGN to late endosomes (Amessou et al., 2007). Thus, reduced levels of VPS45, Syntaxin16, and Rabenosyn-5, are likely to impede an efficient fusion of endolysosomal vesicles and collectively cause the formation of the vesicle clusters, which were observed in *VPS45* KO cells.

Typically, the defective formation of intracellular organelles induces autophagy to selectively remove these damaged organelles (Anding and Baehrecke, 2017). Similarly, aggregated and enlarged endolysosomal vesicles might trigger the autophagy pathway in the absence of VPS45. The levels of the autophagy marker LC3BII were indeed significantly increased in *VPS45* KO HeLa cells as compared to control cells, indicating an enhanced formation of autophagosomes (Tanida et al., 2008). Like endosome maturation, autophagosome maturation is controlled by Rab5 and Rab7 GTPases (Ao et al., 2014). The fusion of Rab5-positive vesicles was impaired in the absence of VPS45, resulting in a defective maturation of endosomes. Likewise, it is conceivable that the fusion of autophagosomal vesicles is perturbed, resulting in a disrupted autophagosome maturation and the accumulation of LC3BII in VPS45-deficient cells. The hampered maturation of Rab5-positive vesicles in either degradation or autophagy pathways might be a consequence of reduced protein levels of the Rab5 effector Rabenosyn-5. Besides, the yeast homolog of Syntaxin16, Tlg2p, has been shown to play a role in autophagy activity and directing the transport of Atg9, a protein required for the formation of autophagosomes (Nair et al., 2011). Thus, reduced levels of both Rabenosyn-5 and Syntaxin16 may impact on the autophagy pathway and affect the efficient clearance of damaged organelles in the absence of VPS45.

Studies in Drosophila and *C. elegans* suggest a role of both Vps45 and Rabenosyn-5 in cargo uptake (Gengyo-Ando et al., 2007; Morrison et al., 2008). In human cells, however, VPS45 was dispensable for cargo internalization. Both clathrin-dependent and clathrin-independent mechanisms of uptake were studied in the absence of VPS45 using various cargos, such as OVA, EGFR, and G-CSFR. All tested cargos reached the early endosomal compartment efficiently. Thus, this work shows that VPS45 is not

required for endocytosis. In contrast, VPS45-deficient HeLa cells exhibited defects at later stages of the endocytic pathway, specifically in cargo recycling and degradation. In particular, Rabenosyn-5 might contribute to the observed phenotypes in *VPS45* KO cells concerning its implications in both recycling and degradation pathways.

Recycling of Tf was significantly delayed in the absence of VPS45 in HeLa cells. The fast recycling pathway is mainly controlled by Rab4, whereas the slow recycling pathway is regulated by Rab11 (van der Sluijs et al., 1992; Ullrich, 1996; Sheff et al., 1999; Schlierf et al., 2000). Previous studies described a high initial association of roughly 90% of intracellular Tf with Rab4-positive endosomes during the first 5 minutes of recycling and a steady association of Rab4 with Tf over time. In comparison, the initial association of Tf with Rab11-positive recycling endosomes was rather low but increased over time to roughly 55% after 30 minutes (Sönnichsen et al., 2000). Rabenosyn-5 interacts with VPS45 and functions as a dual Rab4 and Rab5 effector at early endosomes (Renzis et al., 2002). Although the depletion of VPS45 did not affect endogenous protein amounts of Rab4 or Rab5, it reduced the expression levels of the Rabenosyn-5 protein, which has been shown to play a role in Tf recycling (Navaroli et al., 2012). Thus, it is likely that decreased levels of VPS45 and Rabenosyn-5 reduced the Rab4-mediated recycling rate of Tf from early endosomes during the initial phase. At later time points, it is conceivable that Rab11-mediated recycling compensated for the delayed Rab4-mediated recycling. On the other hand, Rabenosyn-5 has been shown to interact with EHD1, a protein implicated in the slow recycling route (Naslavsky et al., 2004). Thus, impaired vesicle fusion of early endosomes might affect both fast and slow recycling pathways. Besides, aggregated early endosomes resulting from VPS45 depletion might additionally impede efficient Tf recycling.

Rabenosyn-5 not only controls the recycling of cargo by interacting with Rab4 and EHD1 but also regulates the degradation of cargo by promoting vesicle fusion as a Rab5 effector (Nielsen et al., 2000). Although the endogenous expression levels of both Rab5 and Rab7 were not altered, VPS45-deficient cells failed to deliver cargo from early endosomes to the degradative compartment. This work demonstrates that mistrafficking of cargo is caused by a defect in the switch of early endosomal Rab5 to late endosomal Rab7 in the absence of VPS45. Likely, destabilization of Rabenosyn-5 results in an insufficient initiation of Rab5-mediated fusion of early endosomes with late endosomes, which in turn causes trapping of cellular cargos in these vesicles and prevents their degradation in the lysosomal compartment. This accords with previous studies in yeast, which postulate a role of Vps45p in the delivery of vesicles from the Golgi apparatus to the prevacuolar compartment (Piper et al., 1994; Cowles et al., 1994; Bryant and James, 2001).

Notably, patients with VPS45 and Rabenosyn-5 deficiencies show a phenotypic overlap. Patients with loss-of-function mutations in *VPS45* present with severe neutropenia and Rabenosyn-5-deficient patients exhibit at least transient severe neutropenia. Moreover, refractoriness to therapy with G-CSF is observed for both, VPS45-deficient and Rabenosyn-5-deficient patients (Vilboux et al., 2013; Stepensky et al., 2013; Meerschaut et al., 2015; Shah et al., 2017; Magoulas et al., 2018). The depletion of VPS45 in HeLa cells resulted in an aggregation of endosomes and lysosomes, showing that VPS45 is essential in maintaining the intracellular organization of these vesicles. Similarly, fibroblasts of Rabenosyn-5-deficient patients revealed an aberrant morphology and distribution of early endosomes, which were enlarged and clustered (Magoulas et al., 2018). These fibroblasts further showed a delay in Tf recycling, which was also observed in VPS45-deficient HeLa cells. Loss-of-function mutations in *RBSN* caused a complete absence of the protein in patient cells (Magoulas et al., 2018). In contrast, expression levels of VPS45 in patient cells were partly retained but not completely absent. Of note, one patient with a pathogenic variant in *RBSN* and only transient neutropenia was reported to have normal protein amounts. This patient revealed an increased rate of Tf recycling, suggesting a gain-of-function mutation. Moreover, patient fibroblasts showed reduced levels of the mature form of cathepsin D, indicating a function of Rabenosyn-5 in the transport of the protease through the endolysosomal compartment (Stockler et al., 2014). Likewise, this work demonstrates a role of VPS45 in the maturation and transport of cathepsin D.

The transport and maturation of the protease cathepsin D might not only be regulated by the interaction of VPS45 with Rabenosyn-5 but also by the binding of VPS45 to Syntaxin16. Syntaxin16 is involved in the retrograde transport by controlling vesicle trafficking between the TGN and endolysosomal vesicles (Amessou et al., 2007). VPS45-deficient cells revealed lowered levels of Syntaxin16, as well as increased amounts of immature forms of the lysosomal protease cathepsin D. Maturation of cathepsin D requires an intact trafficking of the immature protease from the Golgi apparatus to the endosomal and lysosomal system, involving endosome maturation and retrograde trafficking of the M6PR. Thus, an accumulation of immature forms of cathepsin D might be explained not only by aberrant endosome maturation but also defective retrograde transport due to decreased expression levels of Syntaxin16 in VPS45-depleted cells.

5.2 The role of VPS45 for G-CSFR trafficking

Receptor internalization and transport through various intracellular compartments regulate its signal strength, time course, and specificity (Sorkin and Zastrow, 2009). While

the signaling of some receptors is terminated upon internalization, the signaling of other receptors continues at early endosomes or late endosomes (Sorkin and Zastrow, 2002). G-CSF activates multiple tyrosine kinases, such as the Janus kinases JAK1 and JAK2, members of the Src family of kinases, including Lyn and Hck, as well as SYK and TNK. The main downstream pathways of the G-CSFR comprise the JAK/STAT, PI3K/AKT, and the MAPK/ERK pathways. In particular, the balanced activation of both STAT3 and STAT5 is supposed to be crucial for the differentiation and proliferation of myeloid cells (Liongue and Ward, 2014; Dwivedi and Greis, 2017). The G-CSFR is critical for the survival, proliferation, and differentiation of neutrophil granulocytes. This is emphasized by the finding that patients with loss-of-function mutations in the *CSF3R* gene encoding the G-CSFR are severely neutropenic and refractory to G-CSF treatment (Triot et al., 2014; Klimiankou et al., 2015). Analysis of the patient's bone marrows revealed a normal maturation of neutrophil granulocytes (Triot et al., 2014; Klimiankou et al., 2015). However, cellular studies showed an aberrant glycosylation pattern of the G-CSFR. Besides, the mutant receptor was retained in the ER and inefficiently targeted to the cell surface. Importantly, phosphorylation levels of STAT3 and STAT5 were reduced, demonstrating abrogated downstream signaling of the mutant receptor (Triot et al., 2014). These studies highlight the importance of proper trafficking and signaling of the G-CSFR for neutrophil homeostasis.

In this work, VPS45 depletion resulted in an impaired trafficking and mislocalization of the G-CSFR, which potentially results in altered downstream signaling pathways. Thus, the aberrant trafficking of the G-CSFR might be associated with the hyporesponsiveness of VPS45-deficient patients to even high doses of G-CSF. This is supported by a previous study, in which mutations resulted in the accumulation of the G-CSFR in early endosomes and caused a sustained signaling of the receptor from this compartment. Importantly, the dysregulated signaling led to an imbalanced proliferation and differentiation of myeloid progenitor cells (Irandoust et al., 2007). Although STAT3 was not differentially activated in this work, other G-CSF-induced signaling pathways might be affected in the absence of VPS45. Mistrafficking resulting in a dysregulated signaling is also observed for other immune receptors. For instance, the Lyst protein regulates the maturation of phagosomes and its loss leads to an impaired TLR3- and TLR4-mediated IRF3 activation in murine macrophages (Westphal et al., 2017). Notably, as mentioned in 1.5, patients with mutations in the *LYST* gene suffer from CHS and are neutropenic (Kaplan et al., 2008; Dame et al., 2019).

Overall, VPS45 depletion does not seem to cause mistrafficking of specific receptors or molecules but rather affects the global transport of cellular cargos following the endocytic route.

5.3 Disease-related mutations in *VPS45*

VPS45 is implicated in vesicle trafficking pathways and its deficiency leads to neutropenia in patients (Stepensky et al., 2013; Vilboux et al., 2013; Shah et al., 2017). This is observed for a variety of other genetic defects affecting vesicle transport: mutations in *AP3B1*, *LYST*, *LAMTOR2*, *RAB27A*, and *VPS13B* cause a loss of the neutrophil population in humans, respectively (Barbosa et al., 1996; Kolehmainen et al., 2003; Jung et al., 2006; Bohn et al., 2007; Meeths et al., 2010). Thus, neutrophil granulocytes seem to particularly depend on proper vesicle trafficking pathways.

Both patient-associated VPS45 variants p.Thr224Asn and p.Glu238Lys behave as hypomorphic mutations. Previous computational analyses predicted an instability and dysfunction of both mutants (Vilboux et al., 2013). In line with these predictions, overexpression of mutant VPS45 proteins in HEK293T cells resulted in reduced expression levels as compared to the WT protein, despite higher transfection rates. Thus, it is likely that VPS45 mutations destabilize the protein and induce its degradation. A previous study proposed that, like its binding partners, VPS45 is degraded via the proteasomal pathway, as the treatment of VPS45-deficient HeLa cells with the proteasomal inhibitor lactacystin restored the expression of VPS45 (Rahajeng et al., 2010).

To analyze whether the mutations influence the intracellular localization of the VPS45 protein, WT and mutant GFP fusion proteins were stably expressed in HeLa cells. Like the WT protein, the mutant proteins showed a net-like distribution throughout the cytoplasm. Thus, the mutations did not affect the intracellular localization of VPS45. These results are in contrast to findings obtained in a previous study in patient fibroblasts and neutrophils, in which the endogenous staining of the WT protein revealed a punctate localization in the proximity of the nucleus, while the mutant protein was more diffusely present throughout the cytoplasm (Vilboux et al., 2013). Besides the artificial overexpression of GFP-tagged proteins, attempts were made to further analyze the intracellular localization of VPS45 by comparing endogenous VPS45 staining in WT cells and patient-specific knockin cells. However, the respective antibodies revealed an unspecific binding and the CRISPR/Cas9-mediated knockin of patient mutations in HeLa cells was not successful.

Mutations in *VPS45* did not abrogate its interaction with the known binding partners Rabenosyn-5 and Syntaxin16. However, the interaction of mutant VPS45 proteins with both binding partners was reduced. In addition, rescue studies showed that the exogenous expression of either WT or mutant VPS45 proteins restored the degradation of

cellular cargo. These results indicate that mutant proteins are at least partially functional. It is conceivable that the overexpression of mutant proteins in *VPS45* KO cells provides these cells with enough amounts to exert functions in the endocytic pathway, including endosome maturation and cargo delivery to the degradative compartment. Thus, this work suggests that cells might require only little amounts of the VPS45 protein to function properly. On the contrary, residual VPS45 levels observed in patient neutrophils may not be enough to efficiently execute cargo transport through the endosomal transport.

Importantly, the rescue of the cargo degradation in *VPS45* KO cells gives a hint that the phenotypes observed in these cells are specific for the deletion of VPS45 and do not reflect off-target effects caused by CRISPR/Cas9 engineering.

5.4 The significance of VPS45 for mouse development

To further investigate the biological relevance of VPS45 during mouse development, a KO mouse model was generated. In this study, the *Vps45* locus was disrupted by an insertion of the KO-first allele following the EUCOMM gene targeting strategy. Patient-associated mutations in *VPS45* cause a reduction in protein levels in various cell types but do not completely abrogate its expression (Vilboux et al., 2013; Stepensky et al., 2013). Since it was conceivable that the global loss of VPS45 expression results in embryonic lethality in mice, the flexible KO-first strategy was chosen to generate a VPS45-deficient mouse model in this study to readily convert the KO allele into a conditional allele (Skarnes et al., 2011).

The depletion of VPS45 severely affected embryogenesis, resulting in an early embryonic lethality at around E7. Similarly, the total loss of the VPS45 protein might cause lethality in humans, which is supported by the fact that no individuals with a complete lack of VPS45 expression are known to date.

Notably, mice with a KO in other genes involved in vesicular trafficking pathways are early embryonic lethal as well, highlighting the relevance of proper vesicle transport in mouse development. For instance, mice deficient in Rab11a lack an important regulator of the recycling pathway and die shortly after the implantation stage (Yu et al. 2014). In addition, Rab10 is implicated in the recycling pathway and mice deficient in this protein die at E7.5 of embryonic development (Lv et al. 2015). Furthermore, Rab6a is involved in vesicle transport at the Golgi apparatus and mice with a global KO of *Rab6a* die early during embryogenesis (Bardin et al. 2015). The SNARE protein SEC22b, which is highly conserved throughout evolution, is implicated in a multitude of cellular

processes, including phagocytosis, autophagy, cell growth, and protein secretion. A complete lack of SEC22b results in an early embryonic death at E8.5 (Shin-Rong J. Wu et al., 2019). Likewise, mice deficient in CHMP5, a protein involved in the mammalian MVB pathway, die approximately at E10 (Shim et al., 2006). Besides, mice completely deficient in Rabenosyn-5 are lethal at the preweaning stage (Phenotyping center, Wellcome Trust Sanger Institute). Thus, Rabenosyn-5 might be crucial at a later stage of mouse development than VPS45. Considering its role in vesicle trafficking through the endosomal system in human cells, it is likely that the early mortality of VPS45-deficient mice is caused by the wide-spread mistrafficking of cellular cargo molecules.

Mice lacking VPS45 were embryonic lethal at around E7.5 and appeared as an overall smaller and disorganized cell mass, which prevented from the discrimination of any germ layers. The formation of the three germ layers is termed gastrulation, a process that takes place at around E6.5 in the mouse embryo (Rivera-Pérez and Hadjantonakis, 2015). Since the formation of germ layers seemed to be disturbed in VPS45-deficient embryos, the process of gastrulation may be impaired in these embryos (Tam and Loebel, 2007). Importantly, blood cells start to develop in the extra-embryonic mesoderm in the yolk sac at E7 (Silver and Palis, 1997; Medvinsky et al., 2011; Yamane, 2018). Thus, VPS45 might also play a role in the early hematopoiesis in mouse embryos. Here, a more comprehensive study is required to define the developmental process, in which VPS45 is required. One possibility to analyze gene expression patterns is the generation of lacZ reporter mice, which express β-galactosidase instead of the gene of interest. This would require breeding of the mice carrying the *Vps45* KO-first allele with Cre-expressing mice. Usually mice heterozygous for the resulting lacZ-tagged null allele can be used to analyze gene expression patterns (Coleman et al., 2015).

5.5 The impact of VPS45 on neutrophil differentiation

Based on the findings in patients, VPS45 seems to have a critical function in immune cells, particularly in facilitating the intracellular trafficking in the myeloid compartment. The early embryonic death of VPS45-deficient mice precluded from investigating the role of VPS45 for the differentiation of neutrophils. Thus, two *Vps45*$^{fl/fl;LysM\text{-}Cre}$ and *Vps45*$^{fl/fl;Vav\text{-}Cre}$ conditional KO mouse lines were generated to disrupt *Vps45* expression in myeloid cells and hematopoietic cells, respectively. However, western blot analysis revealed an inefficient deletion of the VPS45 protein in targeted cells of both mouse lines. The LysM-Cre strain has been shown to deplete genes in macrophages with a high efficiency. However, studies suggest that the LysM-Cre strain induces gene

deletion in roughly 50-70% of neutrophils in the bone marrow and peripheral blood (Abram et al., 2014; Shi et al., 2018). Thus, VPS45 might not be depleted in the majority of neutrophils of *Vps45*$^{fl/fl;LysM\text{-}Cre}$ mice and VPS45-sufficient neutrophils might compensate for VPS45-deficient neutrophils in these mice. Similarly, few hematopoietic progenitors with an incomplete deletion of VPS45 might compensate for the development of blood cells in *Vps45*$^{fl/fl;Vav\text{-}Cre}$ mice, although Vav-Cre is known to induce recombination in hematopoietic cells with a high efficiency (Boer et al., 2003; Siegemund et al., 2015). Besides, studies show that *vav* expression starts from E11.5 (Bustelo et al., 1993; Zmuidzinas et al., 1995). Since the depletion of VPS45 was embryonic lethal already before that stage of development at around E7, another cause for the inefficient deletion might be that VPS45 is essential before *vav* is being expressed during embryonic development.

Since the inefficient deletion of VPS45 in both *Vps45*$^{fl/fl;LysM\text{-}Cre}$ and *Vps45*$^{fl/fl;Vav\text{-}Cre}$ conditional KO mouse lines precluded from further analysis of neutrophil development, VPS45 was depleted in murine LSK cells *ex vivo* by the transduction with Cre-expressing viruses. Over time, VPS45-depleted LSK cells showed a reduced capacity to differentiate into neutrophil granulocytes. These results reflect the neutropenic phenotype observed in VPS45-patients and emphasize the importance of VPS45 for neutrophil differentiation (Stepensky et al., 2013; Vilboux et al., 2013; Meerschaut et al., 2015; Shah et al., 2017).

Notably, only few mouse models reflect the neutropenic phenotype observed in humans. Mice deficient in the G-CSFR reveal a significant loss of the neutrophil population in the peripheral blood. Moreover, hematopoietic progenitors were severely reduced in the bone marrow of these mice (Liu et al., 1996). In addition, G6PC3-deficient mice show reduced levels of neutrophils and impaired neutrophil functions, which is in accordance with the phenotype observed in human patients (Cheung et al., 2007; Boztug et al., 2009). Thus, these mice are relevant models to study the impact of gene loss on neutrophil biology. On the contrary, a multitude of genetically modified mice do not reveal a loss of the neutrophil population and thus do not reflect the phenotype in humans, including mice with deficiencies in Rab27a, Lyst, and AP3B1 (Gallin et al., 1974; Feng et al., 1999; Johnson et al., 2011). In addition, neutropenia is not listed as a phenotype of VPS13B-deficient mice. Of note, the genes, which are associated with neutropenia in humans but not in mice, are all implicated in vesicular trafficking pathways. Since there seems to be a discordance in the impact of trafficking defects on neutrophils between mice and humans, the mouse might not always be the appropriate model to study neutropenia-related questions.

6 Conclusion and outlook

This study on VPS45 advances the understanding of its molecular implications in endocytic trafficking.

First, it shows that VPS45 is a critical regulator of the intracellular organization of endolysosomal vesicles, as its complete loss results in a severe aggregation of endosomal and lysosomal vesicles. Second, VPS45 promotes vesicle fusion at early endosomes and its depletion causes cargo mistrafficking through the endosomal system: cargo recycling is delayed and cargo destined for lysosomal degradation is captured in early endosomes, while it fails to transit to the degradative compartment, due to a defective early-to-late endosome conversion. Besides, the loss of VPS45 causes aberrant trafficking of the G-CSFR, which might be associated with the severe neutropenic phenotype of VPS45-deficient patients and their poor response to G-CSF treatment. Analysis of the disease-related mutations show that they behave as hypomorphs. Importantly, VPS45 is essential for mouse development, as VPS45-deficient embryos cannot survive beyond an early stage of embryogenesis. It is thus conceivable that humans with a complete lack of the VPS45 protein might not survive, which is supported by the fact that such individuals are not known to date.

Thus, this work highlights the significance of VPS45 for intact vesicular trafficking through the endocytic system and early embryogenesis of mice. Overall, the results obtained in this thesis do not only contribute to the understanding of basic principles governing endosomal vesicle fusion but also give insights into endosome function in health and disease.

The exact impact of VPS45 on neutrophils, however, remains elusive. The processes of granule fusion and formation as well as phagolysosomal maturation may be impaired in neutrophil granulocytes of patients with VPS45 deficiencies. Consequently, the intracellular cargo trafficking, destruction of engulfed pathogens, and signaling of various receptors, including the G-CSFR, might be disrupted in these cells. It also remains unclear why specifically neutrophil granulocytes are affected by reduced amounts of VPS45 proteins. Based on the findings here, VPS45 is a crucial regulator of the endocytic pathway and specifically involved in cargo recycling and endosome maturation. These processes are not only essential in neutrophil granulocytes but are crucial in multiple immune cells. Hence, rather than neutropenia, a broader defect would be expected in VPS45-deficient patients. On the other hand, mutations in the *VPS13B*, *RAB27A*, and *LAMTOR2* genes are known to affect endosome integrity and

specifically cause neutropenia in patients, emphasizing the importance of intact vesicular trafficking for neutrophil granulocytes (Kolehmainen et al., 2003; Bohn et al., 2007; Meeths et al., 2010).

The lack of appropriate models prevented from studying the significance of VPS45 for neutrophil biology. In particular, the VPS45-deficient mouse models were expected to give further insights into molecular mechanisms affecting neutrophils. However, the complete lack of VPS45 induced embryonic death at an early stage and the deletion of VPS45 in the conditional mouse models was inefficient. In the future, the successful generation of a VPS45-deficient mouse model could contribute to the understanding of underlying pathomechanisms. Alternatively, reprogrammed induced pluripotent stem cells carrying the disease-related *VPS45* mutations might provide a useful tool to study their impact on neutrophils.

Future investigations could address multiple aspects of the function of VPS45, however, the following questions addressing the pathomechanisms underlying VPS45 deficiencies would be of particular interest:

1) Which process is affected in VPS45-deficient neutrophils?
2) At which stage of the neutrophil life cycle does VPS45 play an essential role?
3) Why does VPS45 deficiency specifically affect neutrophil granulocytes?
4) Why are VPS45-deficient patients refractory to G-CSF treatment?

List of figures

List of tables

List of references

Abram, C. L., G. L. Roberge, Y. Hu, and C. A. Lowell. 2014. Comparative analysis of the efficiency and specificity of myeloid-Cre deleting strains using ROSA-EYFP reporter mice. *Journal of immunological methods* 408:89–100. doi:10.1016/j.jim.2014.05.009.

Aivazian, D., R. L. Serrano, and S. Pfeffer. 2006. TIP47 is a key effector for Rab9 localization. *J Cell Biol* 173(6):917–926. doi:10.1083/jcb.200510010.

Akbar, M. A., R. Mandraju, C. Tracy, W. Hu, C. Pasare, and H. Krämer. 2016. ARC Syndrome-linked Vps33B protein is required for inflammatory endosomal maturation and signal termination. *Immunity* 45(2):267–279. doi:10.1016/j.immuni.2016.07.010.

Akopian, D., K. Shen, X. Zhang, and S.-o. Shan. 2013. Signal recognition particle: an essential protein-targeting machine. *Annual review of biochemistry* 82:693–721. doi:10.1146/annurev-biochem-072711-164732.

Almeida, C. J. G. de. 2017. Caveolin-1 and Caveolin-2 Can Be Antagonistic Partners in Inflammation and Beyond. *Frontiers in Immunology* 8. doi:10.3389/fimmu.2017.01530.

Amara, J. F., S. H. Cheng, and A. E. Smith. 1992. Intracellular protein trafficking defects in human disease. *Trends in cell biology* 2(5):145–149. doi:10.1016/0962-8924(92)90101-R.

Amessou, M., A. Fradagrada, T. Falguières, J. M. Lord, D. C. Smith, L. M. Roberts, C. Lamaze, and L. Johannes. 2007. Syntaxin 16 and Syntaxin 5 are Required for Efficient Retrograde Transport of Several Exogenous and Endogenous Cargo Proteins. *Journal of cell science* 120(Pt 8):1457–1468. doi:10.1242/jcs.03436.

Ancliff, P. J., M. P. Blundell, G. O. Cory, Y. Calle, A. Worth, H. Kempski, S. Burns, G. E. Jones, J. Sinclair, C. Kinnon, I. M. Hann, R. E. Gale, D. C. Linch, and A. J. Thrasher. 2006. Two novel activating mutations in the Wiskott-Aldrich syndrome protein result in congenital neutropenia. *Blood* 108(7):2182–2189. doi:10.1182/blood-2006-01-010249.

Anding, A. L., and E. H. Baehrecke. 2017. Cleaning House: Selective Autophagy of Organelles. *Developmental Cell* 41(1):10–22. doi:10.1016/j.devcel.2017.02.016.

Antonin, W., C. Holroyd, D. Fasshauer, S. Pabst, G. F. von Mollard, and R. Jahn. 2000. A SNARE complex mediating fusion of late endosomes defines conserved properties of SNARE structure and function. *EMBO J* 19(23):6453–6464. doi:10.1093/emboj/19.23.6453.

Ao, X., L. Zou, and Y. Wu. 2014. Regulation of autophagy by the Rab GTPase network. *Cell death and differentiation* 21(3):348–358. doi:10.1038/cdd.2013.187.

Araki, N., Y. Egami, Y. Watanabe, and T. Hatae. 2007. Phosphoinositide metabolism during membrane ruffling and macropinosome formation in EGF-stimulated A431 cells. *Experimental cell research* 313(7):1496–1507. doi:10.1016/j.yexcr.2007.02.012.

Autenrieth, S. E., and I. B. Autenrieth. 2009. Variable antigen uptake due to different expression of the macrophage mannose receptor by dendritic cells in various inbred mouse strains. *Immunology* 127(4):523–529. doi:10.1111/j.1365-2567.2008.02960.x.

Bahl, K., S. Xie, G. Spagnol, P. Sorgen, N. Naslavsky, and S. Caplan. 2016. EHD3 Protein Is Required for Tubular Recycling Endosome Stabilization, and an Asparagine-Glutamic Acid Residue Pair within Its Eps15 Homology (EH) Domain Dictates Its Selective Binding to NPF Peptides. *The Journal of biological chemistry* 291(26):13465–13478. doi:10.1074/jbc.M116.716407.

Baker, R. W., P. D. Jeffrey, and F. M. Hughson. 2013. Crystal Structures of the Sec1/Munc18 (SM) Protein Vps33, Alone and Bound to the Homotypic Fusion and Vacuolar Protein Sorting (HOPS) Subunit Vps16*. *PloS one* 8(6):e67409. doi:10.1371/journal.pone.0067409.

Bakker, J., M. Spits, J. Neefjes, and I. Berlin. 2017. The EGFR odyssey - from activation to destruction in space and time. *Journal of cell science* 130(24):4087–4096. doi:10.1242/jcs.209197.

Balderhaar, H. J. k., and C. Ungermann. 2013. CORVET and HOPS tethering complexes - coordinators of endosome and lysosome fusion. *Journal of cell science* 126(Pt 6):1307–1316. doi:10.1242/jcs.107805.

Bankaitis, V. A., L. M. Johnson, and S. D. Emr. 1986. Isolation of yeast mutants defective in protein targeting to the vacuole. *Proceedings of the National Academy of Sciences* 83(23):9075–9079. doi:10.1073/pnas.83.23.9075.

Banta, L. M., J. S. Robinson, D. J. Klionsky, and S. D. Emr. 1988. Organelle assembly in yeast: characterization of yeast mutants defective in vacuolar biogenesis and protein sorting. *J Cell Biol* 107(4):1369–1383. doi:10.1083/jcb.107.4.1369.

Barbosa, M. D., Q. A. Nguyen, V. T. Tchernev, J. A. Ashley, J. C. Detter, S. M. Blaydes, S. J. Brandt, D. Chotai, C. Hodgman, R. C. Solari, M. Lovett, and S. F. Kingsmore. 1996. Identification of the homologous beige and Chediak-Higashi syndrome genes. *Nature* 382(6588):262–265. doi:10.1038/382262a0.

Bar-Sagi, D., and J. R. Feramisco. 1986. Induction of membrane ruffling and fluid-phase pinocytosis in quiescent fibroblasts by ras proteins. *Science (New York, N.Y.)* 233(4768):1061–1068. doi:10.1126/science.3090687.

BasuRay, S., S. Mukherjee, E. G. Romero, M. N. J. Seaman, and A. Wandinger-Ness. 2013. Rab7 mutants associated with Charcot-Marie-Tooth disease cause

delayed growth factor receptor transport and altered endosomal and nuclear signaling. *The Journal of biological chemistry* 288(2):1135–1149. doi:10.1074/jbc.M112.417766.

Belaaouaj, A. 2002. Neutrophil elastase-mediated killing of bacteria: lessons from targeted mutagenesis. *Microbes and infection* 4(12):1259–1264. doi:10.1016/s1286-4579(02)01654-4.

Bem, D., H. Smith, B. Banushi, J. J. Burden, I. J. White, J. Hanley, N. Jeremiah, F. Rieux-Laucat, R. Bettels, G. Ariceta, A. D. Mumford, S. G. Thomas, S. P. Watson, and P. Gissen. 2015. VPS33B regulates protein sorting into and maturation of α-granule progenitor organelles in mouse megakaryocytes. *Blood* 126(2):133–143. doi:10.1182/blood-2014-12-614677.

Benham, A. M. 2012. Protein secretion and the endoplasmic reticulum. *Cold Spring Harbor perspectives in biology* 4(8):a012872. doi:10.1101/cshperspect.a012872.

Blum, J. S., P. A. Wearsch, and P. Cresswell. 2013. Pathways of antigen processing. *Annual review of immunology* 31:443–473. doi:10.1146/annurev-immunol-032712-095910.

Bock, J. B., J. Klumperman, S. Davanger, and R. H. Scheller. 1997. Syntaxin 6 functions in trans-Golgi network vesicle trafficking. *Molecular biology of the cell* 8(7):1261–1271. doi:10.1091/mbc.8.7.1261.

Boer, J. de, A. Williams, G. Skavdis, N. Harker, M. Coles, M. Tolaini, T. Norton, K. Williams, K. Roderick, A. J. Potocnik, and D. Kioussis. 2003. Transgenic mice with hematopoietic and lymphoid specific expression of Cre. *European journal of immunology* 33(2):314–325. doi:10.1002/immu.200310005.

Bohn, G., A. Allroth, G. Brandes, J. Thiel, E. Glocker, A. A. Schaffer, C. Rathinam, N. Taub, D. Teis, C. Zeidler, R. A. Dewey, R. Geffers, J. Buer, L. A. Huber, K. Welte, B. Grimbacher, and C. Klein. 2007. A novel human primary immunodeficiency syndrome caused by deficiency of the endosomal adaptor protein p14. *Nature medicine* 13(1):38–45. doi:10.1038/nm1528.

Bonifacino, J. S., and L. M. Traub. 2003. Signals for sorting of transmembrane proteins to endosomes and lysosomes. *Annual review of biochemistry* 72:395–447. doi:10.1146/annurev.biochem.72.121801.161800.

Boztug, K., G. Appaswamy, A. Ashikov, A. A. Schäffer, U. Salzer, J. Diestelhorst, M. Germeshausen, G. Brandes, J. Lee-Gossler, F. Noyan, A.-K. Gatzke, M. Minkov, J. Greil, C. Kratz, T. Petropoulou, I. Pellier, C. Bellanné-Chantelot, N. Rezaei, K. Mönkemöller, N. Irani-Hakimeh, H. Bakker, R. Gerardy-Schahn, C. Zeidler, B. Grimbacher, K. Welte, and C. Klein. 2009. A syndrome with congenital neutropenia and mutations in G6PC3. *The New England journal of medicine* 360(1):32–43. doi:10.1056/NEJMoa0805051.

Boztug, K., P. M. Järvinen, E. Salzer, T. Racek, S. Mönch, W. Garncarz, E. M. Gertz, A. A. Schäffer, A. Antonopoulos, S. M. Haslam, L. Schieck, J. Puchałka, J.

Diestelhorst, G. Appaswamy, B. Lescoeur, R. Giambruno, J. W. Bigenzahn, U. Elling, D. Pfeifer, C. D. Conde, M. H. Albert, K. Welte, G. Brandes, R. Sherkat, J. van der Werff ten Bosch, N. Rezaei, A. Etzioni, C. Bellanné-Chantelot, G. Superti-Furga, J. M. Penninger, K. L. Bennett, J. von Blume, A. Dell, J. Donadieu, and C. Klein. 2014. JAGN1 deficiency causes aberrant myeloid cell homeostasis and congenital neutropenia. *Nature genetics* 46(9):1021–1027. doi:10.1038/ng.3069.

Bryant, N. J., and D. E. James. 2001. Vps45p stabilizes the syntaxin homologue Tlg2p and positively regulates SNARE complex formation. *EMBO J* 20(13):3380–3388. doi:10.1093/emboj/20.13.3380.

Bryant, N. J., R. C. Piper, S. R. Gerrard, and T. H. Stevens. 1998. Traffic into the prevacuolar/endosomal compartment of Saccharomyces cerevisiae: a VPS45-dependent intracellular route and a VPS45-independent, endocytic route. *European journal of cell biology* 76(1):43–52. doi:10.1016/S0171-9335(98)80016-2.

Burgdorf, S., V. Lukacs-Kornek, and C. Kurts. 2006. The mannose receptor mediates uptake of soluble but not of cell-associated antigen for cross-presentation. *Journal of immunology (Baltimore, Md. 1950)* 176(11):6770–6776. doi:10.4049/jimmunol.176.11.6770.

Burnicka-Turek, O., A. Kata, B. Buyandelger, L. Ebermann, N. Kramann, P. Burfeind, S. Hoyer-Fender, W. Engel, and I. M. Adham. 2010. Pelota interacts with HAX1, EIF3G and SRPX and the resulting protein complexes are associated with the actin cytoskeleton. *BMC cell biology* 11:28. doi:10.1186/1471-2121-11-28.

Bustelo, X. R., S. D. Rubin, K. L. Suen, D. Carrasco, and M. Barbacid. 1993. Developmental expression of the vav protooncogene. *Cell growth & differentiation the molecular biology journal of the American Association for Cancer Research* 4(4):297–308.

Cabrera, M., and C. Ungermann. 2010. Guiding endosomal maturation. *Cell* 141(3):404–406. doi:10.1016/j.cell.2010.04.013.

Cai, H., K. Reinisch, and S. Ferro-Novick. 2007. Coats, Tethers, Rabs, and SNAREs Work Together to Mediate the Intracellular Destination of a Transport Vesicle. *Developmental Cell* 12(5):671–682. doi:10.1016/j.devcel.2007.04.005.

Casanova, J. E., and B. Winckler. 2017. A new Rab7 effector controls phosphoinositide conversion in endosome maturation. *The Journal of cell biology* 216(10):2995–2997. doi:10.1083/jcb.201709034.

Casey, J. R., S. Grinstein, and J. Orlowski. 2010. Sensors and regulators of intracellular pH. *Nat Rev Mol Cell Biol* 11(1):50–61. doi:10.1038/nrm2820.

Caswell, P. T., S. Vadrevu, and J. C. Norman. 2009. Integrins: masters and slaves of endocytic transport. *Nature Reviews Molecular Cell Biology* 10(12):843. doi:10.1038/nrm2799.

Cavnar, P. J., E. Berthier, D. J. Beebe, and A. Huttenlocher. 2011. Hax1 regulates neutrophil adhesion and motility through RhoA. *The Journal of cell biology* 193(3):465–473. doi:10.1083/jcb.201010143.

Chavrier, P., R. G. Parton, H. P. Hauri, K. Simons, and M. Zerial. 1990. Localization of low molecular weight GTP binding proteins to exocytic and endocytic compartments. *Cell* 62(2):317–329. doi:10.1016/0092-8674(90)90369-p.

Chen, A. H., and P. A. Silver. 2012. Designing biological compartmentalization. *Trends in cell biology* 22(12):662–670. doi:10.1016/j.tcb.2012.07.002.

Chen, C. C.-H., P. J. Schweinsberg, S. Vashist, D. P. Mareiniss, E. J. Lambie, and B. D. Grant. 2006. RAB-10 is required for endocytic recycling in the Caenorhabditis elegans intestine. *Molecular biology of the cell* 17(3):1286–1297. doi:10.1091/mbc.e05-08-0787.

Cherry, S., E. J. Jin, M. N. Ozel, Z. Lu, E. Agi, D. Wang, W.-H. Jung, D. Epstein, I. A. Meinertzhagen, C.-C. Chan, and P. R. Hiesinger. 2013. Charcot-Marie-Tooth 2B mutations in rab7 cause dosage-dependent neurodegeneration due to partial loss of function. *eLife* 2:e01064. doi:10.7554/eLife.01064.

Cheung, Y. Y., S. Y. Kim, W. H. Yiu, C.-J. Pan, H.-S. Jun, R. A. Ruef, E. J. Lee, H. Westphal, B. C. Mansfield, and J. Y. Chou. 2007. Impaired neutrophil activity and increased susceptibility to bacterial infection in mice lacking glucose-6-phosphatase–β. *The Journal of clinical investigation* 117(3):784–793. doi:10.1172/JCI30443.

Chia, P. Z. C., and P. A. Gleeson. 2014. Membrane tethering. *F1000prime reports* 6:74. doi:10.12703/P6-74.

Christoforidis, S., M. Miaczynska, K. Ashman, M. Wilm, L. Zhao, S. C. Yip, M. D. Waterfield, J. M. Backer, and M. Zerial. 1999. Phosphatidylinositol-3-OH kinases are Rab5 effectors. *Nature cell biology* 1(4):249–252. doi:10.1038/12075.

Cobbold, C. 2003. Aberrant trafficking of transmembrane proteins in human disease. *Trends in cell biology* 13(12):639–647. doi:10.1016/j.tcb.2003.10.008.

Coleman, J. L. J., K. Brennan, T. Ngo, P. Balaji, R. M. Graham, and N. J. Smith. 2015. Rapid Knockout and Reporter Mouse Line Generation and Breeding Colony Establishment Using EUCOMM Conditional-Ready Embryonic Stem Cells: A Case Study. *Frontiers in Endocrinology* 6. doi:10.3389/fendo.2015.00105.

Cossart, P., and A. Helenius. 2014. Endocytosis of viruses and bacteria. *Cold Spring Harbor perspectives in biology* 6(8). doi:10.1101/cshperspect.a016972.

Cosson, P., and F. Letourneur. 1994. Coatomer interaction with di-lysine endoplasmic reticulum retention motifs. *Science (New York, N.Y.)* 263(5153):1629–1631. doi:10.1126/science.8128252.

Cowles, C. R., S. D. Emr, and B. F. Horazdovsky. 1994. Mutations in the VPS45 gene, a SEC1 homologue, result in vacuolar protein sorting defects and accumulation of membrane vesicles. *Journal of cell science* 107 (Pt 12):3449–3459.

Da Costa, R., M. Bordessoules, M. Guilleman, V. Carmignac, V. Lhussiez, H. Courot, A. Bataille, A. Chlémaire, C. Bruno, P. Fauque, C. Thauvin, L. Faivre, and L. Duplomb. 2020. Vps13b is required for acrosome biogenesis through functions in Golgi dynamic and membrane trafficking. *Cellular and molecular life sciences CMLS* 77(3):511–529. doi:10.1007/s00018-019-03192-4.

Dale, D. C., R. E. Person, A. A. Bolyard, A. G. Aprikyan, C. Bos, M. A. Bonilla, L. A. Boxer, G. Kannourakis, C. Zeidler, K. Welte, K. F. Benson, and M. Horwitz. 2000. Mutations in the gene encoding neutrophil elastase in congenital and cyclic neutropenia. *Blood* 96(7):2317–2322.

Dame, J. A., L.-A. Phillips, N. de Villiers, K. Pillay, C. Hlela, and B. Eley. 2019. A novel LYST mutation causing Chédiak Higashi syndrome in a South African child. *Pediatric Hematology Oncology Journal* 4(2):44–46. doi:10.1016/j.phoj.2019.08.178.

Dautry-Varsat, A., A. Ciechanover, and H. F. Lodish. 1983. pH and the recycling of transferrin during receptor-mediated endocytosis. *Proceedings of the National Academy of Sciences* 80(8):2258–2262. doi:10.1073/pnas.80.8.2258.

del Brío Castillo, R., J. E. Squires, and P. J. McKiernan. 2019. A novel mutation in VPS33B gene causing a milder ARC syndrome phenotype with prolonged survival. *JIMD Reports* 47(1):4–8. doi:10.1002/jmd2.12027.

Demircioglu, F. E., P. Burkhardt, and D. Fasshauer. 2014. The SM protein Sly1 accelerates assembly of the ER-Golgi SNARE complex. *Proceedings of the National Academy of Sciences of the United States of America* 111(38):13828–13833. doi:10.1073/pnas.1408254111.

Deneka, M., M. Neeft, I. Popa, M. van Oort, H. Sprong, V. Oorschot, J. Klumperman, P. Schu, and P. van der Sluijs. 2003. Rabaptin-5α/rabaptin-4 serves as a linker between rab4 and γ1-adaptin in membrane recycling from endosomes. *EMBO J* 22(11):2645–2657. doi:10.1093/emboj/cdg257.

Devriendt, K., A. S. Kim, G. Mathijs, S. G. Frints, M. Schwartz, J. J. van den Oord, G. E. Verhoef, M. A. Boogaerts, J. P. Fryns, D. You, M. K. Rosen, and P. Vandenberghe. 2001. Constitutively activating mutation in WASP causes X-linked severe congenital neutropenia. *Nature genetics* 27(3):313–317. doi:10.1038/85886.

Di Fiore, P. P., and M. von Zastrow. 2014. Endocytosis, signaling, and beyond. *Cold Spring Harbor perspectives in biology* 6(8). doi:10.1101/cshperspect.a016865.

Díaz, E., and S. R. Pfeffer. 1998. TIP47: A Cargo Selection Device for Mannose 6-Phosphate Receptor Trafficking. *Cell* 93(3):433–443. doi:10.1016/S0092-8674(00)81171-X.

Donadieu, J., O. Fenneteau, B. Beaupain, N. Mahlaoui, and C. B. Chantelot. 2011. Congenital neutropenia: diagnosis, molecular bases and patient management. *Orphanet journal of rare diseases* 6:26. doi:10.1186/1750-1172-6-26.

Duclos, S., R. Corsini, and M. Desjardins. 2003. Remodeling of endosomes during lysosome biogenesis involves 'kiss and run' fusion events regulated by rab5. *Journal of cell science* 116(Pt 5):907–918. doi:10.1242/jcs.00259.

Dull, T., R. Zufferey, M. Kelly, R. J. Mandel, M. Nguyen, D. Trono, and L. Naldini. 1998. A third-generation lentivirus vector with a conditional packaging system. *Journal of virology* 72(11):8463–8471.

Dulubova, I., T. Yamaguchi, Y. Gao, S.-W. Min, I. Huryeva, T. C. Südhof, and J. Rizo. 2002. How Tlg2p/syntaxin 16 'snares' Vps45. *EMBO J* 21(14):3620–3631. doi:10.1093/emboj/cdf381.

Dwivedi, P., and K. D. Greis. 2017. Granulocyte colony-stimulating factor receptor signaling in severe congenital neutropenia, chronic neutrophilic leukemia, and related malignancies. *Experimental hematology* 46:9–20. doi:10.1016/j.exphem.2016.10.008.

Eathiraj, S., X. Pan, C. Ritacco, and D. G. Lambright. 2005. Structural basis of family-wide Rab GTPase recognition by rabenosyn-5. *Nature* 436(7049):415–419. doi:10.1038/nature03798.

Eckenroth, B. E., A. N. Steere, N. D. Chasteen, S. J. Everse, and A. B. Mason. 2011. How the binding of human transferrin primes the transferrin receptor potentiating iron release at endosomal pH. *Proceedings of the National Academy of Sciences of the United States of America* 108(32):13089–13094. doi:10.1073/pnas.1105786108.

Egami, Y., T. Taguchi, M. Maekawa, H. Arai, and N. Araki. 2014. Small GTPases and phosphoinositides in the regulatory mechanisms of macropinosome formation and maturation. *Frontiers in physiology* 5:374. doi:10.3389/fphys.2014.00374.

El-Husseini, A. E., H. Guthrie, T. P. Snutch, and S. R. Vincent. 1997. Molecular cloning of a mammalian homologue of the yeast vesicular transport protein vps45. *Biochimica et biophysica acta* 1325(1):8–12. doi:10.1016/s0005-2736(97)00014-x.

Elkin, S. R., A. M. Lakoduk, and S. L. Schmid. 2016. Endocytic pathways and endosomal trafficking: a primer. *Wiener medizinische Wochenschrift (1946)* 166(7-8):196–204. doi:10.1007/s10354-016-0432-7.

Ellgaard, L., N. McCaul, A. Chatsisvili, and I. Braakman. 2016. Co- and Post-Translational Protein Folding in the ER. *Traffic (Copenhagen, Denmark)* 17(6):615–638. doi:10.1111/tra.12392.

Eskelinen, E.-L., and P. Saftig. 2009. Autophagy: a lysosomal degradation pathway with a central role in health and disease. *Biochimica et biophysica acta* 1793(4):664–673. doi:10.1016/j.bbamcr.2008.07.014.

Fasshauer, D. 2003. Structural insights into the SNARE mechanism. *Biochimica et Biophysica Acta (BBA) - Molecular Cell Research* 1641(2):87–97. doi:10.1016/S0167-4889(03)00090-9.

Federica Brandizzi, and Charles Barlowe. Organization of the ER–Golgi interface for membrane traffic control.

Feliciano, W. D., S. Yoshida, S. W. Straight, and J. A. Swanson. 2011. Coordination of the Rab5 cycle on macropinosomes. *Traffic (Copenhagen, Denmark)* 12(12):1911–1922. doi:10.1111/j.1600-0854.2011.01280.x.

Feng, L., A. B. Seymour, S. Jiang, A. To, A. A. Peden, E. K. Novak, L. Zhen, M. E. Rusiniak, E. M. Eicher, M. S. Robinson, M. B. Gorin, and R. T. Swank. 1999. The beta3A subunit gene (Ap3b1) of the AP-3 adaptor complex is altered in the mouse hypopigmentation mutant pearl, a model for Hermansky-Pudlak syndrome and night blindness. *Human molecular genetics* 8(2):323–330. doi:10.1093/hmg/8.2.323.

Francis, G. L. 2010. Albumin and mammalian cell culture: implications for biotechnology applications. *Cytotechnology* 62(1):1–16. doi:10.1007/s10616-010-9263-3.

Frankel, E. B., and A. Audhya. 2017. ESCRT-dependent cargo sorting at multivesicular endosomes. *Seminars in cell & developmental biology* 74:4–10. doi:10.1016/j.semcdb.2017.08.020.

Freeman, S. A., and S. Grinstein. 2014. Phagocytosis: receptors, signal integration, and the cytoskeleton. *Immunological reviews* 262(1):193–215. doi:10.1111/imr.12212.

Futosi, K., S. Fodor, and A. Mócsai. 2013. Neutrophil cell surface receptors and their intracellular signal transduction pathways. *International immunopharmacology* 17(3):638–650. doi:10.1016/j.intimp.2013.06.034.

Gallin, J. I., J. S. Bujak, E. Patten, and S. M. Wolff. 1974. Granulocyte function in the Chediak-Higashi syndrome of mice. *Blood* 43(2):201–206.

Ganley, I. G., K. Carroll, L. Bittova, and S. Pfeffer. 2004. Rab9 GTPase regulates late endosome size and requires effector interaction for its stability. *Molecular biology of the cell* 15(12):5420–5430. doi:10.1091/mbc.e04-08-0747.

Gengyo-Ando, K., H. Kuroyanagi, T. Kobayashi, M. Murate, K. Fujimoto, S. Okabe, and S. Mitani. 2007. The SM protein VPS-45 is required for RAB-5-dependent endocytic transport in Caenorhabditis elegans. *EMBO reports* 8(2):152–157. doi:10.1038/sj.embor.7400882.

Germeshausen, M., S. Deerberg, Y. Peter, C. Reimer, C. P. Kratz, and M. Ballmaier. 2013. The spectrum of ELANE mutations and their implications in severe congenital and cyclic neutropenia. *Human mutation* 34(6):905–914. doi:10.1002/humu.22308.

Gieselmann, V., A. Hasilik, and K. von Figura. 1985. Processing of human cathepsin D in lysosomes in vitro. *The Journal of biological chemistry* 260(5):3215–3220.

Gieselmann, V., R. Pohlmann, A. Hasilik, and K. von Figura. 1983. Biosynthesis and transport of cathepsin D in cultured human fibroblasts. *The Journal of cell biology* 97(1):1–5. doi:10.1083/jcb.97.1.1.

Gillingham, A. K., and S. Munro. 2003. Long coiled-coil proteins and membrane traffic. *Biochimica et Biophysica Acta (BBA) - Molecular Cell Research* 1641(2):71–85. doi:10.1016/S0167-4889(03)00088-0.

Gissen, P., and E. R. Maher. 2007. Cargos and genes: insights into vesicular transport from inherited human disease. *Journal of medical genetics* 44(9):545–555. doi:10.1136/jmg.2007.050294.

Goldenring, J. R. 2015. Recycling endosomes. *Current opinion in cell biology* 35:117–122. doi:10.1016/j.ceb.2015.04.018.

Gonzalez, L., and R. H. Scheller. 1999. Regulation of Membrane Trafficking. *Cell* 96(6):755–758. doi:10.1016/S0092-8674(00)80585-1.

Gordon, S. 2016. Phagocytosis: An Immunobiologic Process. *Immunity* 44(3):463–475. doi:10.1016/j.immuni.2016.02.026.

Grant, B. D., and J. G. Donaldson. 2009. Pathways and mechanisms of endocytic recycling. *Nature reviews. Molecular cell biology* 10(9):597–608. doi:10.1038/nrm2755.

Grenda, D. S., M. Murakami, J. Ghatak, J. Xia, L. A. Boxer, D. Dale, M. C. Dinauer, and D. C. Link. 2007. Mutations of the ELA2 gene found in patients with severe congenital neutropenia induce the unfolded protein response and cellular apoptosis. *Blood* 110(13):4179–4187. doi:10.1182/blood-2006-11-057299.

Grzybowska, E. A., V. Zayat, R. Konopiński, A. Trębińska, M. Szwarc, E. Sarnowska, E. Macech, J. Korczyński, A. Knapp, and J. A. Siedlecki. 2013. HAX-1 is a nucleocytoplasmic shuttling protein with a possible role in mRNA processing. *The FEBS journal* 280(1):256–272. doi:10.1111/febs.12066.

Haddad, E. K., X. Wu, J. A. Hammer, and P. A. Henkart. 2001. Defective granule exocytosis in Rab27a-deficient lymphocytes from Ashen mice. *J Cell Biol* 152(4):835–842. doi:10.1083/jcb.152.4.835.

Hansen, C. G., G. Howard, and B. J. Nichols. 2011. Pacsin 2 is recruited to caveolae and functions in caveolar biogenesis. *Journal of cell science* 124(Pt 16):2777–2785. doi:10.1242/jcs.084319.

Harder, T., and K. Simons. 1997. Caveolae, DIGs, and the dynamics of sphingolipid-cholesterol microdomains. *Current opinion in cell biology* 9(4):534–542.

Harrison, R. E., C. Bucci, O. V. Vieira, T. A. Schroer, and S. Grinstein. 2003. Phagosomes Fuse with Late Endosomes and/or Lysosomes by Extension of Membrane Protrusions along Microtubules: Role of Rab7 and RILP. *Molecular and Cellular Biology* 23(18):6494–6506. doi:10.1128/MCB.23.18.6494-6506.2003.

Hauck, F., and C. Klein. 2013. Pathogenic mechanisms and clinical implications of congenital neutropenia syndromes. *Current opinion in allergy and clinical immunology* 13(6):596–606. doi:10.1097/ACI.0000000000000014.

Henley, J. R., E. W. Krueger, B. J. Oswald, and M. A. McNiven. 1998. Dynamin-mediated internalization of caveolae. *The Journal of cell biology* 141(1):85–99. doi:10.1083/jcb.141.1.85.

Hermans, M. H.A., C. Antonissen, A. C. Ward, A. E.M. Mayen, R. E. Ploemacher, and I. P. Touw. 1999. Sustained Receptor Activation and Hyperproliferation in Response to Granulocyte Colony-stimulating Factor (G-CSF) in Mice with a Severe Congenital Neutropenia/Acute Myeloid Leukemia–derived Mutation in the G-CSF Receptor Gene. *The Journal of Experimental Medicine* 189(4):683–692.

Hidalgo, A., E. R. Chilvers, C. Summers, and L. Koenderman. 2019. The Neutrophil Life Cycle. *Trends in Immunology* 40(7):584–597. doi:10.1016/j.it.2019.04.013.

Hirst, J., C. E. Futter, and C. R. Hopkins. 1998. The Kinetics of Mannose 6-Phosphate Receptor Trafficking in the Endocytic Pathway in HEp-2 Cells: The Receptor Enters and Rapidly Leaves Multivesicular Endosomes without Accumulating in a Prelysosomal Compartment. *Molecular biology of the cell* 9(4):809–816.

Holers, V. M. 2014. Complement and its receptors: new insights into human disease. *Annual review of immunology* 32:433–459. doi:10.1146/annurev-immunol-032713-120154.

Hong, W. 2005. SNAREs and traffic. *Biochimica et Biophysica Acta (BBA) - Molecular Cell Research* 1744(2):120–144. doi:10.1016/j.bbamcr.2005.03.014.

Hopkins, C. R. 1983. Intracellular routing of transferrin and transferrin receptors in epidermoid carcinoma A431 cells. *Cell* 35(1):321–330. doi:10.1016/0092-8674(83)90235-0.

Horwitz, M., K. F. Benson, R. E. Person, A. G. Aprikyan, and D. C. Dale. 1999. Mutations in ELA2, encoding neutrophil elastase, define a 21-day biological clock in cyclic haematopoiesis. *Nature genetics* 23(4):433–436. doi:10.1038/70544.

Hu, Y.-B., E. B. Dammer, R.-J. Ren, and G. Wang. 2015. The endosomal-lysosomal system: from acidification and cargo sorting to neurodegeneration. *Translational Neurodegeneration* 4. doi:10.1186/s40035-015-0041-1.

Huotari, J., and A. Helenius. 2011. Endosome maturation. *The EMBO journal* 30(17):3481–3500. doi:10.1038/emboj.2011.286.

Hurley, J. H., and H. Stenmark. 2011. Molecular mechanisms of ubiquitin-dependent membrane traffic. *Annual review of biophysics* 40:119–142. doi:10.1146/annurev-biophys-042910-155404.

Hyttinen, J. M.T., M. Niittykoski, A. Salminen, and K. Kaarniranta. 2013. Maturation of autophagosomes and endosomes: A key role for Rab7. *Biochimica et Biophysica Acta (BBA) - Molecular Cell Research* 1833(3):503–510. doi:10.1016/j.bbamcr.2012.11.018.

Irandoust, M. I., L. H. J. Aarts, O. Roovers, J. Gits, S. J. Erkeland, and I. P. Touw. 2007. Suppressor of cytokine signaling 3 controls lysosomal routing of G-CSF receptor. *EMBO J* 26(7):1782–1793. doi:10.1038/sj.emboj.7601640.

Jackson, C. L. 2009. Mechanisms of transport through the Golgi complex. *Journal of cell science* 122(Pt 4):443–452. doi:10.1242/jcs.032581.

Jackson, I. J. 1997. Homologous pigmentation mutations in human, mouse and other model organisms. *Human molecular genetics* 6(10):1613–1624. doi:10.1093/hmg/6.10.1613.

Jahn, R., and T. C. Südhof. 1999. Membrane fusion and exocytosis. *Annual review of biochemistry* 68:863–911. doi:10.1146/annurev.biochem.68.1.863.

Janbandhu, V. C., D. Moik, and R. Fässler. 2014. Cre recombinase induces DNA damage and tetraploidy in the absence of LoxP sites. *Cell Cycle* 13(3):462–470. doi:10.4161/cc.27271.

Johannes, L., and V. Popoff. 2008. Tracing the retrograde route in protein trafficking. *Cell* 135(7):1175–1187. doi:10.1016/j.cell.2008.12.009.

Johansson, M., N. Rocha, W. Zwart, I. Jordens, L. Janssen, C. Kuijl, V. M. Olkkonen, and J. Neefjes. 2007. Activation of endosomal dynein motors by stepwise assembly of Rab7-RILP-p150Glued, ORP1L, and the receptor betalll spectrin. *The Journal of cell biology* 176(4):459–471. doi:10.1083/jcb.200606077.

Johnson, J. L., H. Hong, J. Monfregola, and S. D. Catz. 2011. Increased Survival and Reduced Neutrophil Infiltration of the Liver in Rab27a- but Not Munc13-4-Deficient Mice in Lipopolysaccharide-Induced Systemic Inflammation ▿. *Infection and Immunity* 79(9):3607–3618. doi:10.1128/IAI.05043-11.

Jovic, M., M. Sharma, J. Rahajeng, and S. Caplan. 2010. The early endosome: a busy sorting station for proteins at the crossroads. *Histology and histopathology* 25(1):99–112. doi:10.14670/HH-25.99.

Jung, J., G. Bohn, A. Allroth, K. Boztug, G. Brandes, I. Sandrock, A. A. Schäffer, C. Rathinam, I. Köllner, C. Beger, R. Schilke, K. Welte, B. Grimbacher, and C. Klein. 2006. Identification of a homozygous deletion in the AP3B1 gene causing Hermansky-Pudlak syndrome, type 2. *Blood* 108(1):362–369. doi:10.1182/blood-2005-11-4377.

Junutula, J. R., E. Schonteich, G. M. Wilson, A. A. Peden, R. H. Scheller, and R. Prekeris. 2004. Molecular Characterization of Rab11 Interactions with Members of the Family of Rab11-interacting Proteins. *J. Biol. Chem.* 279(32):33430–33437. doi:10.1074/jbc.M404633200.

Kaplan, J., I. de Domenico, and D. M. Ward. 2008. Chediak-Higashi syndrome. *Current opinion in hematology* 15(1):22–29. doi:10.1097/MOH.0b013e3282f2bcce.

Kawamura, N., G.-H. Sun-Wada, M. Aoyama, A. Harada, S. Takasuga, T. Sasaki, and Y. Wada. 2012. Delivery of endosomes to lysosomes via microautophagy in the visceral endoderm of mouse embryos. *Nature communications* 3:1071. doi:10.1038/ncomms2069.

Kazazic, M., V. Bertelsen, K. W. Pedersen, T. T. Vuong, M. V. Grandal, M. S. Rødland, L. M. Traub, E. Stang, and I. H. Madshus. 2009. Epsin 1 is involved in

recruitment of ubiquitinated EGF receptors into clathrin-coated pits. *Traffic (Copenhagen, Denmark)* 10(2):235–245. doi:10.1111/j.1600-0854.2008.00858.x.

Kim, M. J., R. U. Lee, J. Oh, J. E. Choi, H. Kim, K. Lee, S.-K. Hwang, J.-H. Lee, J.-A. Lee, B.-K. Kaang, C.-S. Lim, and Y.-S. Lee. 2019. Spatial Learning and Motor Deficits in Vacuolar Protein Sorting-associated Protein 13b (Vps13b) Mutant Mouse. *Experimental neurobiology* 28(4):485–494. doi:10.5607/en.2019.28.4.485.

Kinchen, J. M., and K. S. Ravichandran. 2010. Identification of two evolutionarily conserved genes regulating processing of engulfed apoptotic cells. *Nature* 464(7289):778–782. doi:10.1038/nature08853.

Kirchhausen, T., D. Owen, and S. C. Harrison. 2014. Molecular structure, function, and dynamics of clathrin-mediated membrane traffic. *Cold Spring Harbor perspectives in biology* 6(5):a016725. doi:10.1101/cshperspect.a016725.

Klein, C. 2011. Genetic defects in severe congenital neutropenia: emerging insights into life and death of human neutrophil granulocytes. *Annual review of immunology* 29:399–413. doi:10.1146/annurev-immunol-030409-101259.

Klein, C. 2017. Kostmann's Disease and HCLS1-Associated Protein X-1 (HAX1). *Journal of clinical immunology* 37(2):117–122. doi:10.1007/s10875-016-0358-2.

Klein, C., M. Grudzien, G. Appaswamy, M. Germeshausen, I. Sandrock, A. A. Schäffer, C. Rathinam, K. Boztug, B. Schwinzer, N. Rezaei, G. Bohn, M. Melin, G. Carlsson, B. Fadeel, N. Dahl, J. Palmblad, J.-I. Henter, C. Zeidler, B. Grimbacher, and K. Welte. 2007. HAX1 deficiency causes autosomal recessive severe congenital neutropenia (Kostmann disease). *Nature genetics* 39(1):86–92. doi:10.1038/ng1940.

Klimiankou, M., O. Klimenkova, M. Uenalan, A. Zeidler, S. Mellor-Heineke, S. Kandabarau, J. Skokowa, C. Zeidler, and K. Welte. 2015. GM-CSF stimulates granulopoiesis in a congenital neutropenia patient with loss-of-function biallelic heterozygous CSF3R mutations. *Blood* 126(15):1865–1867. doi:10.1182/blood-2015-07-661264.

Kloepper, T. H., C. N. Kienle, and D. Fasshauer. 2007. An elaborate classification of SNARE proteins sheds light on the conservation of the eukaryotic endomembrane system. *Molecular biology of the cell* 18(9):3463–3471. doi:10.1091/mbc.e07-03-0193.

Koenderman, L. 2019. Inside-Out Control of Fc-Receptors. *Frontiers in Immunology* 10:544. doi:10.3389/fimmu.2019.00544.

Kolehmainen, J., G. C. M. Black, A. Saarinen, K. Chandler, J. Clayton-Smith, A.-L. Träskelin, R. Perveen, S. Kivitie-Kallio, R. Norio, M. Warburg, J.-P. Fryns, A. de La Chapelle, and A.-E. Lehesjoki. 2003. Cohen syndrome is caused by mutations in a novel gene, COH1, encoding a transmembrane protein with a presumed role in vesicle-mediated sorting and intracellular protein transport. *American journal of human genetics* 72(6):1359–1369. doi:10.1086/375454.

Köllner, I., B. Sodeik, S. Schreek, H. Heyn, N. von Neuhoff, M. Germeshausen, C. Zeidler, M. Krüger, B. Schlegelberger, K. Welte, and C. Beger. 2006. Mutations in neutrophil elastase causing congenital neutropenia lead to cytoplasmic protein accumulation and induction of the unfolded protein response. *Blood* 108(2):493–500. doi:10.1182/blood-2005-11-4689.

KOSTMANN, R. 1956. Infantile genetic agranulocytosis; agranulocytosis infantilis hereditaria. *Acta paediatrica. Supplementum* 45(Suppl 105):1–78.

Kouranti, I., M. Sachse, N. Arouche, B. Goud, and A. Echard. 2006. Rab35 Regulates an Endocytic Recycling Pathway Essential for the Terminal Steps of Cytokinesis. *Current Biology* 16(17):1719–1725. doi:10.1016/j.cub.2006.07.020.

Kumari, S., S. Mg, and S. Mayor. 2010. Endocytosis unplugged: multiple ways to enter the cell. *Cell research* 20(3):256–275. doi:10.1038/cr.2010.19.

Kurt von Figura and Andrej Hasilik. LYSOSOMAL ENZYMES AND THEIR RECEPTORS.

Lahoz-Beneytez, J., M. Elemans, Y. Zhang, R. Ahmed, A. Salam, M. Block, C. Niederalt, B. Asquith, and D. Macallan. 2016. Human neutrophil kinetics: modeling of stable isotope labeling data supports short blood neutrophil half-lives. *Blood* 127(26):3431–3438. doi:10.1182/blood-2016-03-700336.

Laufman, O., W. Hong, and S. Lev. 2011. The COG complex interacts directly with Syntaxin 6 and positively regulates endosome-to-TGN retrograde transport. *The Journal of cell biology* 194(3):459–472. doi:10.1083/jcb.201102045.

Lawrence, S. M., R. Corriden, and V. Nizet. 2018. The Ontogeny of a Neutrophil: Mechanisms of Granulopoiesis and Homeostasis. *Microbiology and Molecular Biology Reviews MMBR* 82(1). doi:10.1128/MMBR.00057-17.

Lemansky, P., M. Gerecitano-Schmidek, R. C. Das, B. Schmidt, and A. Hasilik. 2003. Targeting myeloperoxidase to azurophilic granules in HL-60 cells. *Journal of leukocyte biology* 74(4):542–550. doi:10.1189/jlb.1202616.

Lemmon, M. A., J. Schlessinger, and K. M. Ferguson. 2014. The EGFR Family: Not So Prototypical Receptor Tyrosine Kinases. *Cold Spring Harbor perspectives in biology* 6(4). doi:10.1101/cshperspect.a020768.

Li, H.-H., J. Li, K. J. Wasserloos, C. Wallace, M. G. Sullivan, P. M. Bauer, D. B. Stolz, J. S. Lee, S. C. Watkins, C. M. St Croix, B. R. Pitt, and L.-M. Zhang. 2013. Caveolae-dependent and -independent uptake of albumin in cultured rodent pulmonary endothelial cells. *PloS one* 8(11):e81903. doi:10.1371/journal.pone.0081903.

Li, L., T. Wan, M. Wan, B. Liu, R. Cheng, and R. Zhang. 2015. The effect of the size of fluorescent dextran on its endocytic pathway. *Cell biology international* 39(5):531–539. doi:10.1002/cbin.10424.

Lieber, J. G., S. Webb, B. T. Suratt, S. K. Young, G. L. Johnson, G. M. Keller, and G. S. Worthen. 2004. The in vitro production and characterization of neutrophils from embryonic stem cells. *Blood* 103(3):852–859. doi:10.1182/blood-2003-04-1030.

Liongue, C., and A. C. Ward. 2014. Granulocyte Colony-Stimulating Factor Receptor Mutations in Myeloid Malignancy. *Front. Oncol.* 4:93. doi:10.3389/fonc.2014.00093.

Lippe, R., M. Miaczynska, V. Rybin, A. Runge, and M. Zerial. 2001. Functional synergy between Rab5 effector Rabaptin-5 and exchange factor Rabex-5 when physically associated in a complex. *Molecular biology of the cell* 12(7):2219–2228. doi:10.1091/mbc.12.7.2219.

Liu, F., G. Kunter, M. M. Krem, W. C. Eades, J. A. Cain, M. H. Tomasson, L. Hennighausen, and D. C. Link. 2008. Csf3r mutations in mice confer a strong clonal HSC advantage via activation of Stat5. *The Journal of clinical investigation* 118(3):946–955. doi:10.1172/JCI32704.

Liu, F., H. Y. Wu, R. Wesselschmidt, T. Kornaga, and D. C. Link. 1996. Impaired production and increased apoptosis of neutrophils in granulocyte colony-stimulating factor receptor-deficient mice. *Immunity* 5(5):491–501. doi:10.1016/s1074-7613(00)80504-x.

Liu, K., R. Xing, Y. Jian, Z. Gao, X. Ma, X. Sun, Y. Li, M. Xu, X. Wang, Y. Jing, W. Guo, and C. Yang. 2017. WDR91 is a Rab7 effector required for neuronal development. *The Journal of cell biology* 216(10):3307–3321. doi:10.1083/jcb.201705151.

Lobingier, B. T., and A. J. Merz. 2012. Sec1/Munc18 protein Vps33 binds to SNARE domains and the quaternary SNARE complex. *Molecular biology of the cell* 23(23):4611–4622. doi:10.1091/mbc.E12-05-0343.

Longva, K. E., F. D. Blystad, E. Stang, A. M. Larsen, L. E. Johannessen, and I. H. Madshus. 2002. Ubiquitination and proteasomal activity is required for transport of the EGF receptor to inner membranes of multivesicular bodies. *J Cell Biol* 156(5):843–854. doi:10.1083/jcb.200106056.

Lou, J., J. Rossy, Q. Deng, S. V. Pageon, and K. Gaus. 2016. New Insights into How Trafficking Regulates T Cell Receptor Signaling. *Frontiers in Cell and Developmental Biology* 4:77. doi:10.3389/fcell.2016.00077.

Lou, X., and Y.-K. Shin. 2016. SNARE zippering. *Bioscience Reports* 36(3). doi:10.1042/BSR20160004.

Lürick, A., D. Kümmel, and C. Ungermann. 2018. Multisubunit tethers in membrane fusion. *Current Biology* 28(8):R417-R420. doi:10.1016/j.cub.2017.12.012.

Łyszkiewicz, M., D. Kotlarz, N. Ziętara, G. Brandes, J. Diestelhorst, S. Glage, E. Hobeika, M. Reth, L. A. Huber, A. Krueger, and C. Klein. 2019. LAMTOR2 (p14) Controls B Cell Differentiation by Orchestrating Endosomal BCR Trafficking. *Frontiers in Immunology* 10:497. doi:10.3389/fimmu.2019.00497.

Łyszkiewicz, M., N. Ziętara, L. Frey, U. Pannicke, M. Stern, Y. Liu, Y. Fan, J. Puchałka, S. Hollizeck, I. Somekh, M. Rohlfs, T. Yilmaz, E. Ünal, M. Karakukcu, T. Patiroğlu, C. Kellerer, E. Karasu, K.-W. Sykora, A. Lev, A. Simon, R. Somech,

J. Roesler, M. Hoenig, O. T. Keppler, K. Schwarz, and C. Klein. 2020. Human FCHO1 deficiency reveals role for clathrin-mediated endocytosis in development and function of T cells. *Nature communications* 11(1):1031. doi:10.1038/s41467-020-14809-9.

Madshus, I. H., and E. Stang. 2009. Internalization and intracellular sorting of the EGF receptor: a model for understanding the mechanisms of receptor trafficking. *Journal of cell science* 122(Pt 19):3433–3439. doi:10.1242/jcs.050260.

Magoulas, P. L., O. A. Shchelochkov, M. N. Bainbridge, S. Ben-Shachar, S. Yatsenko, L. Potocki, R. A. Lewis, C. Searby, A. N. Marcogliese, M. T. Elghetany, G. Zapata, P. P. Hernández, M. Gadkari, D. Einhaus, D. M. Muzny, R. A. Gibbs, A. A. Bertuch, D. A. Scott, S. Corvera, and L. M. Franco. 2018. Syndromic congenital myelofibrosis associated with a loss-of-function variant in RBSN. *Blood* 132(6):658–662. doi:10.1182/blood-2017-12-824433.

Mahul-Mellier, A.-L., F. Strappazzon, A. Petiot, C. Chatellard-Causse, S. Torch, B. Blot, K. Freeman, L. Kuhn, J. Garin, J.-M. Verna, S. Fraboulet, and R. Sadoul. 2008. Alix and ALG-2 are involved in tumor necrosis factor receptor 1-induced cell death. *The Journal of biological chemistry* 283(50):34954–34965. doi:10.1074/jbc.M803140200.

Makaryan, V., C. Zeidler, A. A. Bolyard, J. Skokowa, E. Rodger, M. L. Kelley, L. A. Boxer, M. A. Bonilla, P. E. Newburger, A. Shimamura, B. Zhu, P. S. Rosenberg, D. C. Link, K. Welte, and D. C. Dale. 2015. The diversity of mutations and clinical outcomes for ELANE-associated neutropenia. *Current opinion in hematology* 22(1):3–11. doi:10.1097/MOH.0000000000000105.

Mallard, F., C. Antony, D. Tenza, J. Salamero, B. Goud, and L. Johannes. 1998. Direct pathway from early/recycling endosomes to the Golgi apparatus revealed through the study of shiga toxin B-fragment transport. *J Cell Biol* 143(4):973–990. doi:10.1083/jcb.143.4.973.

Marat, A. L., and V. Haucke. 2016. Phosphatidylinositol 3-phosphates—at the interface between cell signalling and membrane traffic. *The EMBO journal* 35(6):561–579. doi:10.15252/embj.201593564.

Marchetti, M., M.-N. Monier, A. Fradagrada, K. Mitchell, F. Baychelier, P. Eid, L. Johannes, and C. Lamaze. 2006. Stat-mediated signaling induced by type I and type II interferons (IFNs) is differentially controlled through lipid microdomain association and clathrin-dependent endocytosis of IFN receptors. *Molecular biology of the cell* 17(7):2896–2909. doi:10.1091/mbc.e06-01-0076.

Matteis, M. A. D., and A. Luini. 2008. Exiting the Golgi complex. *Nature Reviews Molecular Cell Biology* 9(4):273. doi:10.1038/nrm2378.

Maxfield, F. R., and T. E. McGraw. 2004. Endocytic recycling. *Nature reviews. Molecular cell biology* 5(2):121–132. doi:10.1038/nrm1315.

Mayor, S., and R. E. Pagano. 2007. Pathways of clathrin-independent endocytosis. *Nature reviews. Molecular cell biology* 8(8):603–612. doi:10.1038/nrm2216.

McBride, H. M., V. Rybin, C. Murphy, A. Giner, R. Teasdale, and M. Zerial. 1999. Oligomeric Complexes Link Rab5 Effectors with NSF and Drive Membrane Fusion via Interactions between EEA1 and Syntaxin 13. *Cell* 98(3):377–386. doi:10.1016/S0092-8674(00)81966-2.

McCaffrey, M. W., A. Bielli, G. Cantalupo, S. Mora, V. Roberti, M. Santillo, F. Drummond, and C. Bucci. 2001. Rab4 affects both recycling and degradative endosomal trafficking. *FEBS Letters* 495(1-2):21–30. doi:10.1016/S0014-5793(01)02359-6.

McLauchlan, H., J. Newell, N. Morrice, A. Osborne, M. West, and E. Smythe. 1998. A novel role for Rab5-GDI in ligand sequestration into clathrin-coated pits. *Current Biology* 8(1):34–45. doi:10.1016/s0960-9822(98)70018-1.

McMahon, H. T., and E. Boucrot. 2011. Molecular mechanism and physiological functions of clathrin-mediated endocytosis. *Nature reviews. Molecular cell biology* 12(8):517–533. doi:10.1038/nrm3151.

Medvinsky, A., S. Rybtsov, and S. Taoudi. 2011. Embryonic origin of the adult hematopoietic system: advances and questions. *Development (Cambridge, England)* 138(6):1017–1031. doi:10.1242/dev.040998.

Meerschaut, I., V. Bordon, C. Dhooge, P. Delbeke, A. V. Vanlander, A. Simon, C. Klein, R. F. Kooy, R. Somech, and B. Callewaert. 2015. Severe congenital neutropenia with neurological impairment due to a homozygous VPS45 p.E238K mutation: A case report suggesting a genotype–phenotype correlation. *American Journal of Medical Genetics Part A* 167(12):3214–3218. doi:10.1002/ajmg.a.37367.

Meeths, M., Y. T. Bryceson, E. Rudd, C. Zheng, S. M. Wood, K. Ramme, K. Beutel, H. Hasle, C. Heilmann, K. Hultenby, H.-G. Ljunggren, B. Fadeel, M. Nordenskjöld, and J.-I. Henter. 2010. Clinical presentation of Griscelli syndrome type 2 and spectrum of RAB27A mutations. *Pediatric blood & cancer* 54(4):563–572. doi:10.1002/pbc.22357.

Melin, M., M. Entesarian, G. Carlsson, D. Garwicz, C. Klein, B. Fadeel, M. Nordenskjöld, J. Palmblad, J. I. Henter, and N. Dahl. 2007. Assignment of the gene locus for severe congenital neutropenia to chromosome 1q22 in the original Kostmann family from Northern Sweden. *Biochemical and biophysical research communications* 353(3):571–575. doi:10.1016/j.bbrc.2006.12.086.

Mellman, I. 1996. Endocytosis and molecular sorting. *Annual review of cell and developmental biology* 12:575–625. doi:10.1146/annurev.cellbio.12.1.575.

Mettlen, M., P.-H. Chen, S. Srinivasan, G. Danuser, and S. L. Schmid. 2018. Regulation of Clathrin-Mediated Endocytosis. *Annual review of biochemistry* 87:871–896. doi:10.1146/annurev-biochem-062917-012644.

Misteli, T. 2001. The concept of self-organization in cellular architecture. *The Journal of cell biology* 155(2):181–185. doi:10.1083/jcb.200108110.

Mizuno, K., A. Kitamura, and T. Sasaki. 2003. Rabring7, a novel Rab7 target protein with a RING finger motif. *Molecular biology of the cell* 14(9):3741–3752. doi:10.1091/mbc.e02-08-0495.

Morrison, H. A., H. Dionne, T. E. Rusten, A. Brech, W. W. Fisher, B. D. Pfeiffer, S. E. Celniker, H. Stenmark, and D. Bilder. 2008. Regulation of early endosomal entry by the Drosophila tumor suppressors Rabenosyn and Vps45. *Molecular biology of the cell* 19(10):4167–4176. doi:10.1091/mbc.e08-07-0716.

Munro, S., and H. R. Pelham. 1987. A C-terminal signal prevents secretion of luminal ER proteins. *Cell* 48(5):899–907. doi:10.1016/0092-8674(87)90086-9.

Munson, M. 2014. To protect or reject. *eLife* 3:e03374. doi:10.7554/eLife.03374.

Murphy, M. A., R. G. Schnall, D. J. Venter, L. Barnett, I. Bertoncello, C. B. Thien, W. Y. Langdon, and D. D. Bowtell. 1998. Tissue hyperplasia and enhanced T-cell signalling via ZAP-70 in c-Cbl-deficient mice. *Molecular and Cellular Biology* 18(8):4872–4882. doi:10.1128/mcb.18.8.4872.

Nag, S., S. Rani, S. Mahanty, C. Bissig, P. Arora, C. Azevedo, A. Saiardi, P. van der Sluijs, C. Delevoye, G. van Niel, G. Raposo, and S. R. Setty. 2018. Rab4A organizes endosomal domains for sorting cargo to lysosome-related organelles. *Journal of cell science* 131(18). doi:10.1242/jcs.216226.

Nagle, D. L., M. A. Karim, E. A. Woolf, L. Holmgren, P. Bork, D. J. Misumi, S. H. McGrail, B. J. Dussault, C. M. Perou, R. E. Boissy, G. M. Duyk, R. A. Spritz, and K. J. Moore. 1996. Identification and mutation analysis of the complete gene for Chediak-Higashi syndrome. *Nature genetics* 14(3):307–311. doi:10.1038/ng1196-307.

Nair, U., A. Jotwani, J. Geng, N. Gammoh, D. Richerson, W.-L. Yen, J. Griffith, S. Nag, K. Wang, T. Moss, M. Baba, J. A. McNew, X. Jiang, F. Reggiori, T. J. Melia, and D. J. Klionsky. 2011. SNARE proteins are required for macroautophagy. *Cell* 146(2):290–302. doi:10.1016/j.cell.2011.06.022.

Naramura, M., H. K. Kole, R. J. Hu, and H. Gu. 1998. Altered thymic positive selection and intracellular signals in Cbl-deficient mice. *Proceedings of the National Academy of Sciences* 95(26):15547–15552. doi:10.1073/pnas.95.26.15547.

Naslavsky, N., M. Boehm, P. S. Backlund, and S. Caplan. 2004. Rabenosyn-5 and EHD1 Interact and Sequentially Regulate Protein Recycling to the Plasma Membrane. *Molecular biology of the cell* 15(5):2410–2422. doi:10.1091/mbc.E03-10-0733.

Navaroli, D. M., K. D. Bellvé, C. Standley, L. M. Lifshitz, J. Cardia, D. Lambright, D. Leonard, K. E. Fogarty, and S. Corvera. 2012. Rabenosyn-5 defines the fate of the transferrin receptor following clathrin-mediated endocytosis. *Proceedings of*

the National Academy of Sciences of the United States of America 109(8):E471-80. doi:10.1073/pnas.1115495109.

Needham, P. G., C. J. Guerriero, and J. L. Brodsky. 2019. Chaperoning Endoplasmic Reticulum-Associated Degradation (ERAD) and Protein Conformational Diseases. *Cold Spring Harbor perspectives in biology*. doi:10.1101/cshperspect.a033928.

Nguyen, G. T., E. R. Green, and J. Mecsas. 2017. Neutrophils to the ROScue: Mechanisms of NADPH Oxidase Activation and Bacterial Resistance. *Frontiers in Cellular and Infection Microbiology* 7. doi:10.3389/fcimb.2017.00373.

Nguyen-Jackson, H., A. D. Panopoulos, H. Zhang, H. S. Li, and S. S. Watowich. 2010. STAT3 controls the neutrophil migratory response to CXCR2 ligands by direct activation of G-CSF–induced CXCR2 expression and via modulation of CXCR2 signal transduction. *Blood* 115(16):3354–3363. doi:10.1182/blood-2009-08-240317.

Nichols, B. J., J. C. Holthuis, and H. R. Pelham. 1998. The Sec1p homologue Vps45p binds to the syntaxin Tlg2p. *European journal of cell biology* 77(4):263–268. doi:10.1016/s0171-9335(98)80084-8.

Nielsen, E., S. Christoforidis, S. Uttenweiler-Joseph, M. Miaczynska, F. Dewitte, M. Wilm, B. Hoflack, and M. Zerial. 2000. Rabenosyn-5, a novel Rab5 effector, is complexed with hVPS45 and recruited to endosomes through a FYVE finger domain. *J Cell Biol* 151(3):601–612. doi:10.1083/jcb.151.3.601.

Niemann, C. U., M. Abrink, G. Pejler, R. L. Fischer, E. I. Christensen, S. D. Knight, and N. Borregaard. 2007. Neutrophil elastase depends on serglycin proteoglycan for localization in granules. *Blood* 109(10):4478–4486. doi:10.1182/blood-2006-02-001719.

Nimmerjahn, F., and J. V. Ravetch. 2008. Fcgamma receptors as regulators of immune responses. *Nature reviews. Immunology* 8(1):34–47. doi:10.1038/nri2206.

Nogueira, C., P. Erlmann, J. Villeneuve, A. J. M. Santos, E. Martínez-Alonso, J. Á. Martínez-Menárguez, and V. Malhotra. 2014. SLY1 and Syntaxin 18 specify a distinct pathway for procollagen VII export from the endoplasmic reticulum. *eLife* 3. doi:10.7554/eLife.02784.

Ohbayashi, N., S. Mamishi, K. Ishibashi, Y. Maruta, B. Pourakbari, B. Tamizifar, M. Mohammadpour, M. Fukuda, and N. Parvaneh. 2010. Functional characterization of two RAB27A missense mutations found in Griscelli syndrome type 2. *Pigment Cell & Melanoma Research* 23(3):365–374. doi:10.1111/j.1755-148X.2010.00705.x.

Otero, C., M. Groettrup, and D. F. Legler. 2006. Opposite fate of endocytosed CCR7 and its ligands: recycling versus degradation. *Journal of immunology (Baltimore, Md. 1950)* 177(4):2314–2323. doi:10.4049/jimmunol.177.4.2314.

Palande, K., A. Meenhuis, T. Jevdjovic, and I. P. Touw. 2013. Scratching the surface: signaling and routing dynamics of the CSF3 receptor. *Frontiers in bioscience (Landmark edition)* 18:91–105.

Panopoulos, A. D., L. Zhang, J. W. Snow, D. M. Jones, A. M. Smith, K. C. El Kasmi, F. Liu, M. A. Goldsmith, D. C. Link, P. J. Murray, and S. S. Watowich. 2006. STAT3 governs distinct pathways in emergency granulopoiesis and mature neutrophils. *Blood* 108(12):3682–3690. doi:10.1182/blood-2006-02-003012.

Parton, R. G. 2018. Caveolae: Structure, Function, and Relationship to Disease. *Annual review of cell and developmental biology* 34:111–136. doi:10.1146/annurev-cellbio-100617-062737.

Parton, R. G., and M. T. Howes. 2010. Revisiting caveolin trafficking: the end of the caveosome. *The Journal of cell biology* 191(3):439–441. doi:10.1083/jcb.201009093.

Parton, R. G., and K. Simons. 2007. The multiple faces of caveolae. *Nature reviews. Molecular cell biology* 8(3):185–194. doi:10.1038/nrm2122.

Pear, W. S., J. P. Miller, L. Xu, J. C. Pui, B. Soffer, R. C. Quackenbush, A. M. Pendergast, R. Bronson, J. C. Aster, M. L. Scott, and D. Baltimore. 1998. Efficient and rapid induction of a chronic myelogenous leukemia-like myeloproliferative disease in mice receiving P210 bcr/abl-transduced bone marrow. *Blood* 92(10):3780–3792.

Pedruzzi, E., M. Fay, C. Elbim, M. Gaudry, and M.-A. Gougerot-Pocidalo. 2002. Differentiation of PLB-985 myeloid cells into mature neutrophils, shown by degranulation of terminally differentiated compartments in response to N-formyl peptide and priming of superoxide anion production by granulocyte-macrophage colony-stimulating factor. *British journal of haematology* 117(3):719–726. doi:10.1046/j.1365-2141.2002.03521.x.

Pereira, P. N. G., M. P. Dobreva, L. Graham, D. Huylebroeck, K. A. Lawson, and A. N. Zwijsen. 2011. Amnion formation in the mouse embryo: the single amniochorionic fold model. *BMC developmental biology* 11:48. doi:10.1186/1471-213X-11-48.

Perez-Garcia, V., E. Fineberg, R. Wilson, A. Murray, C. I. Mazzeo, C. Tudor, A. Sienerth, J. K. White, E. Tuck, E. J. Ryder, D. Gleeson, E. Siragher, H. Wardle-Jones, N. Staudt, N. Wali, J. Collins, S. Geyer, E. M. Busch-Nentwich, A. Galli, J. C. Smith, E. Robertson, D. J. Adams, W. J. Weninger, T. Mohun, and M. Hemberger. 2018. Placentation defects are highly prevalent in embryonic lethal mouse mutants. *Nature* 555(7697):463–468. doi:10.1038/nature26002.

Person, R. E., F.-Q. Li, Z. Duan, K. F. Benson, J. Wechsler, H. A. Papadaki, G. Eliopoulos, C. Kaufman, S. J. Bertolone, B. Nakamoto, T. Papayannopoulou, H. L. Grimes, and M. Horwitz. 2003. Mutations in proto-oncogene GFI1 cause human

neutropenia and target ELA2. *Nature genetics* 34(3):308–312. doi:10.1038/ng1170.

Peterson, M. R., C. G. Burd, and S. D. Emr. 1999. Vac1p coordinates Rab and phosphatidylinositol 3-kinase signaling in Vps45p-dependent vesicle docking/fusion at the endosome. *Current Biology* 9(3):159–162. doi:10.1016/s0960-9822(99)80071-2.

Pfeffer, S. R. 2013. Rab GTPase regulation of membrane identity. *Current opinion in cell biology* 25(4):414–419. doi:10.1016/j.ceb.2013.04.002.

Piper, R. C., E. A. Whitters, and T. H. Stevens. 1994. Yeast Vps45p is a Sec1p-like protein required for the consumption of vacuole-targeted, post-Golgi transport vesicles. *European journal of cell biology* 65(2):305–318.

Pless, D. d., and R. B. Wellner. 1996. In vitro fusion of endocytic vesicles: Effects of reagents that alter endosomal pH. *J. Cell. Biochem.* 62(1):27–39. doi:10.1002/(SICI)1097-4644(199607)62:1<27:AID-JCB4>3.0.CO;2-3.

Poole, B., and S. Ohkuma. 1981. Effect of weak bases on the intralysosomal pH in mouse peritoneal macrophages. *The Journal of cell biology* 90(3):665–669. doi:10.1083/jcb.90.3.665.

Progida, C., and O. Bakke. 2016. Bidirectional traffic between the Golgi and the endosomes - machineries and regulation. *Journal of cell science* 129(21):3971–3982. doi:10.1242/jcs.185702.

Pryor, P. R., B. M. Mullock, N. A. Bright, S. R. Gray, and J. P. Luzio. 2000. The role of intraorganellar Ca(2+) in late endosome-lysosome heterotypic fusion and in the reformation of lysosomes from hybrid organelles. *The Journal of cell biology* 149(5):1053–1062. doi:10.1083/jcb.149.5.1053.

Pryor, P. R., B. M. Mullock, N. A. Bright, M. R. Lindsay, S. R. Gray, S. C. W. Richardson, A. Stewart, D. E. James, R. C. Piper, and J. P. Luzio. 2004. Combinatorial SNARE complexes with VAMP7 or VAMP8 define different late endocytic fusion events. *EMBO reports* 5(6):590–595. doi:10.1038/sj.embor.7400150.

Racoosin, E. L., and J. A. Swanson. 1992. M-CSF-induced macropinocytosis increases solute endocytosis but not receptor-mediated endocytosis in mouse macrophages. *Journal of cell science* 102 (Pt 4):867–880.

Rahajeng, J., S. Caplan, and N. Naslavsky. 2010. Common and distinct roles for the binding partners Rabenosyn-5 and Vps45 in the regulation of endocytic trafficking in mammalian cells. *Experimental cell research* 316(5):859–874. doi:10.1016/j.yexcr.2009.11.007.

Ravikumar, B., S. Imarisio, S. Sarkar, C. J. O'Kane, and D. C. Rubinsztein. 2008. Rab5 modulates aggregation and toxicity of mutant huntingtin through macroautophagy in cell and fly models of Huntington disease. *Journal of cell science* 121(Pt 10):1649–1660. doi:10.1242/jcs.025726.

Raymond, C. K., I. Howald-Stevenson, C. A. Vater, and T. H. Stevens. 1992. Morphological classification of the yeast vacuolar protein sorting mutants: evidence for a prevacuolar compartment in class E vps mutants. *Molecular biology of the cell* 3(12):1389–1402.

Reggiori, F., and C. Ungermann. 2017. Autophagosome Maturation and Fusion. *Journal of molecular biology* 429(4):486–496. doi:10.1016/j.jmb.2017.01.002.

Renzis, S. de, B. Sönnichsen, and M. Zerial. 2002. Divalent Rab effectors regulate the sub-compartmental organization and sorting of early endosomes. *Nature cell biology* 4(2):124–133. doi:10.1038/ncb744.

Riccardi, C., and I. Nicoletti. 2006. Analysis of apoptosis by propidium iodide staining and flow cytometry. *Nature protocols* 1(3):1458–1461. doi:10.1038/nprot.2006.238.

Richo, G. R., and G. E. Conner. 1994. Structural requirements of procathepsin D activation and maturation. *The Journal of biological chemistry* 269(20):14806–14812.

Rink, J., E. Ghigo, Y. Kalaidzidis, and M. Zerial. 2005. Rab conversion as a mechanism of progression from early to late endosomes. *Cell* 122(5):735–749. doi:10.1016/j.cell.2005.06.043.

Rivera-Pérez, J. A., and A.-K. Hadjantonakis. 2015. The Dynamics of Morphogenesis in the Early Mouse Embryo. *Cold Spring Harbor perspectives in biology* 7(11). doi:10.1101/cshperspect.a015867.

Robinson, M. S. 2004. Adaptable adaptors for coated vesicles. *Trends in cell biology* 14(4):167–174. doi:10.1016/j.tcb.2004.02.002.

Rock, K. L., E. Reits, and J. Neefjes. 2016. Present Yourself! By MHC Class I and MHC Class II Molecules. *Trends in Immunology* 37(11):724–737. doi:10.1016/j.it.2016.08.010.

Rosales, C., and E. Uribe-Querol. 2017. Phagocytosis: A Fundamental Process in Immunity. *BioMed research international* 2017:9042851. doi:10.1155/2017/9042851.

Roskoski, R. 2014. The ErbB/HER family of protein-tyrosine kinases and cancer. *Pharmacological research* 79:34–74. doi:10.1016/j.phrs.2013.11.002.

Rothman, J. E., and F. T. Wieland. 1996. Protein sorting by transport vesicles. *Science (New York, N.Y.)* 272(5259):227–234. doi:10.1126/science.272.5259.227.

Rothman, J. H., I. Howald, and T. H. Stevens. 1989. Characterization of genes required for protein sorting and vacuolar function in the yeast Saccharomyces cerevisiae. *EMBO J* 8(7):2057–2065. doi:10.1002/j.1460-2075.1989.tb03614.x.

Rothman, J. H., and T. H. Stevens. 1986. Protein sorting in yeast: Mutants defective in vacuole biogenesis mislocalize vacuolar proteins into the late secretory pathway. *Cell* 47(6):1041–1051. doi:10.1016/0092-8674(86)90819-6.

Ruggiano, A., O. Foresti, and P. Carvalho. 2014. Quality control: ER-associated degradation: protein quality control and beyond. *The Journal of cell biology* 204(6):869–879. doi:10.1083/jcb.201312042.

Sacher, M., Y.-G. Kim, A. Lavie, B.-H. Oh, and N. Segev. 2008. The TRAPP complex: insights into its architecture and function. *Traffic (Copenhagen, Denmark)* 9(12):2032–2042. doi:10.1111/j.1600-0854.2008.00833.x.

Sallusto, F., M. Cella, C. Danieli, and A. Lanzavecchia. 1995. Dendritic cells use macropinocytosis and the mannose receptor to concentrate macromolecules in the major histocompatibility complex class II compartment: downregulation by cytokines and bacterial products. *The Journal of Experimental Medicine* 182(2):389–400. doi:10.1084/jem.182.2.389.

Sarnowska, E., E. A. Grzybowska, K. Sobczak, R. Konopinski, A. Wilczynska, M. Szwarc, T. J. Sarnowski, W. J. Krzyzosiak, and J. A. Siedlecki. 2007. Hairpin structure within the 3'UTR of DNA polymerase beta mRNA acts as a post-transcriptional regulatory element and interacts with Hax-1. *Nucleic acids research* 35(16):5499–5510. doi:10.1093/nar/gkm502.

Saxena, R. K., Q. B. Saxena, and W. H. Adler. 1982. Defective T-cell response in beige mutant mice. *Nature* 295(5846):240–241. doi:10.1038/295240a0.

Scartozzi, M., I. Bearzi, R. Berardi, A. Mandolesi, C. Pierantoni, and S. Cascinu. 2007. Epidermal growth factor receptor (EGFR) downstream signalling pathway in primary colorectal tumours and related metastatic sites: optimising EGFR-targeted treatment options. *British Journal of Cancer* 97(1):92–97. doi:10.1038/sj.bjc.6603847.

Schäffer, A. A., and C. Klein. 2007. Genetic Heterogeneity in Severe Congenital Neutropenia: How Many Aberrant Pathways Can Kill a Neutrophil? *Current opinion in allergy and clinical immunology* 7(6):481–494. doi:10.1097/ACI.0b013e3282f1d690.

Schambach, A., J. Bohne, S. Chandra, E. Will, G. P. Margison, D. A. Williams, and C. Baum. 2006. Equal potency of gammaretroviral and lentiviral SIN vectors for expression of O6-methylguanine-DNA methyltransferase in hematopoietic cells. *Molecular therapy the journal of the American Society of Gene Therapy* 13(2):391–400. doi:10.1016/j.ymthe.2005.08.012.

Schindler, C., Y. Chen, J. Pu, X. Guo, and J. S. Bonifacino. 2015. EARP is a multisubunit tethering complex involved in endocytic recycling. *Nature cell biology* 17(5):639–650. doi:10.1038/ncb3129.

Schlierf, B., G. H. Fey, J. Hauber, G. M. Hocke, and O. Rosorius. 2000. Rab11b is essential for recycling of transferrin to the plasma membrane. *Experimental cell research* 259(1):257–265. doi:10.1006/excr.2000.4947.

Schonteich, E., G. M. Wilson, J. Burden, C. R. Hopkins, K. Anderson, J. R. Goldenring, and R. Prekeris. 2008. The Rip11/Rab11-FIP5 and kinesin II complex regulates endocytic protein recycling. *Journal of cell science* 121(0 22):3824–3833. doi:10.1242/jcs.032441.

Shah, R. K., M. Munson, K. J. Wierenga, H. R. Pokala, P. E. Newburger, and D. Crawford. 2017. A novel homozygous VPS45 p.P468L mutation leading to severe congenital neutropenia with myelofibrosis. *Pediatric blood & cancer* 64(9). doi:10.1002/pbc.26571.

Shajahan, A. N., B. K. Timblin, R. Sandoval, C. Tiruppathi, A. B. Malik, and R. D. Minshall. 2004. Role of Src-induced dynamin-2 phosphorylation in caveolae-mediated endocytosis in endothelial cells. *The Journal of biological chemistry* 279(19):20392–20400. doi:10.1074/jbc.M308710200.

Shanks, S. G., L. N. Carpp, M. S. Struthers, R. K. McCann, and N. J. Bryant. 2012. The Sec1/Munc18 protein Vps45 regulates cellular levels of its SNARE binding partners Tlg2 and Snc2 in Saccharomyces cerevisiae. *PloS one* 7(11):e49628. doi:10.1371/journal.pone.0049628.

Sheff, D. R., E. A. Daro, M. Hull, and I. Mellman. 1999. The Receptor Recycling Pathway Contains Two Distinct Populations of Early Endosomes with Different Sorting Functions. *J Cell Biol* 145(1):123–139. doi:10.1083/jcb.145.1.123.

Sheshachalam, A., N. Srivastava, T. Mitchell, P. Lacy, and G. Eitzen. 2014. Granule protein processing and regulated secretion in neutrophils. *Frontiers in Immunology* 5:448. doi:10.3389/fimmu.2014.00448.

Shi, J., L. Hua, D. Harmer, P. Li, and G. Ren. 2018. Cre Driver Mice Targeting Macrophages. *Methods in molecular biology (Clifton, N.J.)* 1784:263–275. doi:10.1007/978-1-4939-7837-3_24.

Shim, J.-H., C. Xiao, M. S. Hayden, K.-Y. Lee, E. S. Trombetta, M. Pypaert, A. Nara, T. Yoshimori, B. Wilm, H. Erdjument-Bromage, P. Tempst, B. L. M. Hogan, I. Mellman, and S. Ghosh. 2006. CHMP5 is essential for late endosome function and down-regulation of receptor signaling during mouse embryogenesis. *The Journal of cell biology* 172(7):1045–1056. doi:10.1083/jcb.200509041.

Shin, N., N. Ahn, B. Chang-Ileto, J. Park, K. Takei, S.-G. Ahn, S.-A. Kim, G. Di Paolo, and S. Chang. 2008. SNX9 regulates tubular invagination of the plasma membrane through interaction with actin cytoskeleton and dynamin 2. *Journal of cell science* 121(Pt 8):1252–1263. doi:10.1242/jcs.016709.

Shin-Rong J. Wu, Rami Khoriaty, Stephanie H. Kim, K. Sue O'Shea, Guojing Zhu, Mark Hoenerhoff, Cynthia Zajac, Katherine Oravecz-Wilson, Tomomi Toubai, Yaping Sun, David Ginsburg, and Pavan Reddy. 2019. SNARE protein SEC22B regulates early embryonic development. *Sci Rep* 9(1):1–10. doi:10.1038/s41598-019-46536-7.

Siegemund, S., J. Shepherd, C. Xiao, and K. Sauer. 2015. hCD2-iCre and Vav-iCre Mediated Gene Recombination Patterns in Murine Hematopoietic Cells. *PloS one* 10(4). doi:10.1371/journal.pone.0124661.

Sigismund, S., T. Woelk, C. Puri, E. Maspero, C. Tacchetti, P. Transidico, P. P. Di Fiore, and S. Polo. 2005. Clathrin-independent endocytosis of ubiquitinated cargos. *Proceedings of the National Academy of Sciences* 102(8):2760–2765. doi:10.1073/pnas.0409817102.

Silver, L., and J. Palis. 1997. Initiation of Murine Embryonic Erythropoiesis: A Spatial Analysis. *Blood* 89(4):1154–1164. doi:10.1182/blood.V89.4.1154.

Skarnes, W. C., B. Rosen, A. P. West, M. Koutsourakis, W. Bushell, V. Iyer, A. O. Mujica, M. Thomas, J. Harrow, T. Cox, D. Jackson, J. Severin, P. Biggs, J. Fu, M. Nefedov, P. J. de Jong, A. F. Stewart, and A. Bradley. 2011. A conditional knockout resource for the genome-wide study of mouse gene function. *Nature* 474(7351):337–342. doi:10.1038/nature10163.

Skokowa, J., D. C. Dale, I. P. Touw, C. Zeidler, and K. Welte. 2017. Severe congenital neutropenias. *Nature reviews. Disease primers* 3:17032. doi:10.1038/nrdp.2017.32.

Sönnichsen, B., S. de Renzis, E. Nielsen, J. Rietdorf, and M. Zerial. 2000. Distinct Membrane Domains on Endosomes in the Recycling Pathway Visualized by Multicolor Imaging of Rab4, Rab5, and Rab11. *J Cell Biol* 149(4):901–914. doi:10.1083/jcb.149.4.901.

Sorkin, A., and M. von Zastrow. 2002. Signal transduction and endocytosis: close encounters of many kinds. *Nature reviews. Molecular cell biology* 3(8):600–614. doi:10.1038/nrm883.

Sorkin, A., and M. von Zastrow. 2009. Endocytosis and signalling: intertwining molecular networks. *Nature reviews. Molecular cell biology* 10(9):609–622. doi:10.1038/nrm2748.

Stanley, P. 2011. Golgi glycosylation. *Cold Spring Harbor perspectives in biology* 3(4). doi:10.1101/cshperspect.a005199.

Stenmark, H., G. Vitale, O. Ullrich, and M. Zerial. 1995. Rabaptin-5 is a direct effector of the small GTPase Rab5 in endocytic membrane fusion. *Cell* 83(3):423–432. doi:10.1016/0092-8674(95)90120-5.

Stepensky, P., A. Saada, M. Cowan, A. Tabib, U. Fischer, Y. Berkun, H. Saleh, N. Simanovsky, A. Kogot-Levin, M. Weintraub, H. Ganaiem, A. Shaag, S. Zenvirt, A. Borkhardt, O. Elpeleg, N. J. Bryant, and D. Mevorach. 2013. The Thr224Asn mutation in the VPS45 gene is associated with the congenital neutropenia and primary myelofibrosis of infancy. *Blood* 121(25):5078–5087. doi:10.1182/blood-2012-12-475566.

Stinchcombe, J. C., D. C. Barral, E. H. Mules, S. Booth, A. N. Hume, L. M. Machesky, M. C. Seabra, and G. M. Griffiths. 2001. Rab27a Is Required for Regulated Secretion in Cytotoxic T Lymphocytes. *J Cell Biol* 152(4):825–834.

Stockler, S., S. Corvera, D. Lambright, K. Fogarty, E. Nosova, D. Leonard, R. Steinfeld, C. Ackerley, C. Shyr, N. Au, K. Selby, M. van Allen, H. Vallance, R. Wevers, D. Watkins, D. Rosenblatt, C. J. Ross, E. Conibear, W. Wasserman, and C. van Karnebeek. 2014. Single point mutation in Rabenosyn-5 in a female with intractable seizures and evidence of defective endocytotic trafficking. *Orphanet journal of rare diseases* 9. doi:10.1186/s13023-014-0141-5.

Strydom, N., and S. M. Rankin. 2013. Regulation of circulating neutrophil numbers under homeostasis and in disease. *Journal of innate immunity* 5(4):304–314. doi:10.1159/000350282.

Subramanian, P., I. Mitroulis, G. Hajishengallis, and T. Chavakis. 2016. Regulation of tissue infiltration by neutrophils: Role of integrin α3β1 and other factors. *Current opinion in hematology* 23(1):36–43. doi:10.1097/MOH.0000000000000198.

Suzuki, Y., C. Demoliere, D. Kitamura, H. Takeshita, U. Deuschle, and T. Watanabe. 1997. HAX-1, a novel intracellular protein, localized on mitochondria, directly associates with HS1, a substrate of Src family tyrosine kinases. *Journal of immunology (Baltimore, Md. 1950)* 158(6):2736–2744.

Swanson, J. A. 1989. Phorbol esters stimulate macropinocytosis and solute flow through macrophages. *Journal of cell science* 94 (Pt 1):135–142.

Swanson, J. A. 2014. Phosphoinositides and engulfment. *Cellular microbiology* 16(10):1473–1483. doi:10.1111/cmi.12334.

Tall, G. G., H. Hama, D. B. DeWald, and B. F. Horazdovsky. 1999. The phosphatidylinositol 3-phosphate binding protein Vac1p interacts with a Rab GTPase and a Sec1p homologue to facilitate vesicle-mediated vacuolar protein sorting. *Molecular biology of the cell* 10(6):1873–1889. doi:10.1091/mbc.10.6.1873.

Tam, P. P. L., and D. A. F. Loebel. 2007. Gene function in mouse embryogenesis: get set for gastrulation. *Nature reviews. Genetics* 8(5):368–381. doi:10.1038/nrg2084.

Tanaka, N., M. Kyuuma, and K. Sugamura. 2008. Endosomal sorting complex required for transport proteins in cancer pathogenesis, vesicular transport, and non-endosomal functions. *Cancer science* 99(7):1293–1303. doi:10.1111/j.1349-7006.2008.00825.x.

Tanida, I., T. Ueno, and E. Kominami. 2008. LC3 and Autophagy. *Methods in molecular biology (Clifton, N.J.)* 445:77–88. doi:10.1007/978-1-59745-157-4_4.

Teis, D., N. Taub, R. Kurzbauer, D. Hilber, M. E. de Araujo, M. Erlacher, M. Offterdinger, A. Villunger, S. Geley, G. Bohn, C. Klein, M. W. Hess, and L. A. Huber. 2006. p14–MP1-MEK1 signaling regulates endosomal traffic and cellular proliferation

during tissue homeostasis. *J Cell Biol* 175(6):861–868. doi:10.1083/jcb.200607025.

Tejeda-Muñoz, N., L. V. Albrecht, M. H. Bui, and E. M. de Robertis. 2019. Wnt canonical pathway activates macropinocytosis and lysosomal degradation of extracellular proteins. *Proceedings of the National Academy of Sciences of the United States of America*. doi:10.1073/pnas.1903506116.

Tellam, J. T., D. E. James, T. H. Stevens, and R. C. Piper. 1997. Identification of a mammalian Golgi Sec1p-like protein, mVps45. *The Journal of biological chemistry* 272(10):6187–6193. doi:10.1074/jbc.272.10.6187.

Teng, T.-S., A.-l. Ji, X.-Y. Ji, and Y.-Z. Li. 2017. Neutrophils and Immunity: From Bactericidal Action to Being Conquered. *Journal of Immunology Research* 2017. doi:10.1155/2017/9671604.

Torrisi, M. R., L. V. Lotti, F. Belleudi, R. Gradini, A. E. Salcini, S. Confalonieri, P. G. Pelicci, and P. P. Di Fiore. 1999. Eps15 Is Recruited to the Plasma Membrane upon Epidermal Growth Factor Receptor Activation and Localizes to Components of the Endocytic Pathway during Receptor Internalization. *Molecular biology of the cell* 10(2):417–434.

Traer, C. J., A. C. Rutherford, K. J. Palmer, T. Wassmer, J. Oakley, N. Attar, J. G. Carlton, J. Kremerskothen, D. J. Stephens, and P. J. Cullen. 2007. SNX4 coordinates endosomal sorting of TfnR with dynein-mediated transport into the endocytic recycling compartment. *Nature cell biology* 9(12):1370–1380. doi:10.1038/ncb1656.

Triot, A., P. M. Järvinen, J. I. Arostegui, D. Murugan, N. Kohistani, J. L. Dapena Díaz, T. Racek, J. Puchałka, E. M. Gertz, A. A. Schäffer, D. Kotlarz, D. Pfeifer, C. Díaz de Heredia Rubio, M. A. Ozdemir, T. Patiroglu, M. Karakukcu, J. Sánchez de Toledo Codina, J. Yagüe, I. P. Touw, E. Unal, and C. Klein. 2014. Inherited biallelic CSF3R mutations in severe congenital neutropenia. *Blood* 123(24):3811–3817. doi:10.1182/blood-2013-11-535419.

Tucker, K. A., M. B. Lilly, L. Heck, JR, and T. A. Rado. 1987. Characterization of a new human diploid myeloid leukemia cell line (PLB-985) with granulocytic and monocytic differentiating capacity. *Blood* 70(2):372–378.

Ullrich, O. 1996. Rab11 regulates recycling through the pericentriolar recycling endosome. *J Cell Biol* 135(4):913–924. doi:10.1083/jcb.135.4.913.

Vallejo, M. O., G. P. Niemeyer, A. Vaglenov, T. Hock, B. Urie, P. Christopherson, and C. D. Lothrop. 2013. Decreased hematopoietic progenitor cell mobilization in pearl mice. *Experimental hematology* 41(10):848–857. doi:10.1016/j.exphem.2013.05.002.

van der Beek, J., C. Jonker, R. van der Welle, N. Liv, and J. Klumperman. 2019. CORVET, CHEVI and HOPS - multisubunit tethers of the endo-lysosomal system in health and disease. *Journal of cell science* 132(10). doi:10.1242/jcs.189134.

van der Sluijs, P., M. Hull, P. Webster, P. Mâle, B. Goud, and I. Mellman. 1992. The small GTP-binding protein rab4 controls an early sorting event on the endocytic pathway. *Cell* 70(5):729–740. doi:10.1016/0092-8674(92)90307-X.

van Gele, M., P. Dynoodt, and J. Lambert. 2009. Griscelli syndrome: a model system to study vesicular trafficking. *Pigment Cell & Melanoma Research* 22(3):268–282. doi:10.1111/j.1755-148X.2009.00558.x.

Vilboux, T., A. Lev, M. C. V. Malicdan, A. J. Simon, P. Järvinen, T. Racek, J. Puchalka, R. Sood, B. Carrington, K. Bishop, J. Mullikin, M. Huizing, B. Z. Garty, E. Eyal, B. Wolach, R. Gavrieli, A. Toren, M. Soudack, O. M. Atawneh, T. Babushkin, G. Schiby, A. Cullinane, C. Avivi, S. Polak-Charcon, I. Barshack, N. Amariglio, G. Rechavi, J. van der Werff ten Bosch, Y. Anikster, C. Klein, W. A. Gahl, and R. Somech. 2013. A congenital neutrophil defect syndrome associated with mutations in VPS45. *The New England journal of medicine* 369(1):54–65. doi:10.1056/NEJMoa1301296.

Vorup-Jensen, T., and R. K. Jensen. 2018. Structural Immunology of Complement Receptors 3 and 4. *Frontiers in Immunology* 9:2716. doi:10.3389/fimmu.2018.02716.

Wandinger-Ness, A., and M. Zerial. 2014. Rab proteins and the compartmentalization of the endosomal system. *Cold Spring Harbor perspectives in biology* 6(11):a022616. doi:10.1101/cshperspect.a022616.

Wang, T., L. Li, and W. Hong. 2017. SNARE proteins in membrane trafficking. *Traffic (Copenhagen, Denmark)* 18(12):767–775. doi:10.1111/tra.12524.

Warlich, E., J. Kuehle, T. Cantz, M. H. Brugman, T. Maetzig, M. Galla, A. A. Filipczyk, S. Halle, H. Klump, H. R. Schöler, C. Baum, T. Schroeder, and A. Schambach. 2011. Lentiviral vector design and imaging approaches to visualize the early stages of cellular reprogramming. *Molecular therapy the journal of the American Society of Gene Therapy* 19(4):782–789. doi:10.1038/mt.2010.314.

Weigert, R., A. C. Yeung, J. Li, and J. G. Donaldson. 2004. Rab22a regulates the recycling of membrane proteins internalized independently of clathrin. *Molecular biology of the cell* 15(8):3758–3770. doi:10.1091/mbc.e04-04-0342.

Westphal, A., W. Cheng, J. Yu, G. Grassl, M. Krautkrämer, O. Holst, N. Föger, and K.-H. Lee. 2017. Lysosomal trafficking regulator Lyst links membrane trafficking to toll-like receptor-mediated inflammatory responses. *The Journal of Experimental Medicine* 214(1):227–244. doi:10.1084/jem.20141461.

Wieduwilt, M. J., and M. M. Moasser. 2008. The epidermal growth factor receptor family: biology driving targeted therapeutics. *Cellular and molecular life sciences CMLS* 65(10):1566–1584. doi:10.1007/s00018-008-7440-8.

Willinger, T., M. Staron, S. M. Ferguson, P. de Camilli, and R. A. Flavell. 2015. Dynamin 2-dependent endocytosis sustains T-cell receptor signaling and drives metabolic reprogramming in T lymphocytes. *Proceedings of the National Academy of Sciences* 112(14):4423–4428. doi:10.1073/pnas.1504279112.

Wilson, S. M., R. Yip, D. A. Swing, T. N. O'Sullivan, Y. Zhang, E. K. Novak, R. T. Swank, L. B. Russell, N. G. Copeland, and N. A. Jenkins. 2000. A mutation in Rab27a causes the vesicle transport defects observed in ashen mice. *Proceedings of the National Academy of Sciences* 97(14):7933–7938. doi:10.1073/pnas.140212797.

Wu, B., and W. Guo. 2015. The Exocyst at a Glance. *Journal of cell science* 128(16):2957–2964. doi:10.1242/jcs.156398.

Yamada, E. 1955. THE FINE STRUCTURE OF THE GALL BLADDER EPITHELIUM OF THE MOUSE. *The Journal of Biophysical and Biochemical Cytology* 1(5):445–458.

Yamane, T. 2018. Mouse Yolk Sac Hematopoiesis. *Frontiers in Cell and Developmental Biology* 6. doi:10.3389/fcell.2018.00080.

Yeow, I., G. Howard, J. Chadwick, C. Mendoza-Topaz, C. G. Hansen, B. J. Nichols, and E. Shvets. 2017. EHD Proteins Cooperate to Generate Caveolar Clusters and to Maintain Caveolae during Repeated Mechanical Stress. *Current biology CB* 27(19):2951-2962.e5. doi:10.1016/j.cub.2017.07.047.

Yersin, A., T. Osada, and A. Ikai. 2007. Exploring Transferrin-Receptor Interactions at the Single-Molecule Level. *Biophysical Journal* 94(1):230–240. doi:10.1529/biophysj.107.114637.

Yu, A., Y. Shibata, B. Shah, B. Calamini, D. C. Lo, and R. I. Morimoto. 2014. Protein aggregation can inhibit clathrin-mediated endocytosis by chaperone competition. *Proceedings of the National Academy of Sciences of the United States of America* 111(15):E1481-90. doi:10.1073/pnas.1321811111.

Zerial, M., and H. McBride. 2001. Rab proteins as membrane organizers. *Nature Reviews Molecular Cell Biology* 2(2):107. doi:10.1038/35052055.

Zhang, X., and Y. Wang. 2016. Glycosylation Quality Control by the Golgi Structure. *Journal of molecular biology* 428(16):3183–3193. doi:10.1016/j.jmb.2016.02.030.

Zhou, Y., and J. Zhang. 2014. Arthrogryposis–renal dysfunction–cholestasis (ARC) syndrome: from molecular genetics to clinical features. *Italian Journal of Pediatrics* 40. doi:10.1186/s13052-014-0077-3.

Zmuidzinas, A., K. D. Fischer, S. A. Lira, L. Forrester, S. Bryant, A. Bernstein, and M. Barbacid. 1995. The vav proto-oncogene is required early in embryogenesis but not for hematopoietic development in vitro. *EMBO J* 14(1):1–11. doi:10.1002/j.1460-2075.1995.tb06969.x.

Zorman, S., A. A. Rebane, L. Ma, G. Yang, M. A. Molski, J. Coleman, F. Pincet, J. E. Rothman, and Y. Zhang. 2014. Common intermediates and kinetics, but different

energetics, in the assembly of SNARE proteins. *eLife* 3:e03348. doi:10.7554/eLife.03348.

List of publications

Łyszkiewicz M*, Ziętara N*, **Frey L**, Pannicke U, Stern M, Liu Y, Fan Y, Puchałka J, Hollizeck S, Somekh I, Rohlfs M, Yilmaz T, Ünal E, Karakukcu M, Patiroğlu T, Kellerer C, Karasu E, Sykora KW, Lev A, Simon A, Somech R, Roesler J, Hoenig M, Keppler OT, Schwarz K, Klein C. Human FCHO1 deficiency reveals role for clatrin-mediated endocytosis in development and function of T cells. *Nature communications* 11(1):1031 (2020) DOI:10.1038/s41467-020-14809-9 (*shared first authors)

Frey L, Ziętara N, Łyszkiewicz M, Marquardt B, Mizoguchi Y, Linder MI, Liu Y, Giesert F, Wurst W, Dahlhoff M, Schneider M, Wolf E, Somech R, Klein C. Mammalian VPS45 orchestrates trafficking through the endosomal system. *Blood* 137(14):1932-1944 (2021) DOI:10.1182/blood.2020006871